

KINETICS OF HYDROGEN EVOLUTION AND ABSORPTION DURING
ELECTROCHEMICAL REACTIONS AS DETERMINED BY MONITORING
THE VOLUME OF HYDROGEN BUBBLES.

1359062

REFERENCE
ONLY

City of London Polytechnic
Central House

A thesis submitted to the Council for National Academic
Awards for the degree of Doctor of Philosophy

by

R. Deplanque Dipl. Ing. V.D.I.

Department of Metallurgy and Materials
Sir John Cass School of Science and Technology
City of London Polytechnic
London E1

September 1983



IMAGING SERVICES NORTH

Boston Spa, Wetherby
West Yorkshire, LS23 7BQ
www.bl.uk

BEST COPY AVAILABLE.

VARIABLE PRINT QUALITY

ACKNOWLEDGEMENTS

The author wishes to thank his supervisor, Prof. Dr. L. L. Shreir OBE for the help, advice and encouragement given throughout this work.

Acknowledgements are to be made to the Procurement Executive for support for this work which was carried out under Extramural Contract 2111/023 XR/MAT.

I would also like to express my appreciation to Dr. P. Poole and Dr. V. C. R. McLoughlin of RAE for helpful discussions.

Finally, the author wishes to express gratitude to his colleagues for many valuable discussions, and to thank all members of the staff of the Department of Metallurgy and Materials for their interest, assistance and co-operation.

ABSTRACT

The piezo electric technique (P.E.T) devised in this department is a highly sensitive method for measuring the total volume of gas bubbles suspended in a solution. This is achieved by simply performing a static compressibility test, causing small pressure fluctuations in the volume of a solution enclosed in a rigid vessel.

Volume fluctuations may be produced by utilising the properties of piezo electric materials, which either change their shape in an applied electric field or generate electric fields when under pressure. Applying an ac current to the piezo material positioned in this rigid vessel will cause a cyclic pressure fluctuation which can be measured by a second piezo crystal. On introducing a gas bubble into the system the coupling of both crystals is lessened, which can be measured as a decrease in the e.m.f of the second crystal. This decrease in e.m.f is a direct measure of the amount of gas present in the system.

By cathodically producing H on an electrode which does not absorb hydrogen, and by using a hydrogen saturated solution, it is possible to calibrate the output e.m.f. These results are compared with those obtained using an electrode which does absorb hydrogen and this makes it

possible to calculate the quantitative amount of gas absorbed by the metal.

Experiments were carried out on a variety of metals with low and high hydrogen absorption capabilities. The metals under study included Fe, Au, Cu, Pt, Ti, Al, Al-3Mg, Al-5Mg and Duralumin. Comparative studies were performed between the P.E.T and the solid state vacuum extraction method for Ti, and between P.E.T and the permeation method, as developed by Devanathan for Fe, and good agreement between these three methods was attained.

The diffusion coefficient for Fe was found to be $D_H = 7 \times 10^{-6} \text{ cm}^2 \text{ s}^{-1}$, and for Al, $D_H = 1.87 \times 10^{-9} \text{ cm}^2 \text{ s}^{-1}$, whilst its equilibrium solubility was found to be $S_H = 1 \times 10^{-4} \text{ gH/g Al}$. These results were compared with values found in the literature for Fe ;no values were available for the results on Al.

By introducing As into the electrolyte it was possible to show that at low concentration (2 ppm) As acts as a promoter for the h.a.r on Ti, Al, Al-3Mg, Al-5Mg and as inhibitor in the case of Duralumin. At higher concentrations >5 ppm As acts as inhibitor for the same reaction. A mechanism for this effect is proposed.

A detailed study was made on the growth mechanism of hydrides on Ti with and without As. It was shown that As acts as an inhibitor for the formation of γ -hydrides on Ti.

Proposals for extension of the work and uses in industry and research are made.

1.0	Introduction	1
1.1	Background	1
1.2	Objectives	1
1.3	Scope	1
1.4	Methodology	1
1.5	References	1
2.0	Experimental	2
2.1	Materials	2
2.2	Preparation of samples	2
2.3	Hydrogenation	2
2.4	Analysis	2
2.5	Equilibrium pressure method	2
2.6	Thermogravimetric analysis	2
2.7	Electrode method	2
2.8	Gas chromatography	2
2.9	Mass spectrometry	2
2.10	Neutron activation analysis	2
2.11	Electron microprobe	2
2.12	Hydrogen detection by means of α nuclear	2
2.13	source	2
2.14	Hydrogen analysis by $^1\text{H}(^1\text{H}, \alpha, \gamma)$ nuclear	2
2.15	reaction	2
2.16	Nuclear magnetic resonance (NMR)	2
2.17	Quasi-elastic neutron scattering	2
2.18	Hydrogen permeation current method	2

TABLE OF CONTENTS

	<u>PAGE</u>
<u>INTRODUCTION</u>	
<u>CHAPTER 1</u>	
<u>LITERATURE REVIEW</u>	3
1	3
1.1	3
1.2	3
1.3	4
1.4	4
1.5	5
1.6	5
1.7	6
1.8	6
1.9	6
1.10	7
1.11	7
1.12	8
1.13	8
1.14	9
1.15	10
1.16	11
1.17	11
1.18	12
1.19	13

		<u>Page</u>
2.	The effect of promoters on hydrogen entry	14
3.	Effect of current density on hydrogen absorption	16
<u>CHAPTER 2</u>	<u>THEORY OF HYDROGEN DIFFUSION</u>	18
2.1	Introduction	18
2.2	Adsorption of hydrogen	18
2.3	Dependence of permeation on surface coverage	20
2.4	Diffusion	22
2.5	Methods of measuring diffusion coefficients	24
2.6	Basic mathematics of the time-lag method	26
2.7	Logarithmic representation of the time-lag curve	30
2.8	The rate transient method	30
2.9	Determination of H concentration	33
2.10	The Einstein - Smoluwchosky Equation	34
<u>CHAPTER 3</u>	<u>PIEZO ELECTRIC TECHNIQUE AS ORIGINALLY DEvised</u>	37
3.1	Introduction	37
3.2	Principle of the piezo-electric technique	37
3.3	Description of the original apparatus	38
3.4	Original method used to calibrate the P.E.T.	43
3.5	Experiments performed by Meadows	43
3.6	Results and discussion	45
<u>CHAPTER 4</u>	<u>EXPERIMENTAL</u>	53
4.1	Introduction	53
4.2	Desing of charging cell	53
4.3	The monitoring cell	56
4.4	Electrodes used for volumetric determination of cathodic hydrogen	61

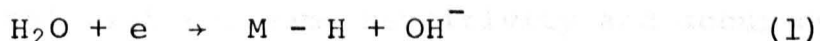
	<u>Page</u>	
4.5	Calibration of electrodes for determination of Faradaic hydrogen evolution	63
4.6	Electrodes used as anodes	64
4.7	The pre-saturation vessel	64
4.8	The noise filter system	66
4.9	Reproducibility	68
<u>CHAPTER 5</u>	<u>CALIBRATION OF THE PIEZO - ELECTRIC - CELL</u>	69
5.1	Calibration of the readout on a digital voltmeter	69
5.2	Experiment to determine H-saturation of 0.05 M H ₂ SO ₄	71
5.3	Experimental procedure	72
5.4	Results	73
5.5	Dissolution of cathodic hydrogen at different metal electrodes using the P.E.T. - cell	75
5.6	Calculation of the amount of hydrogen absorbed by different metals	77
5.7	Calculations	78
<u>CHAPTER 6</u>	<u>HYDROGEN ABSORPTION BY VARIOUS METALS</u>	82
6.1	Effect of current density on hydrogen absorption in various metals	82
6.1.1	Results	82
6.1.2	Conclusions	99
6.2	Hydrogen absorption by a gold electrode	100
6.2.1	Introduction	100
6.2.2	Material and experimental procedure	101
6.2.3	Results	102
	<u>INTRODUCTION</u>	151
	Introduction	151
	Material and experimental	157

		<u>Page</u>
<u>CHAPTER 7</u>	<u>HYDROGEN ABSORPTION IN TITANIUM</u>	105
7.1	Comparison between solid state vacuum extraction (VE) and P.E.T.	107
7.1.1	Introduction	107
7.1.2	Materials	107
7.1.3	Specimen preparation	108
7.1.4	Solution	109
7.2	Estimation of absorbed hydrogen using the P.E.T.	110
7.3	The vacuum extraction apparatus (VEA)	110
7.3.1	Extraction section	111
7.3.2	Analysis section	111
7.3.3	Evacuation section	113
7.3.4	Calculation of results obtained by VEA	114
7.4	Results and discussion	115
7.5	Kinetics of hydride formation on Ti	118
7.6	Results	119
7.7	Hydrogen absorption by Ti in solutions containing As	123
7.7.1	Introduction	124
7.7.2	Material and experimental procedure	126
7.7.3	Results	129
7.7.4	Discussion and conclusion	138
7.7.5	Summary	142
7.8	Cathodic reduction of anodic oxide films on Ti	143
7.8.1	Introduction	143
7.8.2	Results	145
<u>CHAPTER 8</u>	<u>HYDROGEN ABSORPTION IN ALUMINIUM</u>	151
8.1	Introduction	151
8.2	Material and experimental	157

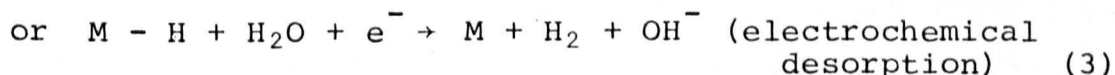
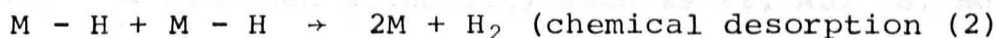
	<u>Page</u>	
8.3	Effect of thickness of foil on D_H in Al and Fe	159
8.4	Aluminium foils	165
8.5	Hydrogen absorption in domestic Al-foils	165
8.6	Influence of alloying additions to Al on the absorption of hydrogen	171
8.6.1	Introduction	172
8.6.3	Results and discussion	173
8.6.4	Conclusions	175
8.6.5	Determination of hydrogen saturated solubilities and diffusion coefficient in pure aluminium	176
8.6.6	Results	177
8.6.7	Cathodic absorption of H in Al using As containing charging solutions	179
8.7	Results	180
<u>CHAPTER 9</u>	<u>GENERAL DISCUSSION AND CONCLUSION</u>	189
9.1	Conclusions	194
9.2	Future work	199
9.3	Further work on H-absorption	199
	<u>REFERENCES</u>	204

1.0 INTRODUCTION

It is well known that the absorption of hydrogen by certain metals and alloys results in the phenomenon of hydrogen embrittlement, and that this in turn may result in fracture of the material at tensile stresses well below the yield stress. Although hydrogen may be introduced into the metal from the gas phase it can also be introduced from aqueous solutions in which the hydrated proton (and/or) water is cathodically reduced (spontaneously or by means of an external emf) to hydrogen atoms which become adsorbed on the surface of the metal.



This adsorbed hydrogen will then form molecular hydrogen by either chemical or electrochemical desorption



The hydrogen may remain as molecular gas and/or dissolve in the solution or the metal. This absorption of hydrogen by metals can be studied by a variety of techniques; for example, by solid - state vacuum extraction or by permeation through a thin metal membrane.

All methods have certain advantages and disadvantages, but in most cases they do not provide accurate information on the initial stages of hydrogen absorption. However, the

piezo-electric technique (P.E.T) which has been used widely in this work has an advantage over the two techniques mentioned above, that it is capable of monitoring the instantaneous evolution of hydrogen on the surface of a cathodically polarized metal foil and this in turn provides a means of monitoring hydrogen absorption.

It has been the purpose of this work to develop a technique and analytical model for determining hydrogen absorption rates in a variety of metals. It has been established that it is possible to use this technique to determine *equilibrium* solubilities and diffusion coefficients for hydrogen in metals. This can, of course, be achieved by other methods, but not with the same sensitivity and accuracy as the P.E.T. The high sensitivity of the P.E.T for measuring the kinetics of hydrogen evolution described by Meadows and Shreir⁽⁷⁰⁾ is particularly suitable for metals with unknown or very low hydrogen solubility such as Pt, Au, Cd, Hg and Al.

⁷⁰ signifies hydrogen irrespective of form, monatomic, molecular, etc.

CHAPTER 1
LITERATURE REVIEW

1. HYDROGEN ESTIMATION METHODS

1.1 Introduction

In view of the novelty of the piezo-electric method an extensive literature survey was carried out on techniques used for studying hydrogen absorption in order to establish the advantages and limitation of the former.

The determination of hydrogen in a variety of metals has been reviewed by several authors⁽¹⁻⁴⁶⁾ and the principles of the method are considered very briefly below. However some emphasis will be placed on newer less well known techniques.

1.2 Sieverts' Method^(106,1,2)

This was one of the earliest methods in which the change in volume of H^{*} gas in contact with an iron-specimen, both of which were contained in a glass vessel at a predetermined pressure, were determined after various time intervals. This method provided a means of determining H solubility.

The apparatus consisted of a glass vessel, which could be introduced in a furnace so that it could be heated to a predetermined temperature, attached to a mercury barometer. This gave a direct measurement of the volume of H evolved from the metal specimen during heating.

* H signifies 'hydrogen' irrespective of form, monatomic, molecular, etc.

1.3 Vacuum-fusion⁽³⁾

This term is applied to methods in which the metal sample contained in a graphite crucible which could be heated to a high temperature, is melted, usually in the range 1500 - 2000°C . In this method dissolved hydrogen and nitrogen are evolved as gases and similar consideration apply to dissolved oxygen which is reduced to CO. These gaseous products are then transferred to a conventional gas analytical apparatus in which their volumes are determined.

The disadvantages of this method as far as hydrogen is concerned is that the hydrogen evolved may be only a small proportion of the total gases absorbed so that, depending on the method used for analysing the gases, the accuracy may not be high.

1.4 Vacuum extraction using the liquid tin-fusion method

The hydrogen content is determined by using tin to lower the melting point of the metal under test thus allowing the gases to be extracted by vacuum fusion at a relatively low temperature. Of the low melting point metals only tin is used in this liquid-metal technique, since in addition to the low m.p (232°C) it has a low vapour pressure when just molten.

Carney, Chipman and Grant⁽⁴⁾ used an induction heated bath of 130g Sn + 0.7g Si + 2g of sample, which were contained in a silica crucible heated at 1150°C. All the hydrogen was evolved in about 5 min, and an accuracy of 0.1 ppm was claimed for the method.

The difficulties of this method are mainly due to the evaporation of films from the surface and the collection time varies between 5 min and 1.5 h, where the latter is the more usual time required to collect the whole amount of gas^(5,6) .

1.5 Solid-state vacuum extraction from the solid (Vacuum Heating) (5 - 13)

This is regarded as the simplest and most accurate of the vacuum extraction procedures. The apparatus required consists in principle of a furnace tube exhausted by vacuum pumps (backing pumps and Hg diffusion-pump) which transfers the gas evolved into a fixed volume in which the pressure is measured, the whole apparatus being exhausted by a Hg diffusion-pump. This method will be described in detail in Chapter 4.

The disadvantage of the method is the relatively long time often required for the extraction of all hydrogen from the specimen.

1.6 Inert gas carrier method⁽¹⁴⁾

In this method the hydrogen is allowed to diffuse out of the heated specimen into the surrounding atmosphere and is swept away by a stream of an inert gas (Ar, N₂, etc.).

After drying the gas completely the volume of hydrogen is evaluated by passing it over hot copper oxide to convert the hydrogen to water, which is then determined gravimet-

rically. This method suffers presumably from the difficulty of all continuous gas-flow methods, ie. the initial gas content of the system is relatively large in comparison to the volume of H in the metal.

1.7 Ionic bombardment (15,16)

The hydrogen-containing sample is made the cathode in a gas discharge tube operating at a moderate vacuum, and the gases evolved are collected and analysed. Bobalek and Shrader⁽¹⁶⁾ concluded that this method even though it gave reproducible results was difficult and inconvenient.

1.8 Combustion methods (17-20)

The basic principle of this method is the total oxidation of the metal in pure oxygen at elevated temperatures. The gaseous products formed are then separated by then freezing and fractional distillation. Unsatisfactory results have been obtained from the type of apparatus used, and in addition the method is complex and liable to error.

1.9 Reactive carrier gas methods

Sauerwald⁽¹⁹⁾ has used a method for estimating hydrogen in magnesium in which chlorine is bubbled through the molten metal to form hydrogen chloride, which is then oxidised with oxygen and copper oxide and the hydrogen determined as water. However, Moore⁽²⁰⁾ using this method had difficulty in obtaining accurate results for H in steel.

1.10 Chemical Methods

Chretien et al⁽²¹⁾ dissolved aluminium in liquid bromine under carbon disulphide. Any dissolved hydrogen in the Al was converted to HBr which was determined gravimetrically as silver bromide. Any unoxidised hydrogen or its gaseous compounds was separately oxidised with hot copper oxide and weighed as water.

Mannchen and Fischer⁽²²⁾ found this method unreliable owing to side reactions.

1.11 Equilibrium pressure method⁽²³⁾

The metal specimen is placed in an evacuated hot enclosure containing a known quantity of hydrogen which is allowed to equilibriate with the metal. The apparatus consists of a furnace tube with a pressure gauge attached, and the change in pressure is determined at the temperature under study for a predetermined time.

The method for determining the pressure change suffers from the disadvantage that the result depends on knowing the equilibrium solubility of H in the particular metal at the operating temperature, and is limited to cases in which the equilibrium hydrogen pressure can be built up without removing a significant proportion of the hydrogen from the specimen.

1.12 Isotopic equilibrium method (24)

The sample is heated in an enclosure with a known quantity of hydrogen-containing deuterium. It is assumed that the hydrogen in the metal and in the deuterium in the gas distribute themselves in the same way between the gas phase and the metal, and by determining the equilibrium content of deuterium in the gas phase, the hydrogen content of the metal can be calculated.

Hydrogen from the apparatus or from the surface films on the specimen affects both these equilibrium methods (Nos. 1.11 and 1.12), and also the results. The method thus appears to be unsatisfactory.

1.13 Telegas method (equilibrium pressure method for liquid metals) (25-27)

The method is basically an equilibrium-pressure method utilising molten metal and a carrier-gas. A small quantity of nitrogen gas is repeatedly bubbled through the melt by means of a special probe and the amount of H taken up by the N₂ corresponds with the partial pressure of H in the melt.

The method which is used for controlling the H content of melts, has all the disadvantages of an equilibrium method, but is useful since it gives a reasonably accurate result in a very short time (2 - 3 min) .

1.14 Ion probe spectrometer (26)

An ion beam is used to sputter material from the surface of the sample, and the secondary ions resulting from the bombardment are then analysed in a mass spectrometer.

By varying the intensity of the bombarding ion beam the method can be used for both surface and depth analysis. It also has the advantage that there is equal sensitivity over the whole mass range and only a small quantity of material is analysed. By monitoring a single species as a function of time, concentration profiles can be measured as sputtering proceeds. Mass analysis is carried out using a Mattauch-Herzog focusing mass-spectrometer, in which electrostatic and magnetic fields are employed. A detailed description of the electrostatic and magnetic sections of the apparatus is given by Herzog (158).

In the mass spectrometer an electrostatic field acts as an energy analyser while the magnetostatic section separates the ions of different mass. As the magnet current of the mass spectrometer is slowly increased each mass/charge ratio can be detected and the results recorded on an x - y recorder. The magnetic current may also be used to detect a single element of specific mass, and the behaviour of this species can be monitored as a function of time.

Major difficulties with the instrument are the lack of spatial and depth resolution and the inability to analyse elements that diffuse only slowly to the surface being examined.

1.15 Hydrogen detection by means of a nuclear method⁽³¹⁾

By using the resonance reaction reported by Landford⁽³²⁾



it is possible to determine the quantity of hydrogen absorbed within a metal foil. To utilise this reaction a hydrogen-containing material is bombarded with ${}^{15}\text{N}$ -ions and the yield of 4.43 MeV γ -rays is measured using a NaI scintillation counter. The characteristic γ -rays provides a means of calculating the hydrogen content. However the quantity of the γ -rays is dependent on the reaction probability, and if the energy is less than 6.385 MeV no γ -rays will be emitted. When the energy is raised to the resonance energy, hydrogen at the surface of the sample will be detected. If the incident beam of ${}^{15}\text{N}$ has an energy above 6.385 MeV it will lose energy by penetrating the sample until it falls to 6.385 MeV, ie. the nuclear reaction will occur at a certain depth inside the sample.

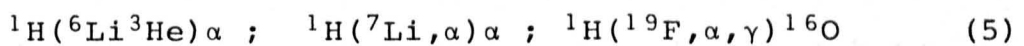
Due to the narrowness of the resonance in the cross section of the metal specimen⁽³⁴⁾ hydrogen can be identified in a small layer of a defined depth, which can be calculated from the known energy loss of ${}^{15}\text{N}$ -ions⁽³³⁾. In this way depth profiles of hydrogen concentration can be determined with a resolution of about 3 - 10 nm.

The sensitivity of the method allows hydrogen concentration down to only 30 ppm to be detected within the analysed layer.

1.16 Hydrogen analysis by ${}^1\text{H}({}^{11}\text{B},\alpha)\alpha\alpha$ nuclear reaction (34,35)

Analysis by low energy nuclear reactions is used to investigate phenomena which take place in a thin layer near the surface. The target (eg. foil of 10 μm thickness) is bombarded with 18 MeV protons and the scattered particles are detected by a scintillation counter.

This method allows the separation of hydrogen atoms near the surface from those in the bulk with a depth resolution of about 10 nm. Hydrogen analysis is achieved by γ or α detection. Leich and Tambrello⁽³⁵⁾ use ${}^1\text{H}({}^{19}\text{F}, \alpha, \gamma) {}^{16}\text{O}$ reaction, with the incident energies of ${}^{19}\text{F}$ ions varying from 16 MeV to 18 MeV. The depth of resolution is about 30 nm and depth concentrations can be measured up to 400 nm. It is also possible to analyse hydrogen by means of other nuclear reactions such as



etc., in which the concentration of hydrogen is calculated over the spectrum of charged particles. However, the most common nuclear method for determining H is by means of the ${}^1\text{H}({}^{11}\text{B},\alpha)\alpha$ reaction.

1.17 Nuclear magnetic resonance (NMR) (37)

The NMR technique is well-established method for studying atomic motion in solids. Recently reviews on the application of nuclear magnetic resonance for studying hydrogen diffusion have been written by Pedersen (1965)⁽³⁶⁾, Cotts (1972)⁽³⁷⁾ and Fukai et al⁽⁴³⁾. It is based on measurements of the longitudinal spin-lattice relaxation time T_2 .

From the absolute values of the frequency and its temperature dependence, the rate of atomic motion and the H content can be calculated.

Two relatively new NMR techniques, the so-called 'rotating frame' technique and the direct measurement of the diffusion coefficient by observation of the spin-echo decay in the presence of an applied magnetic field, are beginning to be utilised for studies of diffusion of H in metals⁽³⁸⁾.

1.18 Quasi elastic neutron scattering (QNS)

In 1972 both Springer⁽³⁸⁾ and Gissler⁽³⁹⁾ reviewed this method which was first applied by Skold and Nelim⁽⁴⁰⁾ in 1967, and gave an account of its application to metal-hydrogen systems.

It is based on a monoenergetic neutron beam which is scattered by the protons in the metal. As a result of the diffusion of the protons the beam will be energetically broadened and the width of the line will depend on the rate of diffusion.

With conventional spectrometers, the quasielastic - n-scattering technique is limited to $D_H > 10^{-5} - 10^{-6}$ cm²/s.

However, with the recent development by Alefeld of the high-resolution back-scattering spectrometer⁽⁴¹⁾ diffusion

coefficients which are 1-2 orders of magnitude smaller can be measured.

1.19 Hydrogen permeation current method

Devanathan et al^(42,45,46) developed a method of measuring the instantaneous rate of permeation of cathodic hydrogen through membranes of different metals.

The method involves cathodically charging one side of a thin metal diaphragm in an acid or alkaline solution. Hydrogen ions will be discharged on this side of the diaphragm and a small fraction of the hydrogen atoms thus produced will enter the metal and diffuse through it to the other side, which is in contact with 0.1 NaOH. The hydrogen atoms arriving at the metal/NaOH interface are ionised instantaneously by applying a constant anodic potential of -0.4 V (vs 0.1 M calomel electrode⁽⁴⁶⁾) by means of a potentiostat. The resulting ionisation current (P) is monitored on a sensitive recorder and this current, which corresponds to zero coverage of H on the exit side, is a faradaic measure of the instantaneous rate of permeation of hydrogen. From graphical integration of the P-t record the quantity of hydrogen permeating during a definite period can be calculated.

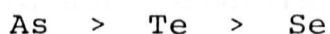
The theory of the method, which has been used to some extent in the present work, will be considered in the experimental section.

2. THE EFFECT OF PROMOTERS ON HYDROGEN ENTRY

Baukloh and Zimmerman⁽⁴⁷⁾ showed in a thorough investigation that many elements of Groups V and VI of the periodic table influence markedly the entry of hydrogen into iron and steel during cathodic polarization. This was studied by measuring the hydrogen permeation through a steel membrane in 1N H₂SO₄ which was cathodically polarized on one side, and the degree of promoting action was shown to be



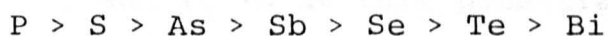
whereas in NaOH



and in acetic acid



The effect of additives has also been studied by determining⁽⁴⁸⁾ the elongation of iron coils during cathodic polarization in H₂SO₄. It was found that at a critical concentration of promoter there were no further increases in hydrogen occlusion. The following order was obtained for maximum promoting ability irrespective of concentration:



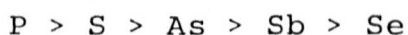
It has been shown⁽⁴⁹⁾ that the nature of the compound containing the promoter has a significant effect on the promoting action e.g. P, when added as hydride PH₃ produced the maximum effect, whereas when added as elemental yellow P, it was shown to have little or no effect.

Promoting action by metalloids is not clearly understood, and several theories have been proposed to explain how they catalyse H absorption. One of these will be discussed in detail in a later Chapter.

Smialowski et al⁽⁴⁸⁾ consider that the formation of a volatile hydride is an essential step in hydrogen entry, a view which is supported by McGraw et al⁽⁴⁹⁾ who are of the opinion that promoters form hydrogen compounds of high stability. Few workers have attempted to explain why promoter action did not correlate with the binding force of the promoter hydrides. The values of binding force computed by Siebert⁽⁵⁰⁾ predicted the order



whereas Newman⁽⁵¹⁾ found experimentally using solid-state vacuum extraction that the order was



A strong argument in favour of the hydride theory is that As only promotes hydrogen entry at potentials more negative than -0.4 V ⁽⁵²⁾, and it is at this potential that As becomes reduced to the AsH_3 ⁽⁵²⁾. New evidence for this theory will be discussed in a later Chapter.

3. EFFECT OF CURRENT DENSITY ON HYDROGEN ABSORPTION

Early work by Sieverts showed that the solubility of H was proportional to the square root of the pressure (p), ie.

$$S = K p^{\frac{1}{2}} \quad (4)$$

Bodenstein⁽¹⁵⁹⁾ showed that an analogous relationship exists between the permeation rate (P) of cathodically evolved hydrogen and the applied current density:

$$P = K i^{\frac{1}{2}} \quad (5)$$

where K is a constant. This analogy is supported further by the work of Borelius and Lindblom⁽¹⁶⁰⁾ who found a departure from the square root relationship at low and high current densities and at low and high gas pressures. They modified the equation for low pressure to

$$p = K (i^{\frac{1}{2}} - i_t^{\frac{1}{2}}) \quad (6)$$

where i_t is the threshold value of the current density which varies with the nature of the metal used and the range of c.ds studied. This established the connection between c.d. and pressure of H just below the surface of the metal.

Later investigators^(53,42) have queried the existence of a threshold value of current density, and have emphasised the importance of the variation of surface coverage with current density. For cathodically polarized mild steel in 1M H_2SO_4 , Baukloh and Zimmerman⁽⁴⁷⁾ found a maximum rate of hydrogen absorption at a critical c.d above which the absorption rate decreased. Certain of this work has been repeated

to check the validity of the P.E.T method, and will be discussed in this work subsequently.

The present study was carried out in order to determine the effect of the concentration of the electrolyte on the rate of the reaction between the hydrogen and the oxygen ions. The results are given in Table I. It is seen that the rate of the reaction increases with increasing concentration of the electrolyte. This is in agreement with the results obtained by other workers in this field.

TABLE I
Rate of reaction between hydrogen and oxygen ions

The rate of reaction between hydrogen and oxygen ions was measured at various concentrations of the electrolyte. The results are given in Table I. It is seen that the rate of the reaction increases with increasing concentration of the electrolyte.

3. Rate of reaction between hydrogen and oxygen ions

The rate of reaction between hydrogen and oxygen ions was measured at various concentrations of the electrolyte. The results are given in Table I. It is seen that the rate of the reaction increases with increasing concentration of the electrolyte. This is in agreement with the results obtained by other workers in this field.

The rate of reaction between hydrogen and oxygen ions was measured at various concentrations of the electrolyte. The results are given in Table I. It is seen that the rate of the reaction increases with increasing concentration of the electrolyte.

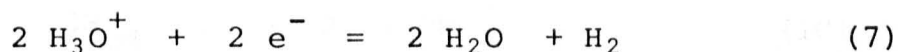


CHAPTER 2

2. THEORIES OF HYDROGEN DIFFUSION

2.1 Introduction

The entry of hydrogen into a cathodically polarized metal electrode or a metal in equilibrium with gaseous hydrogen must be preceded by adsorption of H on the surface of the metal. The hydrogen evolution reaction (h.e.r) can be summarized by the following general equation which involves a number of consecutive steps

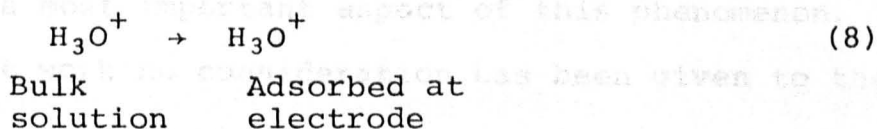


It is necessary to consider the fundamental mechanism of absorption of H_2 , since this explains the kinetics of H_2 evolution and absorption.

2.2 Adsorption of Hydrogen

Adsorption of hydrogen is regarded as being controlled by three different reactions as shown by various workers in this field (see Pöpperling, Ref 54). These may be summarised as follows.

1. Migration and diffusion of the hydrated proton to the surface of the metal electrode



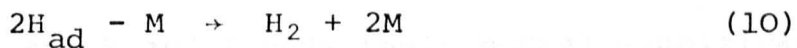
2. Electrochemical discharge of the adsorbed ion to form an adsorbed atom on the surface of the metal



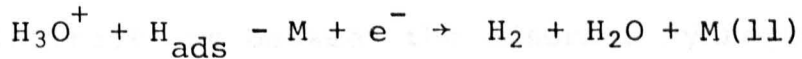
Steps 1 and 2 are generally known as Volmer reactions.

3. The adsorbed hydrogen is then able to react in one of the following ways

- (i) Chemical combination (or chemical desorption)



- (ii) Electrochemical desorption



- (iii) Absorption of hydrogen by the cathode metal



4. Desorption and transport of the hydrogen molecule into the gas phase.

Reaction 12 which leads to the absorption of hydrogen gas into the metal lattice is important in relation to various phenomenon, particularly H stress cracking, and represents therefore a most important aspect of this phenomenon. In the present work no consideration has been given to the effect of a tensile stress.

If adsorption follows the Langmuir Isotherm then there is a relationship between the coverage (θ) and the activity (a_H)

of the adsorbed hydrogen atoms. This can be expressed as (55,56)

$$\theta = \frac{l_O^{\alpha_H}}{1 + l_O^{\alpha_H}} \cdot \frac{\theta}{1 - \theta} = l_O^{\alpha_H} \quad (13)$$

where l_O can be written as

$$l_O = \exp \frac{\Delta G^\theta}{RT} \quad (14)$$

where ΔG^θ is the standard free enthalpy for adsorption and l_O represents the adsorption coefficient as quoted by Moore (20) and R and T have their normal significance.

Equation(14) is only true for a homogeneous surface with no lateral interactions between the adsorbed hydrogen atoms. If this is not the case the Tempkin Isotherm has to be applied (55,56,57)

$$\theta = \frac{1}{\phi} \ln \frac{1 + \alpha_H l_O}{1 + l_O^{\alpha_H} \exp(\phi)} \quad (15)$$

where ϕ is a factor which takes into account lateral interaction, and is generally of the order of 10 to 15 (58).

2.3 Dependence of permeation on surface coverage (θ)

The hydrogen which is brought to the surface of the metal as described in equations 14 and 15 is absorbed according to equation 12 (57).

The reaction kinetics are very much dependent on surface coverage (θ), ie. the fraction of the total sites that are available for adsorption. Shamzul Huq and Rosenberg (58)

showed that the kinetics of the above steps are

$$i_1 = K_1 i_{O,1} (1 - \theta) \exp(-\alpha \eta F/RT) \quad (16)$$

$$i_2 = K_2 i_{O,2} \theta^2 \quad (17)$$

$$i_3 = K_3 i_{O,3} \theta \exp(-\alpha \eta F/RT) \quad (18)$$

where K_1 , K_2 and K_3 are the rate constants, which include a term for the activity of the hydrogen ion, and α is the transfer coefficient. At equilibrium the equilibrium exchange c.d.s in equations 16, 17 and 18 are given by

$$i_{O,1} = K_{O,1} (1 - \theta) \quad (19)$$

$$i_{O,2} = K_{O,2} \theta^2 \quad (20)$$

$$i_{O,3} = K_{O,3} \theta \quad (21)$$

where θ is the equilibrium surface coverage.

When $i_{O,1}$ is significantly smaller than either $i_{O,2}$ or $i_{O,3}$ the reaction kinetics is controlled by slow discharge and is independent of the desorption step.

Adsorbed hydrogen comes to equilibrium by step 2 (equation 17) in which θ is assumed to be independent of η .

Equation 16 and 18 are forms of the Tafel equation

$$\eta = a \pm b \log i \quad (22)$$

where the Tafel slope b , is given by

$$b = \frac{2.303RT}{\alpha F \eta} \quad (23)$$

where n is the number of electrons in the rds. Hence, at 298 K equation 23 becomes

$$b = \frac{0.059}{\alpha n} \quad (24)$$

and $b = 0.118$ V if α is assumed to be 0.5 and n to equal 1. When the rate controlling step is chemical desorption^(58,59) the overall rate is given by equation 22 where

$$a = \frac{2.303RT}{\alpha F} \log i_0 \quad (25)$$

2.4 Diffusion⁽⁶¹⁾

The diffusion flow (flux or current) of a substance in a mixture with other substances is defined as the amount of this substance passing perpendicularly through a reference surface of unit area during unit time.

Fick's 1st law⁽⁶¹⁾ of diffusion may be stated as

$$J = -D \frac{dc}{dx} \quad (26)$$

where J is the diffusion flow, D the coefficient of diffusion and dc/dx is the concentration gradient along the x diffusion axis; the units of D are $m^2 s^{-1}$.*

Most diffusion processes however cause the concentration of the diffusing species to change with time and to take this into account it is assumed that the concentration gradient is responsible for the diffusion flux J_1 across the first reference plane and also causes a flux J_2

* Units of D are quoted as $cm^2 s^{-1}$ or $m^2 s^{-1}$

across a second plane to have the value

$$J_2 = J_1 + \frac{dJ_1}{dx} dx \quad (27)$$

Thus the amount of material (dm) that accumulates in a defined volume element per second is given by

$$dm = J_1 - J_2 = \frac{dJ}{dx} dx = -\frac{d}{dx}(-D\frac{dc}{dx}) dx \quad (28)$$

Since dm/dx is the rate dc/dt at which the concentration in the volume element is changing with time, it can be written as

$$\frac{\partial c}{\partial t} = \frac{\partial}{\partial x} (D \frac{\partial c}{\partial x}) \quad (29)$$

which is the general form of Fick's 2nd law for diffusion in one dimension that applies when the diffusion coefficient D is a function of concentration.

Often D can be considered to be constant, permitting use of the simpler equation

$$\frac{\partial c}{\partial t} = D \frac{\partial^2 c}{\partial x^2} \quad (30)$$

where c is the concentration, t the time (s) and x is the distance (m or cm) at which the reference planes are set in the direction of the x -axis.

Since diffusion is a vectorial property more than one different coefficient ('diffusivity') is required in anisotropic media or when diffusion is not unidirectional. Equations may still be written for diffusion along principal axes

in the form of:

$$J_x = - D_x \left(\frac{dc}{dx} \right) \quad (31)$$

$$J_y = - D_y \left(\frac{dc}{dx} \right) \quad (32)$$

$$J_z = - D_z \left(\frac{dc}{dx} \right) \quad (33)$$

where D_x , D_y and D_z are called the principal coefficients of diffusion.

2.5 Methods of measuring diffusion coefficients ⁽⁶²⁾

The diffusion coefficient D (m^2s^{-1}) may be expressed as follows:

$$D = D_0 \exp \left(-Q_D / RT \right) \quad (34)$$

Q_D = activation energy for diffusion (J/mol)

D_0 = fundamental frequency factor (m^2s^{-1})

R = gas constant ($J K^{-1} mol^{-1}$)

T = absolute temperature (K)

It should be noted that Q_D corresponds to the excess energy necessary for the diffusing particle to overcome the potential barrier separating two interstitial sites in the solvent lattice.

In their general theory of interstitial diffusion Wert and Zener⁽⁶³⁾ considered that the activation energy is associated with the strain energy of the lattice as a result of distortion induced by the interstitial atom around the

octahedral position (1/2 0 0). A similar assumption was made by Ferro⁽⁶⁴⁾ for diffusion in a bcc lattice. Thus, during a jump from one position to another, the atom is regarded as forcing apart two lattice atoms residing between the two octahedral sides by an amount equivalent to the difference between the diameter of the diffusing atom and the height of the cavity. The energy which is necessary to weaken the bond is taken up by the bond after the diffusing atom has passed through the lattice. Under these circumstances the net energy consumption is zero.

The pre-exponential frequency factor D_0 for diffusion in a bcc lattice was evaluated theoretically by Wert and Zener⁽⁶³⁾ in form of the following equation:

$$D_0 = \frac{1}{6} v a^2 \exp \left(\frac{\Delta S}{R} \right) \quad (35)$$

where v is the frequency of vibration of the solute atom in an interstitial position, a is the lattice parameter and ΔS is the entropy of activation.

The entropy of activation was found to be related to the coefficient of the decrease of elastic modulus with temperature as follows^(63,64)

$$\Delta S = \beta Q_D / T_m \quad (36)$$

where β is the coefficient of variation of elastic modulus with temperature, and T_m is the melting point of the metal (K).

The frequency ν has been evaluated by Wach⁽⁶²⁾ as:

$$\nu = (2Q_D / a^2)^{\frac{1}{2}} \quad (37)$$

If Q_D and β are known, then D_O can be evaluated, and using this approach satisfactory results were obtained by Ferro⁽⁶⁴⁾ for several interstitial solid solutions.

2.6 Basic Mathematics of the time-lag method.

The technique most frequently employed in the determination of the diffusion parameters (diffusivity and permeability) of hydrogen in iron and steel is the time-lag method.

This method is based on measurements of the time taken to attain a constant rate of flow through a membrane, with one side of the membrane exposed to the source of hydrogen (either gaseous or electrolytic) and the other exposed to a pre-evacuated system. Changes in concentration gradient take place until the attainment of steady-state conditions, and measurement of the pressure rise in the vacuum side of the system yields characteristic curves of the type shown schematically in Figure 1. The value of the intercept, on the time axis allows the calculation of the diffusion coefficient D from the following equation:

$$D_H = \frac{d^2}{6t_0} \quad (38)$$

where D is the diffusion coefficient ($m^2 s^{-1}$)

d is the thickness of the membrane (m)

and t_0 is the time required to establish constant flow (s)

Pressure

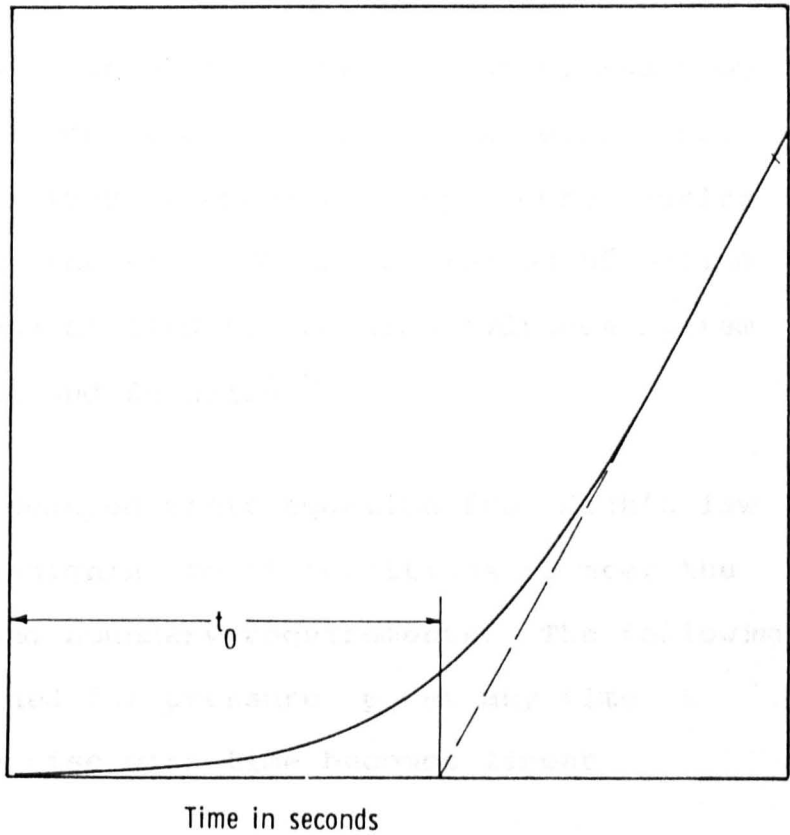


Fig. 1

Theoretical time - lag curve (schematic)

- A is the area of the membrane (cm^2)
- B is the diffusion coefficient (cm^2/sec)
- V is the volume of the collecting system (cm^3)
- r is the thickness of the diaphragm (cm)
- k is the pressure of the gas or the liquid pressure at
- s is the solubility

The term $d^2/4B$ has dimensions of time (s) and can be equated to t_0 , the time required to establish the constant rate of flow (i.e. the intercepts on the time axis)

$$t_0 = \frac{r^2}{4B} \quad \text{or} \quad r = \sqrt{4Bt_0} \quad (40)$$

The rate of hydrogen flow (permeation) can be obtained from the linear portion of the time-lag curve, and from knowledge of the geometry of the diffusion cell. This method has been derived independently by Rogers, Buritz and Alpert⁽⁶⁵⁾ for the study of the diffusion of helium through glasses and applied to the iron-hydrogen system by Eschbach, Gross and Schulien⁽⁶⁶⁾.

Rogers et al⁽⁶⁵⁾ deduced their equation from Fick's law of diffusion by assigning to it conditions to meet the non-steady flow and boundary requirements. The following formula was obtained for pressure p at any time t when the pressure rise with time becomes linear

$$p = \frac{A D S}{V d} p_1 \left(t - \frac{d^2}{6D} \right) \quad (39)$$

p is the pressure on the vacuum side in time (t)

A is the area of the membrane (m^2)

D is the diffusion coefficient ($m^2 s^{-1}$)

V is the volume of the collecting system (m^3)

d is the thickness of the membrane (m)

p_1 is the pressure of the gas on the high

pressure side

S is the solubility

The term $d^2/6D$ has dimensions of time (s) and can be equated to t_0 , the time required to establish the constant rate of flow (ie. the intercept on the time axis)

$$t_0 = \frac{d^2}{6D_H} \quad \text{or} \quad D = \frac{d^2}{6t_0} \quad (40)$$

By putting $t = 0$ in equation (39), the following relationship is obtained

$$S = \frac{6V}{Ad} \times \frac{p_0}{p_1} \quad (41)$$

where p_0 is the intercept which is obtained if the linear steady state curve (c.f Figure 1) is extrapolated to the pressure axis.

This is a convenient method of calculating the solubility, provided p is known which is not the case when hydrogen is introduced from solution by cathodic polarisation of one side of a metal membrane. It is evident from equation (39) that the solubility S is expressed in m^3_H / m^3_{Fe} which is dimensionless. The diffusion parameters are related by:

$$Q = D_H S \quad (42)$$

where Q is the permeability ($m^2 s^{-1}$)

S is the solubility (m^3_H / m^3_{Fe})

Since S is dimensionless then both Q and D will have the same dimensions ($m^2 s^{-1}$).

Mathematical analysis of the time-lag method for cylindrical geometry has been provided by Veysseyre, Asou and Bastien⁽⁶⁷⁾.

2.7 Logarithmic representation of the time-lag curve

By further analysis of the time-lag method Rogers et al⁽⁶⁵⁾ derived a linear representation of the initial portion of the curve (Figure 1)

$$\ln t^{\frac{1}{2}} \times \frac{dp}{dt} = \left(K - \frac{d^2}{4D} \right) \frac{1}{t} \quad (43)$$

This is a linear equation and a plot of $t^{\frac{1}{2}} \frac{dp}{dt}$ vs $\frac{1}{t}$ (Figure 2) yields a straight line of slope m and D_H can then be calculated from the relationship

$$D_H = -\frac{d^2}{4} \frac{1}{m} \quad (44)$$

The linear representation allows an accurate check of the simpler graphical extrapolation and also confirms whether or not the experimental permeation vs t curve is accurately represented by equation 38 or 39, as any anomalies would result in a departure from linearity. An example of data replotted according to this method is given schematically in Figure 2.

2.8 The rate transient method

A third approach is the method of Davanathan⁽⁴²⁾ and Nanis and McBreen⁽⁶⁸⁾ who consider the time - lag curve represented as a rate transient as shown schematically in Figure 3.

From the initial portion of the curve it is possible to obtain the diffusion coefficient using the following relationship

$$t^{\frac{1}{2}} \frac{dp}{dt}$$

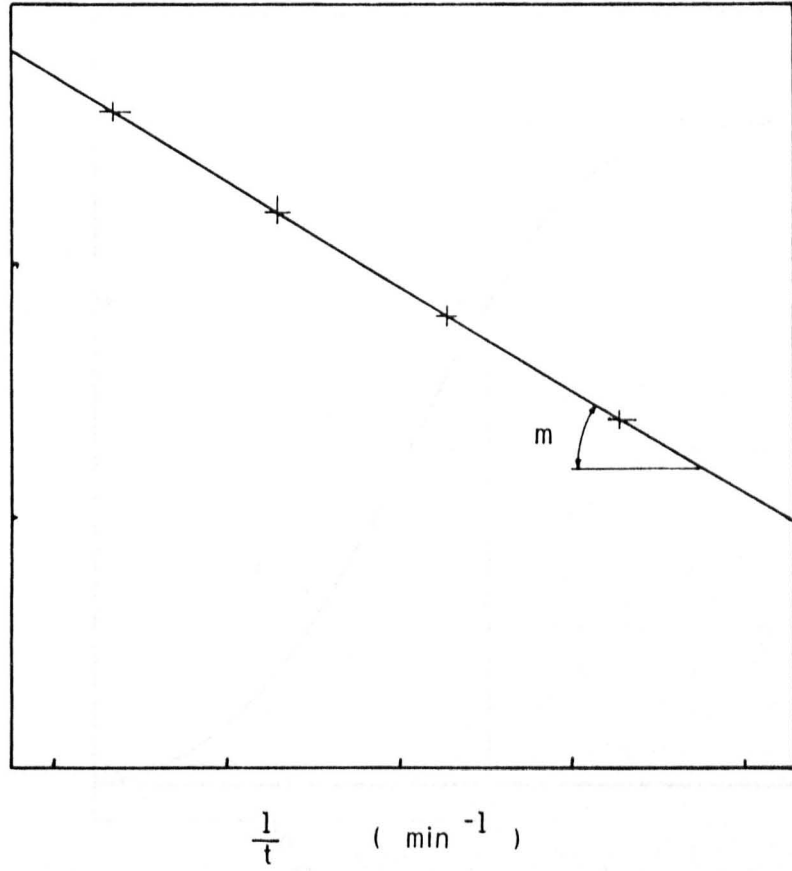


Fig. 2

Logarithmic method of analysing the time lag data of Fig. 1

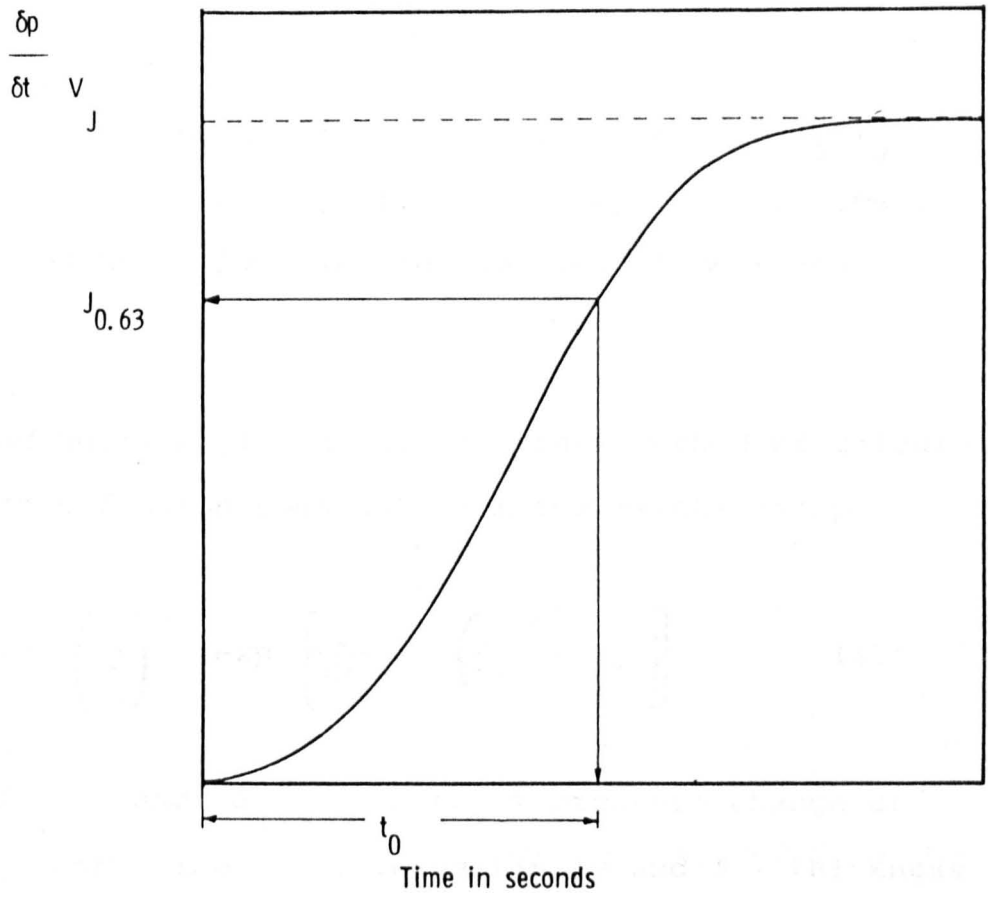


Fig. 3

Schematic time lag curve presented as rate transient

$$D = \frac{d^2}{6t_0} \quad (45)$$

where t_0 is the time required for permeation $(\frac{\partial P}{\partial t})_V$, to obtain 63% of the steady state value J_∞ ; this time is the same as that given in the classical time - lag method.

Nanis and McBreen⁽⁴⁷⁾ give a more accurate method of calculating the diffusion constant from the relationship

$$\frac{J_{t_1}}{J_{t_2}} = \left(\frac{t_2}{t_1}\right)^{\frac{1}{2}} \exp \left[\frac{d^2}{4D_H} \left(\frac{1}{t_1} - \frac{1}{t_2} \right) \right] \quad (46)$$

where J_{t_1} , and J_{t_2} = rate of pressure change at time t_1 and time t_2 , respectively and d = thickness of the membrane (m)

2.9 Determination of H Concentration

Once the diffusion coefficient D , and the permeation P have been determined, the concentration of hydrogen (c) on the input side of the membrane, can be calculated from the relationship:

$$P = \frac{Dc_0}{d} \quad (47)$$

P = permeation ($m^3 m^{-2} s^{-1}$)

D = diffusivity ($m^2 s^{-1}$)

c_0 = concentration (in appropriate units)

d = thickness of the membrane (m)

2.10 The Einstein-Smoluwchosky Equation

The diffusion coefficient D appears in both the macroscopic and the atomistic relationship of diffusion theory. It is given by the empirical approach embodied in Fick's 1st and 2nd laws in which D appears simply as a proportionality constant relating the flux J and the concentration gradient dc/dx .

One different approach is given by the random walk interpretation of the diffusion coefficient as embodied in the Einstein-Smoluchowsky equation described by Bockris and Reddy 1970⁽⁶⁹⁾ which gives the atomistic basis of the diffusion coefficient.

It can be proved that the mean square distance $\langle x^2 \rangle$ travelled by an ion between two reference planes depends on the number of jumps N the ion makes and the mean jump distance (l) is related by:

$$\langle x^2 \rangle = N l^2 \quad (48)$$

By introducing reference planes referred to as transit planes (Fick's 1st and 2nd laws) it is possible to determine the diffusion flux of ions (J) across the transit plane, ie. the net number of moles of ions crossing unit area of transit plane per second from left to right is given by

$$J = \frac{1}{2} \frac{\sqrt{\langle x^2 \rangle}}{t} (c_L - c_R) \quad (49)$$

where c_L is the concentration of ions to the left of the transit plane and c_R the concentration to the right of the

transit plane, t is the time in seconds to make the right (R), and left (L) crossing.

Equation (49) reveals that all that is required for diffusion is a difference in the number of particles per unit volume in two regions. The important point is that no special diffusive force acts on the particles in the direction of the flux.

The concentration gradient dc/dx in the left-to-right direction can be written

$$\frac{dc}{dx} = \frac{c_R - c_L}{\sqrt{\langle x^2 \rangle}} = \frac{c_L - c_R}{\sqrt{\langle x^2 \rangle}} \quad (50)$$

or

$$c_L - c_R = -\sqrt{\langle x^2 \rangle} \frac{dc}{dx} \quad (51)$$

This result for $c_L - c_R$ can be substituted in eq (50) to give

$$J = -\frac{1}{2} \frac{\langle x^2 \rangle}{t} \frac{dc}{dx} \quad (52)$$

and, by equating the coefficient of this equation with that of Fick's 1st law

$$J = -D \frac{dc}{dx} \quad (53)$$

one has

$$\frac{\langle x^2 \rangle}{2t} = D \quad (54)$$

$$\langle x^2 \rangle = 2 D t \quad (55)$$

Equation (55) is the Einstein-Smoluwchowsky equation, which provides a bridge between the microscopic view of random-walking ions and the coefficient D of the macroscopic Fick's law.

The characteristic of random walk in the Einstein-Smoluwchowsky equation is the appearance of the mean square distance (ie. square centimeters), and since this mean square distance is proportional to time (seconds), the proportionality constant D in equation (55) must have the dimensions of cm^2s^{-1} .

CHAPTER 3

3. PIEZO ELECTRIC TECHNIQUE AS ORIGINALLY DEvised⁽⁷⁰⁾

3.1 Introduction

The apparatus devised by Meadows et al⁽⁷⁰⁾ is capable of detecting and measuring small bubbles of gas present in a liquid environment to a sensitivity of 1nl. This technique has been used by him to determine hydrogen and oxygen evolution rates at different cathodically polarised electrodes in a variety of electrolyte solutions. These measurements reveal that in the early stages of electrolysis the gas evolution rates are not in general in accordance with Faraday's law and that the incremental evolution rates determined are multiples of one sixth of the expected theoretical values. This aspect of the work will be discussed subsequently.

3.2 Principle of the piezo electric technique

The piezo electric technique relies on two fundamental properties of a static fluid, ie.

1. The pressure in a static fluid is the same throughout the body of the fluid and is independent of the direction of measurement and
2. The compressibilities of liquids and gases differ markedly.

Thus it is possible to detect the presence of a small bubble of gas within the body of a liquid contained in a rigid

enclosure, by simply performing a static compressibility test. Since there is a large difference in compressibility between gases and liquids, a p-v plot performed on the system, with and without gas bubbles, provides a means of determining the gas volume. This is achieved by causing small fluctuations in the volume of a solution in a rigid vessel. Because this vessel is a rigid enclosure it is evident that the pressure will fluctuate with change in volume of gas.

In practice, a very satisfactory way of inducing volume fluctuations and measuring the pressure variations is to utilize the properties of piezo-electric materials, which either change their shape in an applied electric field or generate electric fields when pressure is applied⁽⁷⁰⁾.

3.3 Description of the original apparatus

The instrument devised by Meadows consists of a monitoring cell and a reaction cell. The monitoring cell is a thick-walled mild steel tube having a diameter of 5 cm, a wall thickness of 0.6 cm and a length of 10.5 cm and is provided with flanges at either end (see Figure 4). One end of the tube is sealed with a steel plate bolted to the flange; this steel plate has two glass taps for introducing a solution and two 0.3 cm diameter Cu tubes that support the piezo-electric transducers and carry the electrical connections. The other end of the steel tube is covered with a polyethylene membrane, which allows the pressure in the monitoring cell to be transmitted to the reaction cell.

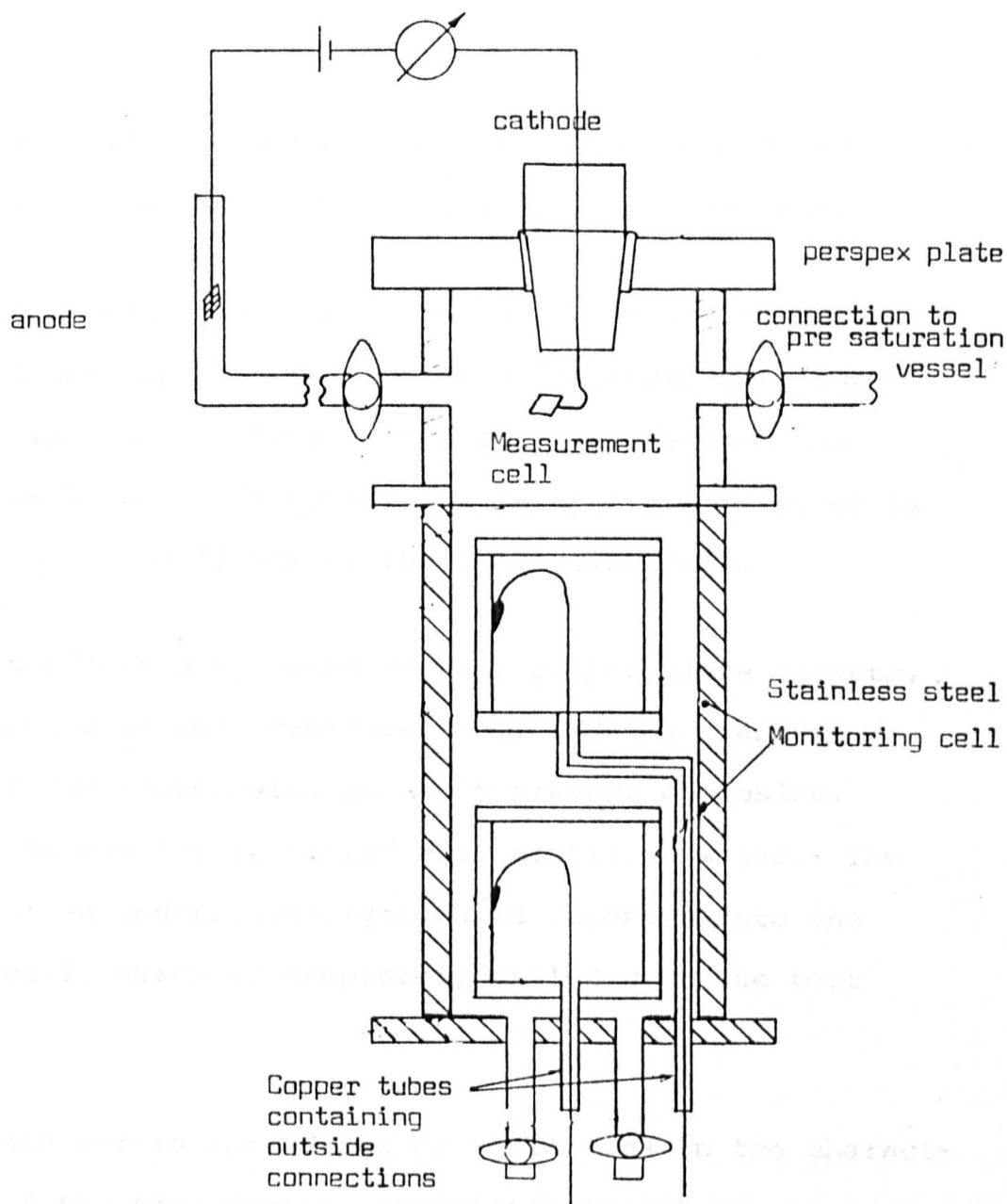


Fig. 4 General view of the piezo - electric system

The reaction cell is in turn clamped to the monitoring cell by brass threaded bolts to form a rigid structure.

The reaction cell is a glass tube (5 cm dia x 3 cm length) with two glass taps fixed into the wall opposite to one another. The end of the reaction cell remote from the membrane is blanked off by a thick Perspex plate, which is also bolted to the flange on the monitoring cell.

Sealing is effected by means of thin polyethylene gaskets, and the inside of the transducer cell and the transducers themselves are coated with paint to prevent corrosion.

This cell is completely filled with distilled water. The metal specimen under investigation is inserted into the reaction cell, which is completely filled with the test solution.

To eliminate errors introduced by variations in the characteristics of the transducers, oscillator amplitude, temperature, etc., two identical cells are used as a differential pair. In this arrangement, one transducer in each cell is energized by a stable oscillator at approximately 20 Hz.

These transducers are connected in opposition so that small differences in the characteristics of the transducers can be accommodated by adjusting the signal input to one of the energized transducers using a potentiometer. Alternatively, if a bubble of gas is already present in the reaction cell or has been deliberately injected, the dissolution of the bubble is signified by a change in the magnitude of the

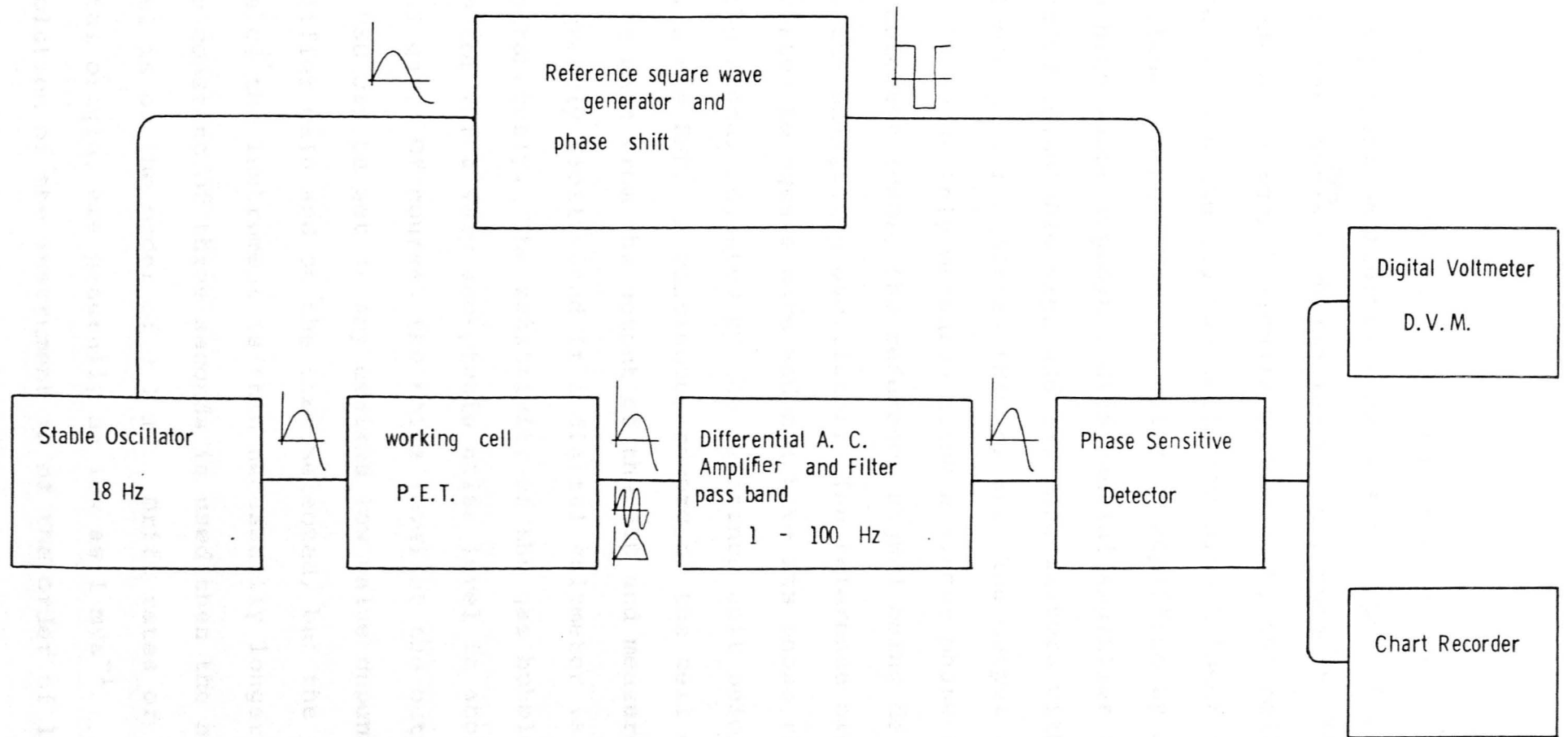


Fig. 5 Schematic diagram of Piezo- electric gas volume determination technique (P.E.T.)

output signal. The output of a pair of cells is much less dependent on fluctuations in the output of the oscillator, and ^{has} a much smaller noise component. This is because any external signals picked up by the cells cancel out, since the two cells are almost identical. The signal output from the cells is amplified by means of a high input impedance differential amplifier incorporating adjustable high and low pass filters with variable gain facilities (Figure 5). The output from this is accurately measured using a linear phase sensitive detector (PSD), the reference signal being derived from the energizing oscillator. The reference signal is converted to square wave and can have its phase relative to the signal adjusted by the reference unit before it enters the PSD. A continuous record of the cell output can be made from the output of the PSD and measurements are greatly facilitated if a digital voltmeter is used simultaneously. The sensitivity of the gas bubble detector for a very acceptable noise level is about $2V/\mu\text{l}$ gas. Of course, the noise level at the output of the PSD can be set at any desired low value depending on amplifier gain and on the time selected, but the response time of the instrument is then necessarily longer. If a time constant of three seconds is used then the noise level is of the order of ± 1 mV. Drift rates of instrumental origin, are generally as low as 1 mVs^{-1} . Thus the resolution of the instrument is of the order of 1 nl of gas.

3.4 Original method used to calibrate the PET

The instrument has been calibrated by injecting small bubbles of gas into a previously H₂-saturated solution using a precision syringe graduated in 0.01 μl. As would be expected from the functioning of the instrument, the voltage output is not linear with volume and the sensitivity diminishes as the bubble volume increases. A plot of volume (V) vs signal (S)^{-3/2} gives a straight line up to a volume of about 14 μl. This non-linearity is of particular importance, and in the present study a method has been devised for making the necessary corrections.

3.5 Experiments performed by Meadows

Meadows studied H evolution from cathodically polarised metal electrodes positioned inside the reaction cell (see Figure 4). This was achieved by means of a counter-electrode placed outside the cell in one of the side arms. To avoid diffusion of O₂ to the cathode, which could interfere with the cathode reaction, electrolytic continuity was achieved by the thin liquid film surrounding one of the two taps which divided the reaction cell from the anode compartment and which had to be closed during measurements. Faraday's Law states that the quantity of gas produced at an electrode is proportional to the amount of charge passed and this can be checked very simply by measuring

the volume of gas produced in a given time by the passage of a known constant current.

However, in practice this procedure is not very satisfactory because steady state conditions are not immediately achieved when the current is first switched on and there is always a short delay before gas evolution commences even though the electrolyte is H-saturated. Thus in Meadows work all measurements using the PET have been made by measuring the slope of the chart recorder trace.

The results obtained by Meadows have been presented in the form of current vs gas evolution rate curves, rather than as charge vs volume curves. Since the atmospheric pressure and temperature vary from day to day, it is necessary to reduce all the volumes measured to STP. Meadows considered that the best test of Faraday's law using the instrument would be by a number of measurements of gas evolution rates over a wide range of c.ds using a given electrolyte system. A graph of current vs gas evolution rate would then be a straight line whose slope would be a sensitive test of the validity of the law. Because Meadows did not determine the surface area of the electrodes used it is not possible to give relationships involving current densities.

3.6 Results and Discussion

Initially measurements made by Meadows were of the hydrogen and oxygen evolution rates from a smooth Pt electrode (wire 3 cm long and 0.2 mm dia) in 0.05M H₂SO₄ acid and in 0.1M NaOH solutions. In all cases it was found by Meadows that both the absolute volumes of gas collected for a given electrical charge and the incremental gas evolution rates were significantly less than those predicted by Faraday's law (Figures 6 to 8). As it is shown in graphs 6 to 8 the incremental evolution rates appear to be multiples of 1/6 of theoretical for most experiments performed. This is shown in Figure 6 where slopes of 4/6 and 1/6 were obtained initially before theoretical evolution occurred. Similar considerations apply to Figure 7 which was performed using the same conditions as those for Figure 6. The poor reproducibility of Meadows' results is evident in Figures 6 to 8.

Great efforts were made to ensure that the discrepancies observed were not simply a result of a rapid dissolution of the evolved gas in the electrolyte. Meadows stated that gas dissolution could be discounted since a small bubble of the appropriate gas injected into the gas-saturated solution in the reaction cell by a calibrated syringe did not change in size.

This operation was used by Meadows to confirm that the electrolyte was completely saturated with H and to calibrate the instrument. Subsequent experiments have shown a number of discrepancies, and it has been established that

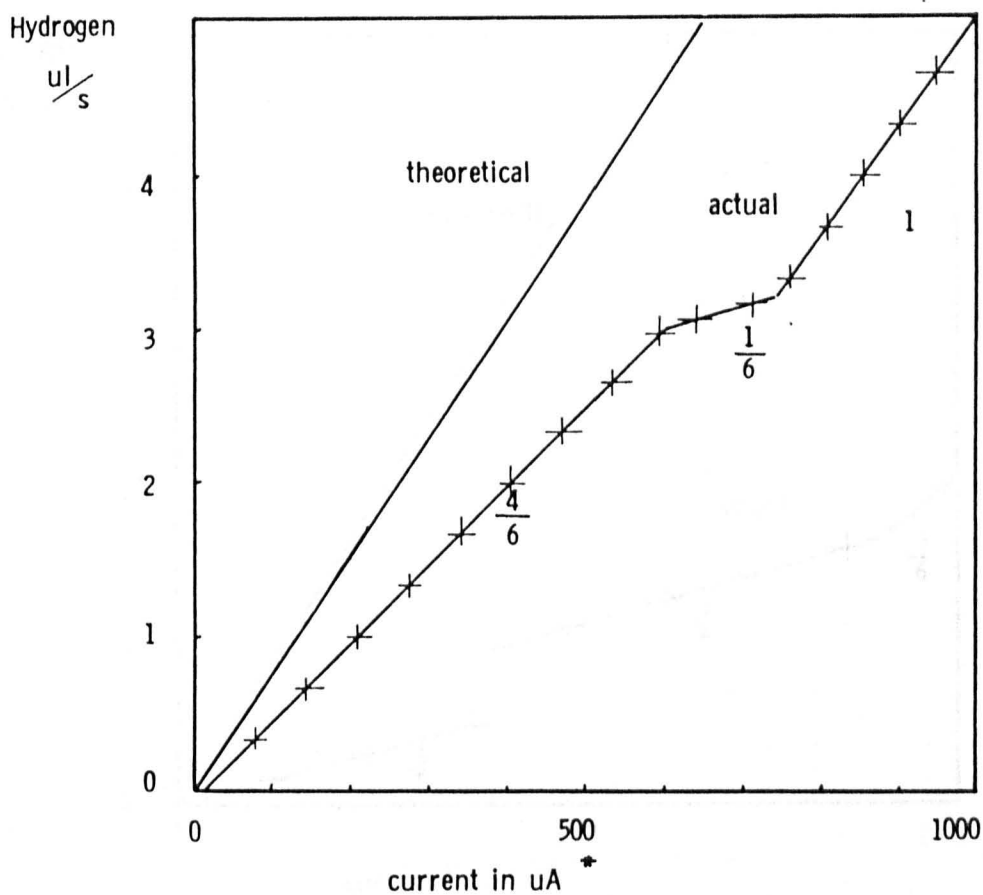


Fig. 6

Hydrogen evolution on a Pt - cathode in 0.05 M H_2SO_4

as performed by Meadows

* Since Meadows took no account of the area of the electrode it is not possible to give the results in $\mu\text{A}/\text{cm}^2$

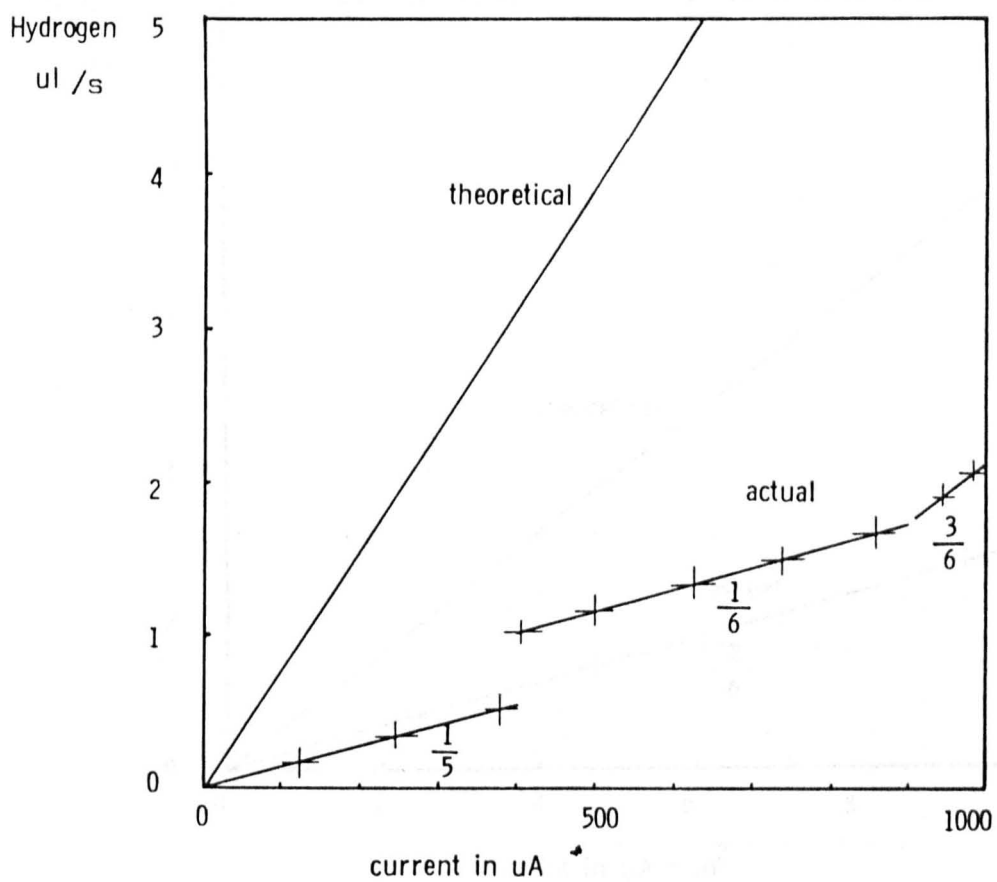


Fig. 7

Hydrogen evolution on a Pt - cathode in 0.05 M H_2SO_4 as performed by Meadows

* see footnote Fig. 6

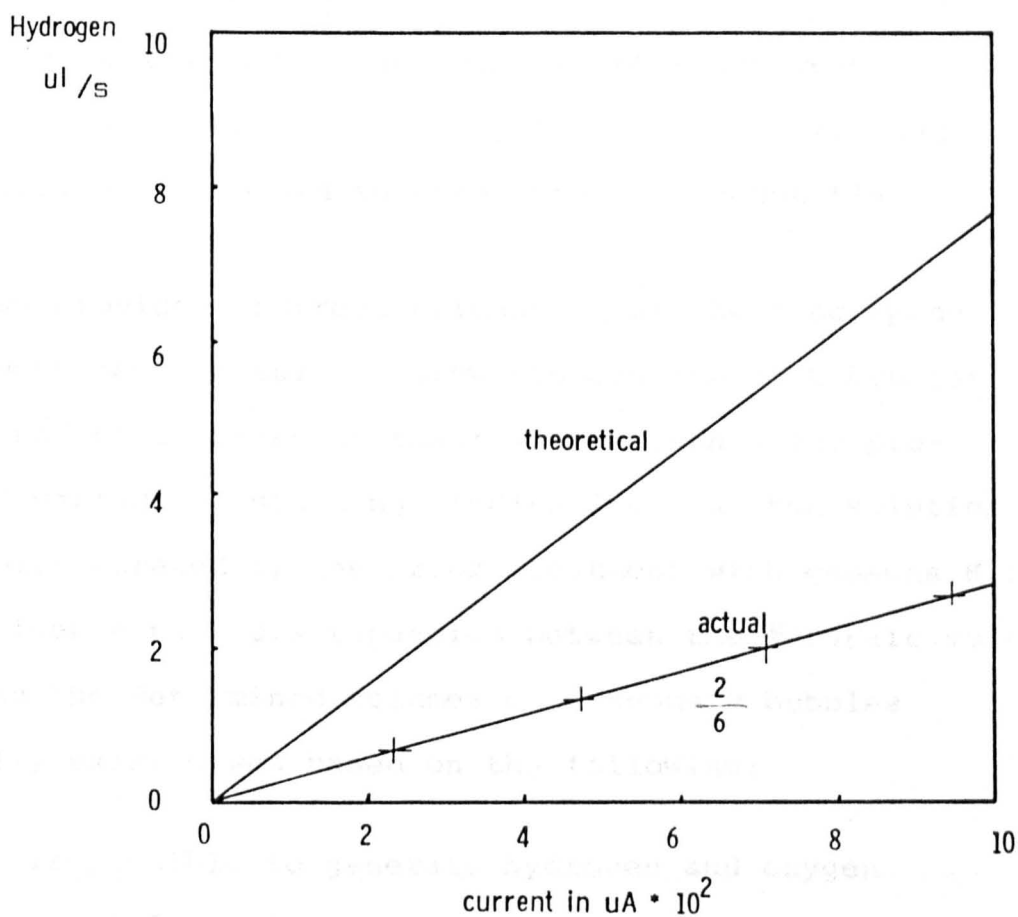


Fig. 8

Hydrogen evolution on a Pt - cathode in 0.05 M H_2SO_4
as performed by Meadows

see footnote Fig. 6

the rate of dissolution of H appears to be related to bubble size and that large bubbles are relatively stable in solutions that are by no means H -saturated. This will be discussed in more detail subsequently.

Meadows provided indirect evidence that the discrepancies were not a result of slow dissolution of H bubbles, and found no decrease in their volume even after prolonged periods of standing, indicating that the solution had been saturated by the prior treatment with gaseous H . The evidence that discrepancies between the Faradaic volume and the determined volumes of gaseous H bubbles actually existed was based on the following:

1. It is possible to generate hydrogen and oxygen at exact faradaic rates provided this takes place at the tip of a very small wire electrode, ie. at very high current densities.
2. The incremental gas evolution rates (ie. the slopes of the graphs of current against evolution rate) appear to have a limited number of discrete values which are multiples of one sixth ($1/6$) of the theoretical rates.

Incremental rates of $1/6$, $2/6$, $3/6$, $4/6$, $5/6$ of the theoretical rates as calculated from Faraday's Law were observed by Meadows during a variety of measurements. These slopes were considered to be a positive indication of a hitherto undiscovered mechanism of ionic discharge and that Faraday's

Law is not valid under these circumstances (see above). In all cases these fractions eventually disappeared, and the curve corresponded to the theoretical.

Meadows made many measurements of hydrogen and oxygen evolution rates in solutions of H_2SO_4 , $NaOH$ and Na_2SO_4 using other electrodes including copper and carbon. In all cases he found, at least during the early stages of electrolysis that the hydrogen and oxygen evolution rates were lower than predicted by theory and that the incremental rates appear only as multiples of one sixth the theoretical value. Meadows argued that it is difficult to see how the simple principle of pairing electrons and ions during an electrochemical reaction, which is Faraday's Law, is operating under the conditions described above, and his theories may be summarized as follows.

The discrepancies from theoretical can only be satisfactorily explained if the electrode reaction proceeds by transfer of packets of charge containing six electrons. This effect must be related to the structure of the solvent water, in some way, although as yet there is no evidence to suggest a particular model. Solubility measurements performed indicated that the hydrogen which fails to appear in the gas phase is actually present in the electrolyte, but probably in a bound form as individual neutral hydrogen atoms, i.e. in a form quite different from that of the dissolved molecular hydrogen. The deficiency of oxygen at the anode cannot be explained in an analogous manner unless a

particularly stable oxygen clathrate is formed. The most likely alternative anode reaction is thus the formation of hydrogen peroxide or possibly a stable ozone compound.

Meadows determined the quantitative difference between a solution charged to saturation with H₂ gas produced by electrolysis and by bubbling H₂ - gas from a cylinder through a non-saturated solution. Both solutions were then heated and the volume of H₂ gas evolved was measured. It was found that solutions in which hydrogen had been cathodically evolved at a Pt electrode contained roughly double the quantity of extractable hydrogen compared with a solution of the same composition that had been saturated with molecular hydrogen from a cylinder of the compressed gas. These measurements indicated that in the former case some new compounds were being formed. Since these discrepancies of the hydrogen and oxygen evolution rates were observed in acid, neutral and alkaline solutions over a wide range of concentrations and with a variety of electrode materials including platinum, copper and carbon it seemed to provide evidence that the observations were of a fundamental nature. Moreover, the observed slopes were related to the Faradaic values by factors of $n/6$, where n is an integer, which suggested that the structure of the solution was involved in some way and that the discharge process requires the participation of electrons and ions.

The views put forward by Meadows to explain the departures

from Faraday's law seemed to be very revolutionary in comparison with the obvious and more simple view that they were simply due to solubility of H in the metal electrode. If the latter is correct it means that the method might be used for determining H solubility in metals and possibly diffusion coefficients. This has proved to be the case, and the PET has provided a means of studying H solubility in a number of metals which have been regarded as having no ability to dissolve H.

Some of the results obtained in this investigation are more detailed than those which are given in the present Chapter.

The results reported in this chapter are those of H₂ and H₂O₂ evolved in the present investigation, (figure 10) but in order to evaluate the solubility of carbonic acid in metal electrodes with accuracy mathematical modifications had to be made to the basic theory of calculating the quantities of gas evolved. Modifications to the experimental technique were also found to be necessary.

4.4 Design of the charging cell

The charging or reaction cell (Figure 9) is a thick walled 1/8 inch glass tube of diameter about 40 mm. One end of the tube is sealed with a thick perspex plate E and polyethylene gasket, in the centre of which is inserted a ground glass joint A (Quickfit 24/29), through which the electrode holder B is introduced into the cell. Two teflon tape F' and F'' of 3 mm bore are connected to the cell at

CHAPTER 4

4. EXPERIMENTAL

4.1 Introduction

The aim of this study was to investigate the absorption of cathodic hydrogen into various metals, particularly Al and its alloys and Ti using the piezo-electric-technique. Other methods of measuring hydrogen in metals, which have been described in various publications, will be discussed in a later Chapter. Although certain aspects of the experimental procedure have been discussed briefly in Chapter 3 a more detailed description will be given in the present Chapter.

The P.E.T apparatus as devised by Meadows and Shreir⁽⁷⁰⁾ was used in the present investigation, (Figure 10), but in order to evaluate the solubility of cathodic H in metal electrodes with accuracy substantial modifications had to be made to the basic theory of calculating the quantities of gas evolved. Modifications to the experimental technique were also found to be necessary.

4.2 Design of the charging cell

The charging or reaction cell (Figure 9) is a thick walled (8 mm) glass tube S of diameter about 40 mm. One end of the tube is sealed with a thick perspex plate E and polyethylene gasket, in the centre of which is inserted a ground glass joint B (Quickfit 24/29), through which the electrode holder H is introduced into the cell. Two teflon taps F' and F'' of 8 mm bore are connected to the cell at

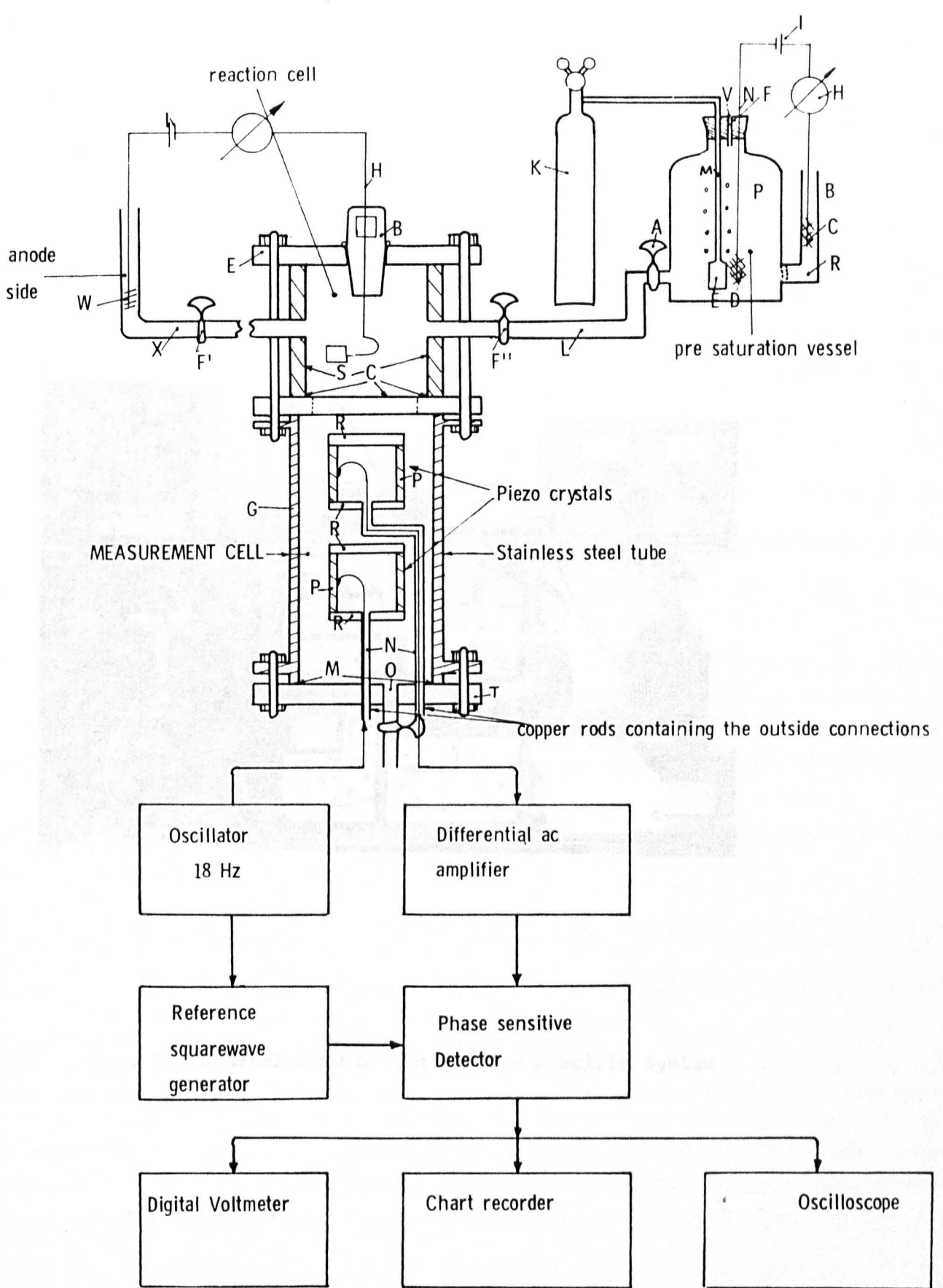
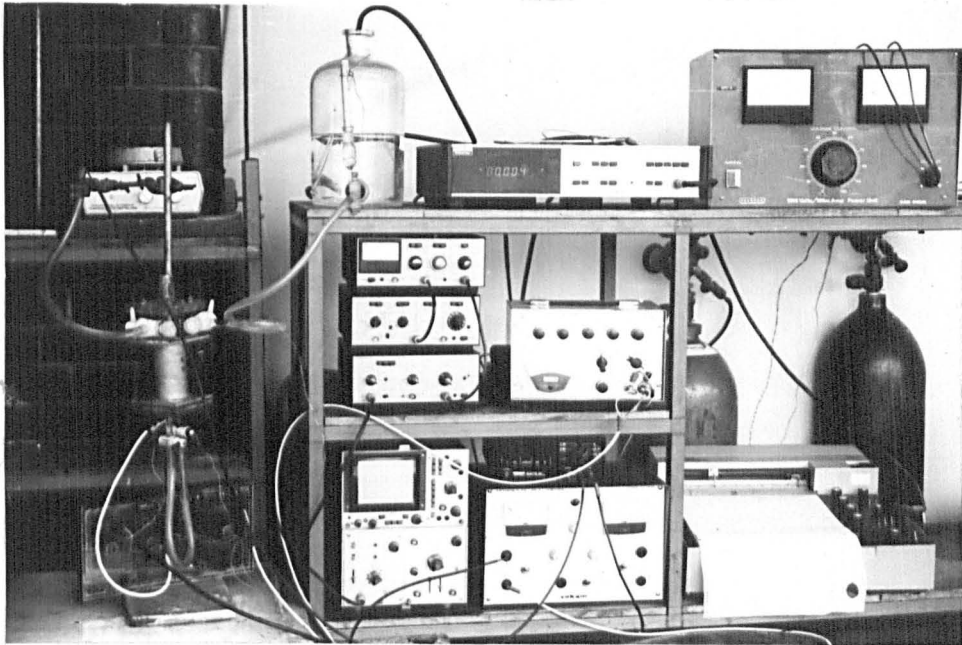


Fig. 9

General view of the piezo electric system



The monitoring cell is a thick walled stainless-steel tube with a flange F at the lower end; the dimensions of this cell are governed by the size of the piezo-electric crystals P contained in the cell and the two different sizes of cells used.

Fig. 10 General view of the piezo - electric system

	Original Design	Modified Design
Wall thickness	0.5 mm	0.5 mm
Diameter	45.0 mm	75.0 mm

Holes were drilled through each of the flanges to connect the nuts and bolts to the reaction cell and the lower flange F, which is a stainless steel plate clamped to the cell tube by means of stainless steel nuts and bolts. A seal is

right-angles. This cell is clamped to the stainless steel monitoring cell G by means of long brass bolts and nuts, and a circular sheet of thin polyethylene C is used as a diaphragm to separate the solution in the glass charging cell from that in the monitoring cell. This gasket also prevents leakage of the solutions in the reaction and monitoring cells.

The interior of the reaction cell must be observed before the experiment to detect and remove any gas bubbles adhering to the cell wall; this is essential since if they are allowed to remain they could introduce errors into the voltage output.

4.3 The monitoring cell

The monitoring cell is a thick walled stainless-steel tube G with a flange T at the lower end; the dimensions of this cell are governed by the size of the piezo-electric crystals P contained in the cell and the two different sizes of cells used had the following dimensions:

	Original Design	Modified Design
Wall thickness	0.5 mm	0.5 mm
Diameter	45.0 mm	75.0 mm

Holes were drilled through each of the flanges to connect the nuts and bolts to the reaction cell and the lower flange T, which is a stainless steel plate clamped to the cell tube by means of stainless steel nuts and bolts. A seal is

effected by a polyethylene ring M situated between the bottom plate and the cell tube.

Cemented into the lower flange are two teflon taps O which have the same function as in the reaction cell. Two copper tubes N are brazed onto the lower flange and these support two piezo-electric crystals are mounted on two steel plates R of the same diameter as the crystals, which are attached to the top of the two copper tubes with Araldite. The piezo crystals P are cylindrical in shape and are situated one above the other, as can be seen in Figure 9, and are sealed on top with a second steel plate attached using Araldite. The exteriors of the piezo crystals, the cover plates and the copper tubes are coated with an electrically conductive silver paint by means of which the copper tubes which pass through the bottom of the cell may be earthed. The piezo crystals were specific-purpose transducers used in such applications as echo sounding equipment, hydrophones and pressure gauges. They were supplied by Vernitron Limited (PZT-5A tubes Part No BSP 10009) and the types used had the following dimensions:

<u>Table 1</u>	<u>Dimensions of piezo-crystals</u>	
<u>Dimension</u>	<u>Size (a)</u>	<u>Size (b)</u>
outside diameter	25.40 mm	50.80 mm
length	25.40 mm	50.80 mm
wall thickness	3.18 mm	5.08 mm

These crystals are a modified lead-zirconate-titanate (Vernitron Limited Bulletin 66 OH/F January 1976), which provide

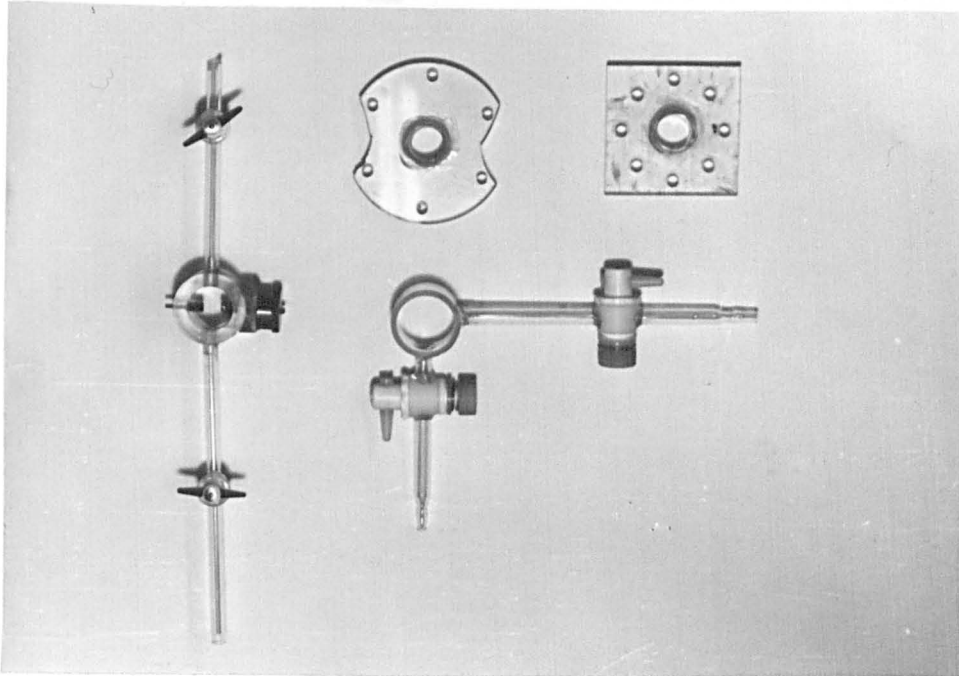
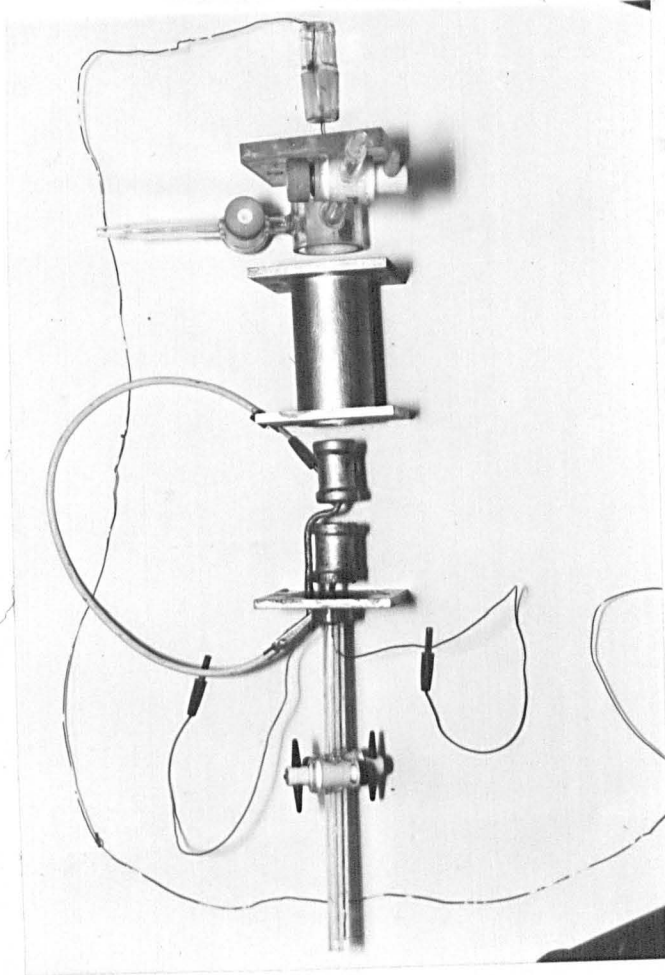


Fig. 11 Different types of reaction cells

Fig. 12

View of photo - electric - cell



Electrode

Perspex top

Reaction - cell

Monitoring - cell

Stainless-steel tube

Piezo-electric-crystals

Stainless-steel bottom

Fig. 11 Different types of piezo - electric cells in present use

Fig. 12

View of piezo - electric - cell

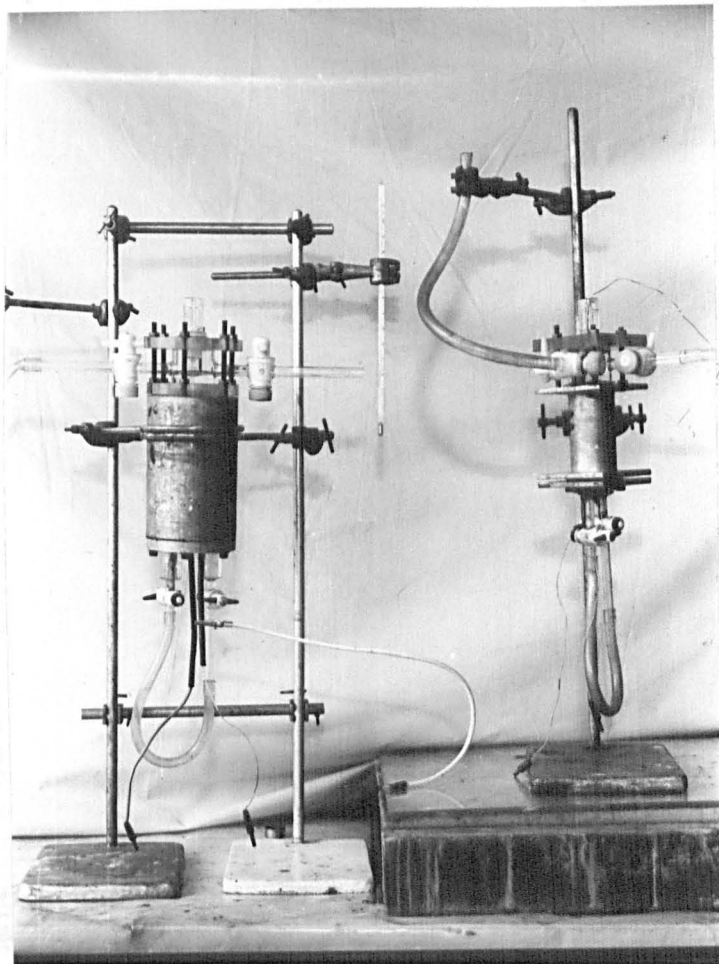


Fig. 13 Different types of piezo - electric cells in present use

a transducer element with a high electro-mechanical coupling coefficient and high charge sensitivity. They have a high curie temperature of above 350°C , which indicates that at ambient temperatures they are very sensitive to small pressure differences within the basic cell.

The monitoring cell was completely filled with de-aerated distilled water, while the reaction vessel could be filled with a variety of hydrogen-charging solutions ranging from acid to alkaline. Entry of the solution into the reaction vessel was effected via the tap F" (Figure 9), whilst the distilled water was introduced into the monitoring cell via the taps O. Fig's 11 - 13 show photographs of the experimental setup.

4.4 Electrodes used for volumetric determination of cathodic hydrogen

For most experiments the metal electrode was in the form of foil of thicknesses ranging from 0.001 to 0.3 mm and of constant dimensions of 5 x 10 mm. These electrodes were mounted in a Quickfit stopper (B) which can be inserted tightly into the top perspex plate of the cell. This wire was glued into the holes using Araldite resin. The copper-wire and the welding point which sits on a small neck at the top of the electrode was covered with 'Lacomite' lacquer for insulation. The current density at the electrode was maintained at 1 mA/cm^2 .

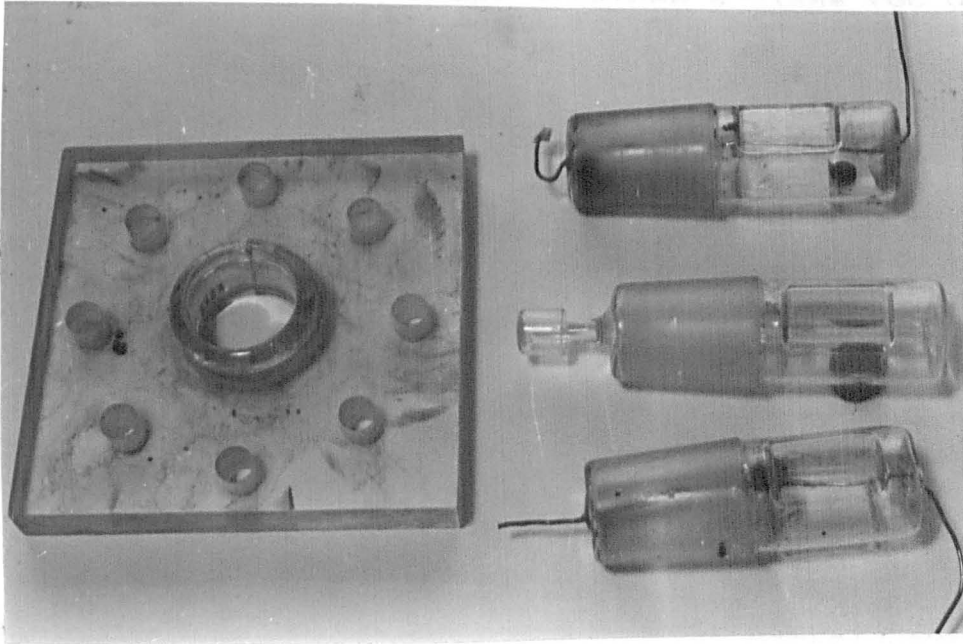


Fig. 14 Different types of electrodes used in the piezo - electric technique

Hydrogen evolution at very low rates was determined using powder metals immersed in various acid and alkaline solution without an external source of e.m.f. For this purpose a Quickfit glass stopper was used to the bottom of which was attached a glass rod of 5 mm diameter and 20 mm length. This glass rod acted as a support for a small circular glass container, as shown in Figure 14 . The powder metal was weighed and then introduced into the glass container, which was then placed into the reaction cell.

4.5 Calibration of Electrode for determination of Faradaic hydrogen evolution.

The electrode used for calibration was produced by immersing a Cu wire in Hg for several hours. The electrode was charged at a constant current of 1 mA. Under these circumstances a single bubble of H was formed, which had a smaller tendency to dissolve in the solution than a number of very small bubbles. This was necessary in case the solution had not been completely saturated with H prior to its introduction into the cell. This point electrode of mercury/copper amalgam does not absorb any hydrogen so that the rate of evolution of H gas bubbles conform with Faraday's law. It was used to produce a calibration curve by means of which the absorption of H by other electrodes could be established. A

more detailed review of the experimental procedure will be given subsequently.

4.6 Electrodes used as anodes.

Platinum in the form of wire or mesh was used for the anode (W in Figure 9), which was situated within the silicone-rubber tube attached to one of the side-arms (F'). This tube is completely filled with the electrolyte and electrical connection between anode and cathode was achieved by the thin electrolyte film around tap F' in the side-arm X. This was necessary to prevent oxygen diffusion from the anode to the cathode, which would interfere with the hydrogen evolution reaction at the cathode. Silicone rubber was chosen because of its low sulphur content, since it is well known that S or S-compounds are promoters for H absorption. The transparency of the rubber provided a means of ensuring that the anode was immersed in the charging electrolyte.

4.7 The pre-saturation vessel

To prevent dissolution of hydrogen gas in the solution and consequent errors in the determination of the volume of H evolved for a given amount of charge it was essential to de-aerate the electrolyte and to saturate it with H. This was done in the pre-saturation vessel (Figure 9), which was connected to the reaction cell by a silicone rubber tube (L).

This direct connection was made to prevent any losses of hydrogen from solution and to prevent any oxygen diffusing into the solution. The H pre-saturation vessel (P) was a 5l glass container with two outlets. The outlet tap A has a silicon-rubber tube (L) which is connected to the reaction cell. Another outlet R is to the anode compartment (B) which is connected to the vessel via a glass frit.

The anode compartment is a bent glass tube open to the atmosphere, which contains a platinum gauze (C) welded to a platinum wire that is connected to a constant current power source (I). The cathode (D) in the glass container is connected to a Pt wire (N). This wire leads to an insulated Cu lead through a stopper (F) to the power source. A milliammeter (H) is connected between anode and cathode to measure the current flow.

A supplementary method of sparging the solution with hydrogen gas is achieved by means of a glass frit (E) which is connected to a glass tube (M) and leads through the stopper (F) to a hydrogen gas cylinder (K). To prevent pressure build up within the glass vessel a small glass tube (V) of 5 mm diameter is incorporated into the stopper.

The general procedure of charging was to sparge the solution with hydrogen gas from the gas cylinder for 15 min and then to further hydrogenate it by means of

of hydrogen evolved from a Pt mesh cathode. This was allowed to continue for at least 4 h using a current of 2 mA. The electrolyte was then introduced into the reaction cell.

Before every experiment, the P.E.T cell was tested to see if the electrolyte was completely saturated with hydrogen gas (see Chapter 5). A fresh solution was introduced into the reaction cell prior to each experiment.

4.8 The Noise Filter System (Figure 9)

The electronic noise filter system amplifies the signals which are emitted by the piezo-electric crystal and cancels out any signal which is not a direct response to bubble growth within the reaction cell. This is achieved by using several filters and an amplifier. The general procedure of measuring the volume of H bubbles with the piezo-electric cell is as follows. One of the two piezo-electric crystals (Figure 9) in the cell G is activated with a 18 Hz signal generated by a stable oscillator (Brookdeal A-level transistor decade oscillator, type ta 66A). This a.c pulse will cause an increase in the size of one of the piezo crystals, which leads to a pressure build up within the closed system. The pressure is measured by the second piezo crystal, which responds by transforming this pressure build-up into an electrical signal. This signal is then introduced into a differential a.c amplifier (Ortel Brookdeal, type 9454). The signal is

amplified and all frequencies below 10 and above 100 Hz are cancelled out. The signal is also introduced into a Reference Unit (Ortec Brookdeal, type 9422) in which the sinusoidal wave is then shifted 90° , which is necessary in order that both waves are in phase, since the 2nd piezo-electric crystal lags the first by 90° . Both signals are then introduced into a phase sensitive detector which compares both signals and filters out all frequencies which are not 18 Hz. This procedure has to be performed because of the high sensitivity of the piezo-electric material, towards outside noises, eg. vibration of the building caused by passing traffic and fluctuation within the main signal which interferes with the measurement.

The reference unit and the P.S.D are monitored by a two channel oscilloscope (Telequipment). The filtered signal is fed into a digital voltmeter (Solatron A 223) and a chart recorder (Bryant Southern Instruments Type 28000, two pen recorder), If a bubble appears either within the monitoring cell or in the reaction cell, the coupling of both piezo-crystals will be influenced by the ease of compression of the bubble in comparison with that of the thick walled ceramic material of the piezo-electric-crystal. This effect is shown on the chart recorder as a decrease in the e.m.f output (referred to as 'voltage output').

Tests were carried out at different frequencies and different voltage, and consequently fluctuations in pressure, to determine their effect on the rate of hydrogen absorption into a metal foil and it was shown that these had little

effect. This can be explained by the fact that although the frequency varies the mean pressure at the sinusoidal wave is always zero.

4.9 Reproducibility

Over 100 experiments were carried out at different c.ds with the non-absorbing Hg-Cu electrode to establish reproducibility, and in general the variation between 3-4 specimens tested under identical conditions was $\sim \pm 1\%$.

In the case of metals and alloys that absorbed H about 16 experiments were carried out for each condition of charging and the agreement between the emf vs time curves produced on the chart recorder normally agreed within the range ± 2 to $\pm 5\%$, but poorer reproducibility was observed in certain parts of the curves for Ti metal and Al-Mg alloys that formed metal hydrides.

CHAPTER 5

5. CALIBRATION OF THE PIEZO-ELECTRIC-CELL (P.E.T)

In order to relate the voltage read-out produced by the piezo-electric crystals to the volume of hydrogen bubbles present in the solution it is essential to calibrate the cell by introducing hydrogen by means of cathodic charging or by the injection of a known amount of H-gas into the measuring compartment of the P.E.T cell. Calibration has been carried out using both methods.

5.1 Calibration of the readout on a digital voltmeter(DVM)

A pre-determined volume of hydrogen gas, saturated with water vapour by bubbling it through an outside container filled with 0.05M H_2SO_4 , was introduced into the measuring compartment of the P.E.T cell by means of a calibrated hypodermic syringe (Hamilton, Schweiz). Prior saturation of the hydrogen gas with water vapour using 0.05M H_2SO_4 was necessary to prevent the increase in bubble size that occurred when a sample of the dry gas was introduced into the charging solution in the cell. The change in output voltage was monitored with a digital voltmeter (DVM) and related to the volume injected. A more convenient way of introducing hydrogen into the cell is to cathodically charge a metal electrode within the cell and plot the DVM readout vs time.

It can be seen from Figure 15 that the relationship is not

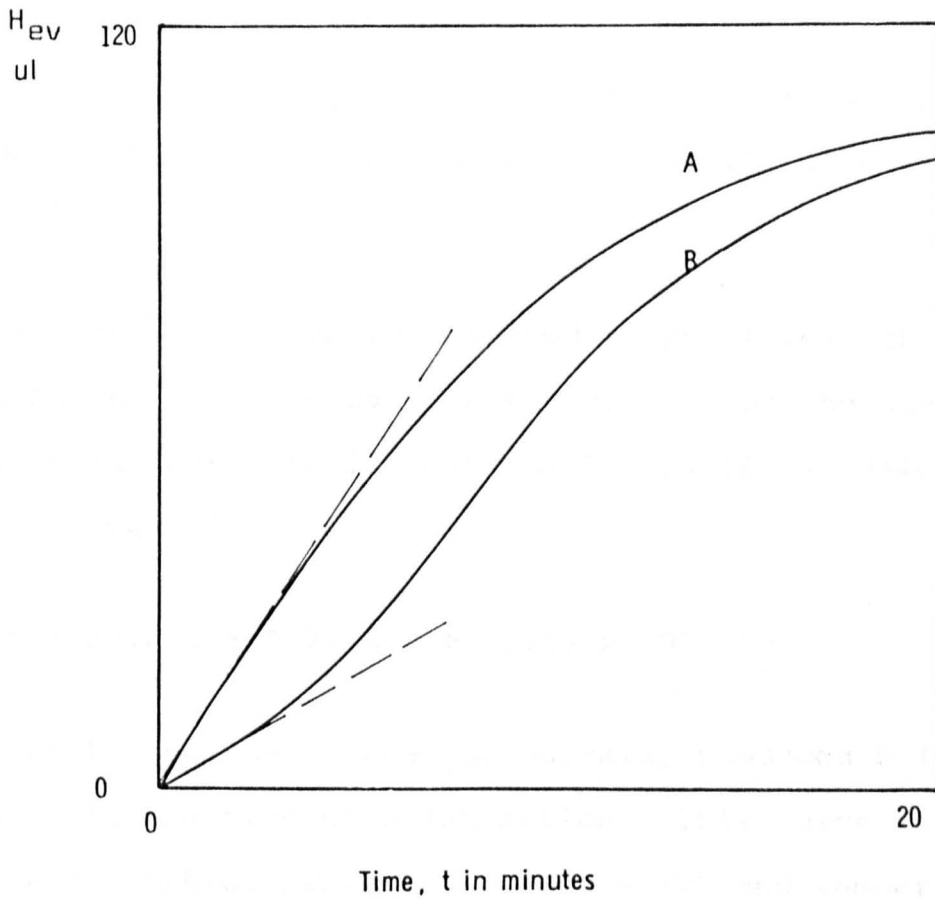


Fig. 15

- A ▪ Calibration curve
- B ▪ Curve obtained by a metal electrode which does absorb hydrogen (schematic)

linear throughout and that the sensitivity decreases (as shown in H slope of the curve) with an increase in the total volume of H .

The linear region, which is confined to small volumes of gas, increase from 5 to 25 μ l with the size of the piezo-crystals used in the cell. Curve A in Figure 15 follows the general equation

$$Y = 22.2 t - 0.37 t^2 + 3.19 \times 10^{-4} t^3 \quad (59)$$

where Y is the volume of the cathodically produced H in μ l, and t is the time of polarisation. This curve is highly reproducible, providing pressure (P) and temperature (T) are kept reasonably constant. This can easily be shown using the general gas equation

$$p \times V = n \times R \times T \quad (60)$$

This method of calibration is more convenient than gas injection. The anode which must be located outside the cell, is connected electrolytically to the cathode via a thin liquid film surrounding one of the taps that connects the anode and cathode compartments.

5.2 Experiment to determine H-saturation 0.05M H₂SO₄

According to Meadows more cathodic H is required to saturate the acid solution than gaseous H introduced from a cylinder. It was essential to check this using a cell

specially designed for this purpose, and preliminary experiments were carried out to see if electrolytic hydrogen was more or less effective than hydrogen gas for saturating the solution with H.

The cell consisted of a glass container of 250 ml volume and H from a cylinder was passed into the cell by means of a glass tube with a glass frit. Attached to the side of the cell was a glass capillary calibrated in 0.1 ml and having a total volume of 10 ml. The electrolyte was maintained at a constant temperature of $293 \pm 0.1\text{K}$, by the means of a thermostatically controlled water bath.

5.3 Experimental Procedure

The 0.05M H_2SO_4 inside the cell was saturated with hydrogen by one of two different methods. Hydrogen gas was passed into the cell by the means of the glass frit, which was connected to a hydrogen gas cylinder, for various periods of time, ie. 15, 30, 60, 120 and 300 min. In each case after sparging the solution with hydrogen gas for a pre-determined interval of time, all outside connections of the cell were closed and the tap connecting the cell to the capillary was taken as zero reading. The temperature of the water bath was then increased to 333K, and since the solubility of hydrogen decreases with temperature H gas was evolved and this was monitored by the changes in solution level in the capillary. When the level of solution in the capillary reached a constant value it was assumed that the solution was saturated at 333 K.

The second method of saturating the electrolyte was by means of cathodic H produced within the cell by cathodically polarizing the Pt mesh electrode (area not determined) at currents of 1mA, 5mA, 10mA and 20mA, for the same time periods and at the same temperature as that used for charging with gaseous H. The method of measuring the volume of H at saturation was the same as that described above for saturation of the acid with H from a cylinder.

5.4 Results

The results are given in Figure 16 in which curve 1 represents the volume change for 0.05M H₂SO₄ in which no H has been introduced.

As it can be seen from Figure 16 that, although the curves for volume increase vs time, have different slopes, the curve for cathodic charging at the highest current having the greatest slope, they all attain the same constant value.

Because of the smaller bubble size of cathodically produced hydrogen the time required to reach saturation is less than with gaseous H taken from a cylinder. The time for saturation decreases with increase in c.d, since it was observed that increase in current reduced bubble size, until at and above a critical current(10mA) the time to reach saturation became constant. This

Vol increase
mL

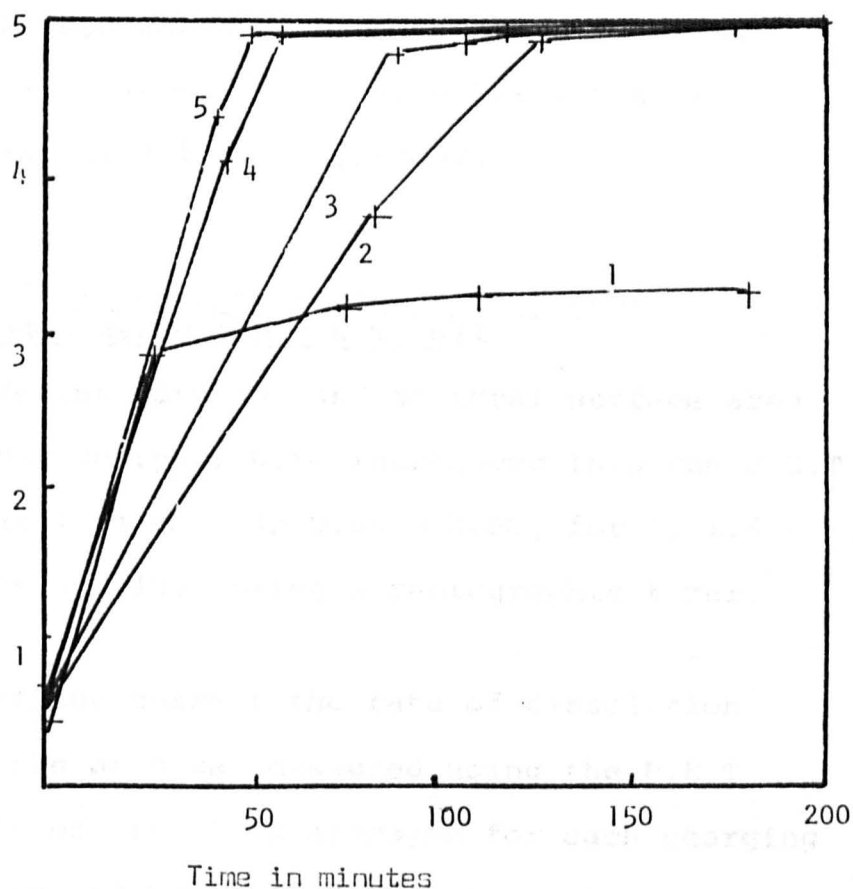


Fig. 16 Hydrogen solubility in 0.05 M H_2SO_4 by charging cathodically at different c. ds. and comparing the results with those obtained by charging the solution with purified H_2 gas from the cylinder.

1 = volume increase due to temperature rise of the solution in the absence of H

2 = charging with purified H_2 gas

3 = charging cathodically at 1 mA

4 = charging cathodically at 2 mA

5 = charging cathodically at 20 mA

leads to the conclusion that the total amount of hydrogen gas dissolved at saturation is the same irrespective of the method of charging, which does not confirm the view expressed by Meadows that electrolytic H has a higher solubility than gaseous H from a cylinder.

5.5 Dissolution of cathodic hydrogen at different metal electrodes using the P.E.T cell

Electrodes of different material and of total surface area of 1 cm^2 (both sides charged) were introduced into the P.E.T cell and charged at 1 mA cm^{-2} in $0.05 \text{ M H}_2\text{SO}_4$ for 1, 1.5, 3, 4, 6, 12, 15, 16 and 18s using a photographic timer.

After switching off the current the rate of dissolution of the bubbles in the acid was measured using the P.E.T. The total amount of dissolved hydrogen for each charging time was then determined by the P.E.T during a total period of 200 s. The results were expressed as volume of H after a predetermined time of charging from which is subtracted the small amount of H remaining after 200 s. The results have been expressed as percentage of H gas dissolved after 200 s vs total gas volume.

Figure 17 shows that the rate of dissolution of H decreased with the total volume of H, and confirms previous assumptions that the rate decreases with increase in bubble volume, which is of course a function of bubble diameter. Comparing both curves it can be seen that the rate of

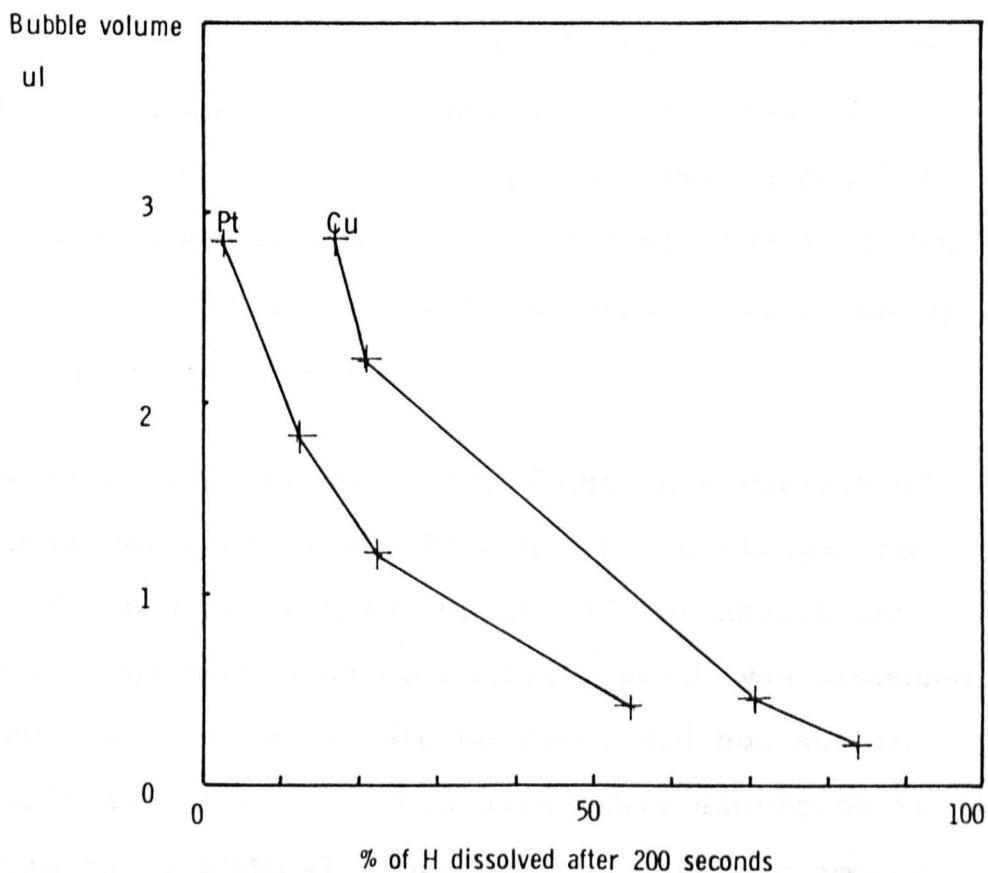


Fig. 17

Dissolution of H in Pt and Cu and in a H_2SO_4 solution showing how this depends on bubble size.

dissolution of H gas evolved at Pt is greater than that evolved at a Cu electrode even though the shape of both graphs is the same. Because they were both charged under the same conditions of c.d., pressure, temperature and using the same solution, it is evident that this can only be due to different absorption rates of hydrogen by the metal electrode itself.

This type of experiment was carried out on a variety of metal electrodes such as Au, Ti and a Hg/Cu amalgam to find out if there was a metal which did not absorb any H. It was found that a Hg/Cu amalgam, which was produced by dipping a Cu electrode into mercury, did not absorb a detectable amount of H. Thus using this electrode it is possible to cathodically produce the Faradaic amount of hydrogen gas, whereas with all other metals the volume H was below the Faradaic volume.

The Hg/Cu alloy was chosen therefore as a calibration electrode to determine the relationship between volume of H gas and output e.m.f produced by the P.E.T.

5.6 Calculation of the amount of hydrogen absorbed by different metals

In order to calculate the amount of hydrogen gas absorbed by different metals the following procedure has been adopted.

Using the copper/mercury electrode it is possible to obtain the theoretical readout, and from the charge passed it is

possible to relate the voltage readout of the D.V.M to the volume of gas produced on the surface of the metal. This can be regarded as a reference curve. From the differences between the curves obtained using metals which do absorb hydrogen and the reference curve it is possible to calculate the exact amount of hydrogen gas which is absorbed in a particular metal.

5.7 Calculation

The Cu amalgam electrode provides a means of obtaining Faradaic H evolution, and from the charge passed it is possible to relate the voltage readout of the D.V.M (digital voltmeter) to the volume of hydrogen gas produced on the surface of the electrode. This may be regarded as the reference curve giving the Faradaic or theoretical evolution of H, but there are a number of complications. Thus account must be taken of the fact that neither this curve nor those obtained with a H-absorbing electrode are linear owing to the decrease in the sensitivity of the piezo crystals as the volume of H in the cell increases. Thus calculation of the absorbed hydrogen is only possible by comparing the values of the e.m.f as given on the y-axis of the chart recorder at different time intervals. The x-axis of the readout is the time (in seconds) of cathodic polarisation of the electrode, which can be converted into μl H gas by combining Faraday's law with the gas law. (In order to convert

pressure in torr (mm of Hg) to Nm^{-2} the factor 1.013×10^5 has been used.)

The voltage readout is set so that it is a maximum of 10 V when no hydrogen bubbles are present, and by using the reference curve it is apparent that this can be expressed in μl of H gas, even though the relationship between voltage readout and time is non-linear.

In order to calculate the volume of H absorbed by a metal (eg. Ti or Al) it is necessary to consider both the calibration curve for a non-absorbing electrode (curve A in Figure 18) and the absorption curve (curve B) for which the volume of H measured is normally less than that of the calibration curve owing to absorption of H by the metal. Curve A, the calibration curve is determined by measuring the readout using a non-absorbing electrode for times of 1, 2 and 3 seconds. In order to determine the volume of H gas evolved (less than that for curve A) at an absorbing electrode the readout is measured after a time that gives 1 μl H gas evolved at a non-absorbing electrode, which corresponds to ac of Figure 18. It follows by simple proportion that the H actually evolved is $ab/ac \times 1 \mu\text{l}$. Similar considerations apply to the other incremental steps in time, but it should be noted that each calculation of the H actually evolved must be based on a voltage readout of similar magnitude to that on the calibration curve. Thus for calculating the H evolved corresponding to point b_1 the ratio will be $b_1b_1/ac \times 1 \mu\text{l}$; for point b_2 the value will be $b_1b_2/cc_1 \times 1 \mu\text{l}$, etc.

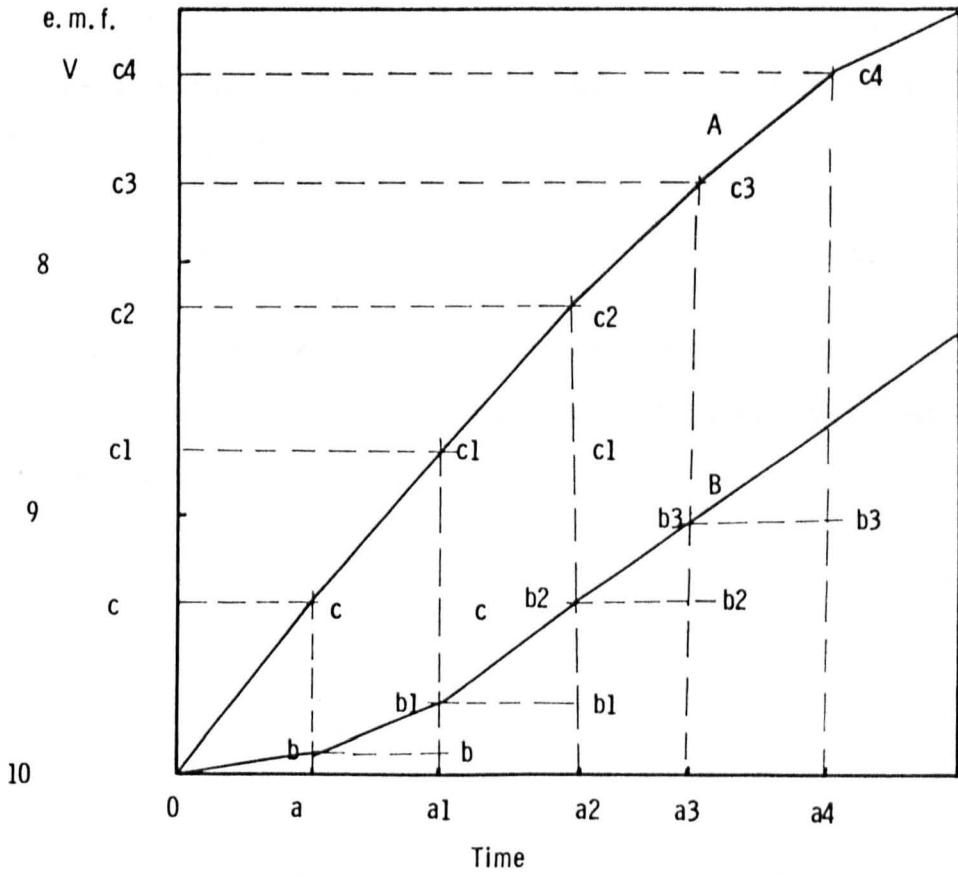


Fig. 18

Calibration diagram

A - Calibration curve

B - Curve obtained by a metal which does absorb hydrogen

By cumulative summation it is possible to follow the volume of H evolved after different times along curve B. The absorption of H by the cathode metal for each 1 μ l of gaseous H₂ formed is given by

$$H_{\text{abs}} = l - \text{evolved hydrogen} \quad (61)$$

and this will become zero when the cathode metal is saturated with hydrogen; and subsequently hydrogen gas evolution will be Faradaic.

CHAPTER 6

6. Hydrogen absorption by various metals

6.1 Effect of current density on hydrogen absorption in various metals

The survey of the literature given in Chapter 1.3 shows that charging a metal electrode at different c.ds has a significant effect on the rate of hydrogen absorption. This effect has been studied by many workers^(42,47,53,83), each of which agree that the permeation (P) vs cd follows the general equation $P \propto i^{\frac{1}{2}}$. However, in more recent publications this approach has been questioned and it is stated that this law extends only over a limited range of c.ds.

An investigation of this relationship has been undertaken using the P.E.T to study the P v i relationship in a range of c.ds using a variety of metal electrodes. The metals were supplied by Goodfellow Metals Ltd and their nominal composition is described in Table 2, together with specimens of Hg/Cu, Ga and Hg. These have been studied as described in Chapter 4 using c.ds in the range 0.2 mA/cm² to 2 mA/cm², the c.ds being increased in steps of 0.2 mA. In order to avoid effects due to rapid H-saturation of the foils the experimental time was kept to a maximum of 150 s.

6.1.1 Results

Figures 19 - 29 show the effect of different c.ds on the eleven metals and to avoid a confusing picture only

Table 2

Typical composition of different metals as supplied by Goodfellow metals Ltd

<u>Element</u>	<u>Analysis in ppm</u>									
Ti	Al	Cr	Fe	Mn	Ni	Si	Sn	C		
	300	-	1500	100	50	300	200	300		
Cd	Al	Cu	Fe	In	K	Sn	Zn			
	200	100	300	200	150	100	1000			
In	Au	Cd	Cu	Fe	K	Mn	Na	Ni	Pb	
	200	30	300	200	50	20	200	500	400	
W	Ca	Cu	Fe	Mo	Ni	Pb	Si	Sn		
	20	20	20	150	20	50	50	30		
Zr	Al	Cr	Fe	Hf	Sn	C				
	50	100	60	65	100	120				
Fe	Ag	Al	Cd	Co	Cu	Ni				
	15	10	40	400	400	400				
Cu	Bi	K	Pb	Ca						
	10	100	100	25						
Pb	Ag	Bi	Cu	Sn						
	20	100	20	70						
Pt	Ag	Al	Ca	Cu	Fe	Ni	Zn			
	50	80	300	250	300	150	150			
Ag	Ca	Cr	Cu	Fe	Pb	Si				
	40	20	20	60	40	20				
Ni	Al	Co	Cr	Cu	Fe	Mg	Mn	Si	Ti	C
	100	600	100	100	400	800	200	100	100	100
Au	Ag	Cu	Ni	Pb						
	300	500	100	15						
Mo	Al	Cr	Fe	Pb	Si	Ti	C			
	20	50	50	30	50	30	40			

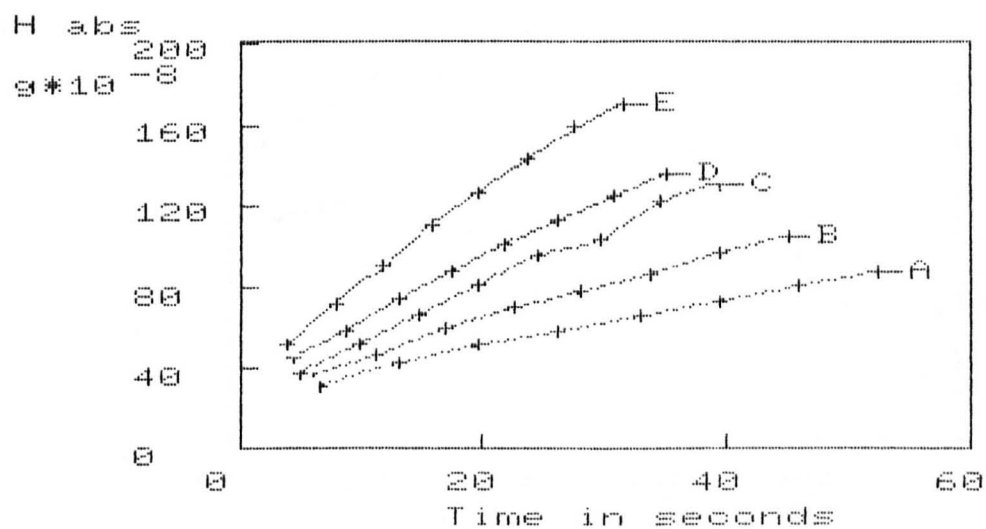


Fig. 19 Hydrogen absorption in Au at various current densities

- A = $1.2 \text{ [mA/cm}^2 \text{]}$
- B = $1.4 \text{ [mA/cm}^2 \text{]}$
- C = $1.6 \text{ [mA/cm}^2 \text{]}$
- D = $1.8 \text{ [mA/cm}^2 \text{]}$
- E = $2.0 \text{ [mA/cm}^2 \text{]}$

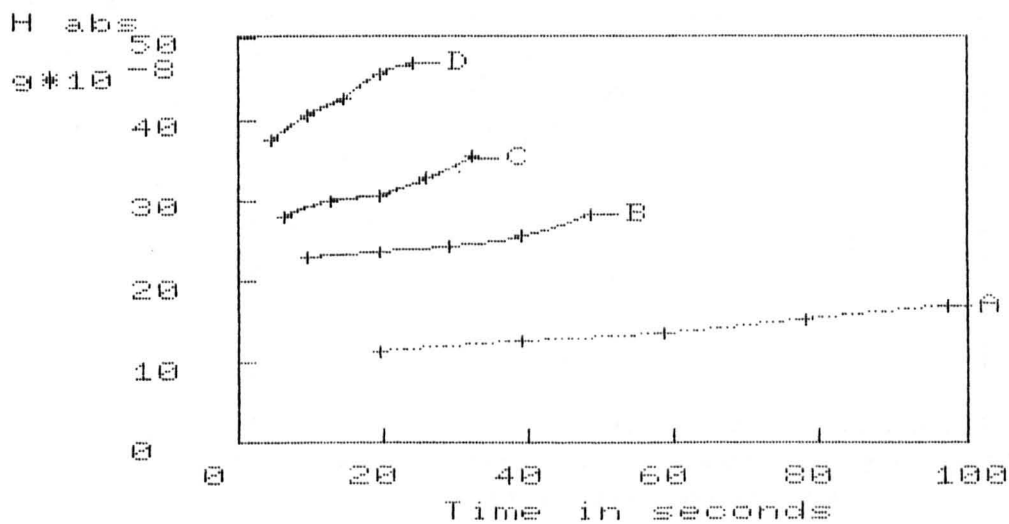


Fig. 20 Hydrogen absorption in Cu at various current densities

- A = 0.4 [mA/cm²]
- B = 0.8 [mA/cm²]
- C = 1.2 [mA/cm²]
- D = 1.6 [mA/cm²]

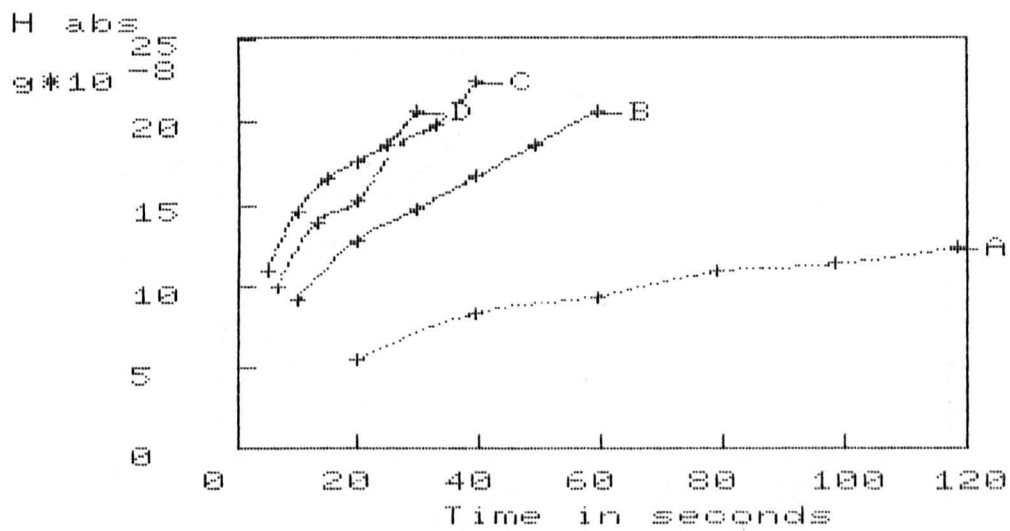


Fig. 21 Hydrogen absorption in In at various current densities

- A = 0.4 [mA/cm²]
- B = 0.8 [mA/cm²]
- C = 1.2 [mA/cm²]
- D = 1.6 [mA/cm²]

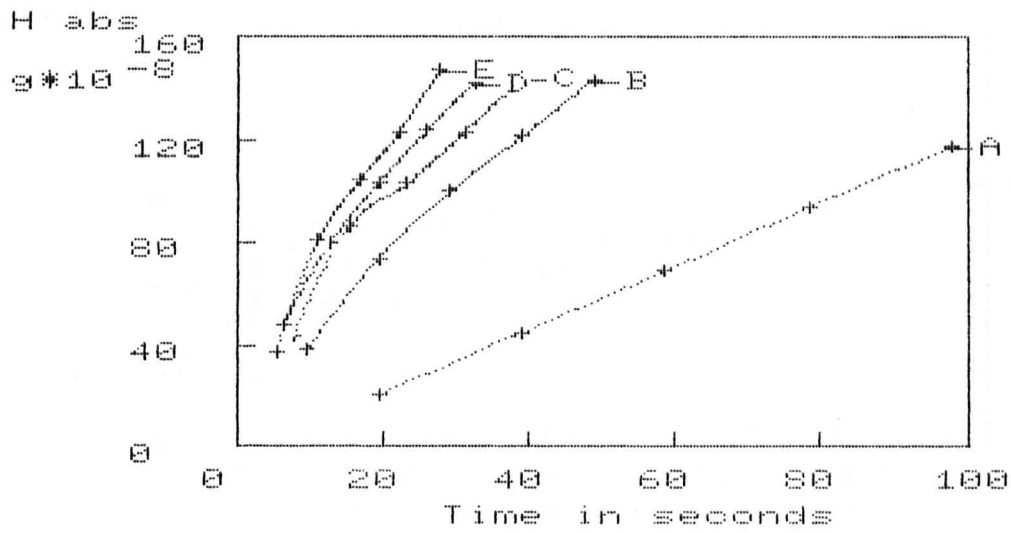


Fig. 22 Hydrogen absorption in Ti at various current densities

- A = 0.4 [mA/cm²]
- B = 0.8 [mA/cm²]
- C = 1.0 [mA/cm²]
- D = 1.2 [mA/cm²]
- E = 1.4 [mA/cm²]

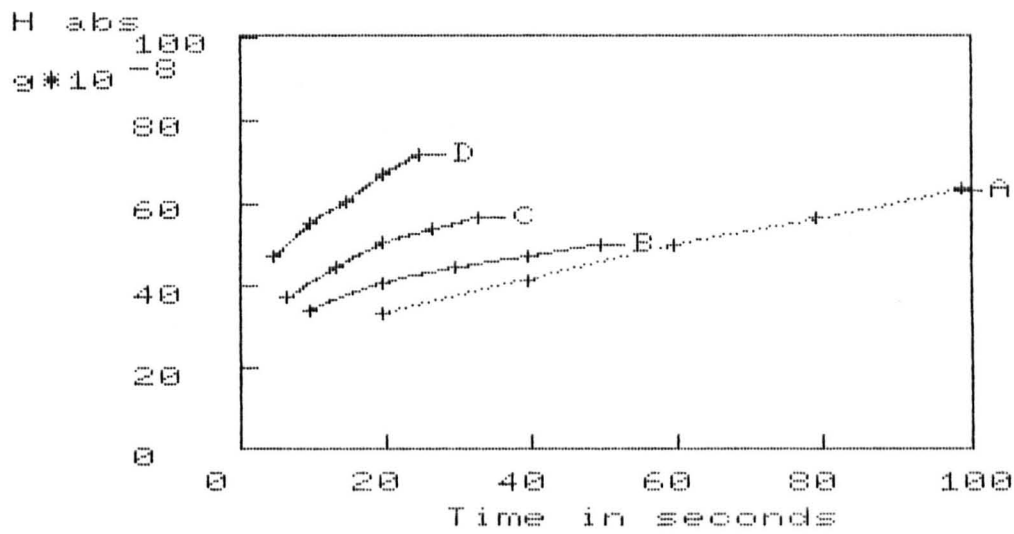


Fig. 23 Hydrogen absorption in Pt at various current densities

- A = 0.4 [mA/cm²]
- B = 0.8 [mA/cm²]
- C = 1.2 [mA/cm²]
- D = 1.6 [mA/cm²]

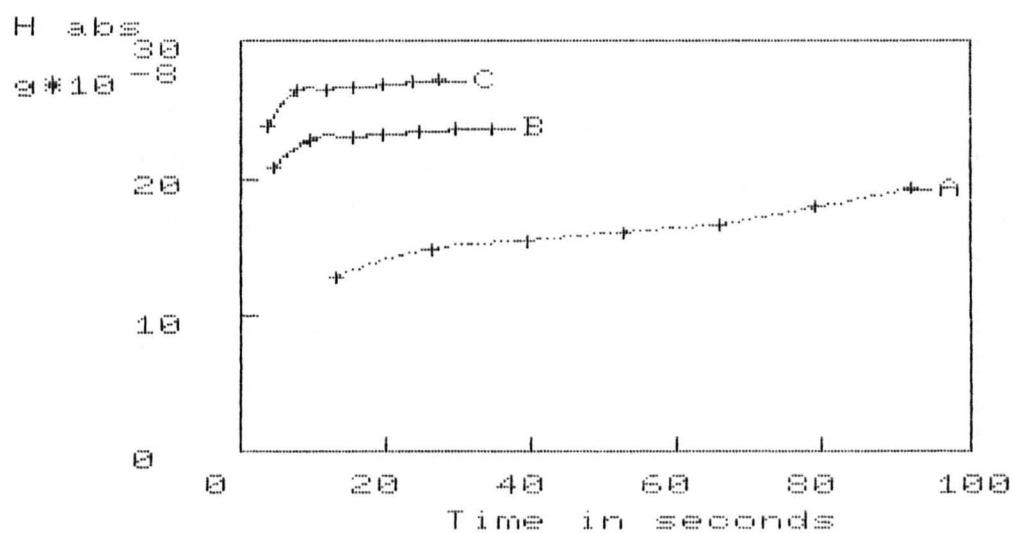


Fig. 24 Hydrogen absorption in W at various current densities

A = 0.6 [mA/cm²]
 B = 1.6 [mA/cm²]
 C = 2.0 [mA/cm²]

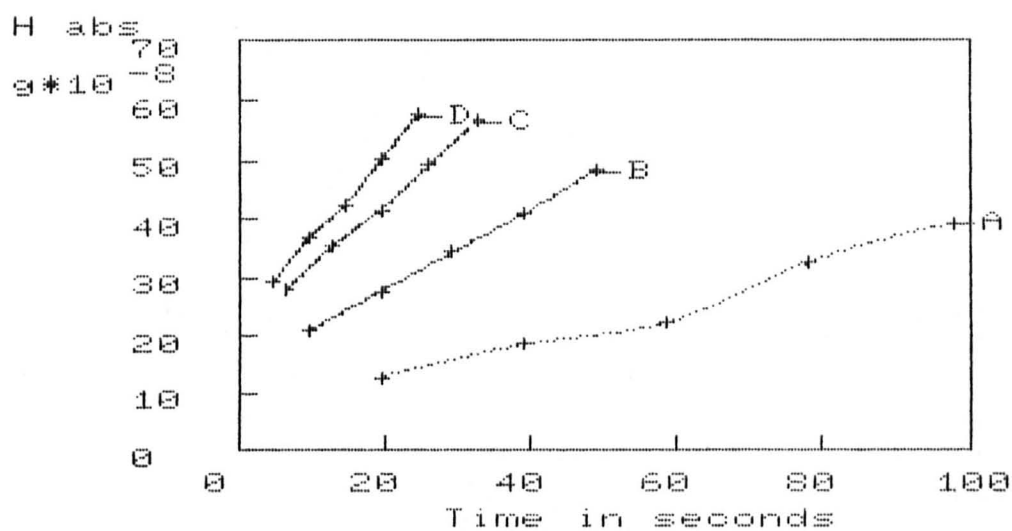


Fig. 25 Hydrogen absorption in Pb at various current densities

- A = 0.4 [mA/cm²]
- B = 0.8 [mA/cm²]
- C = 1.2 [mA/cm²]
- D = 1.6 [mA/cm²]

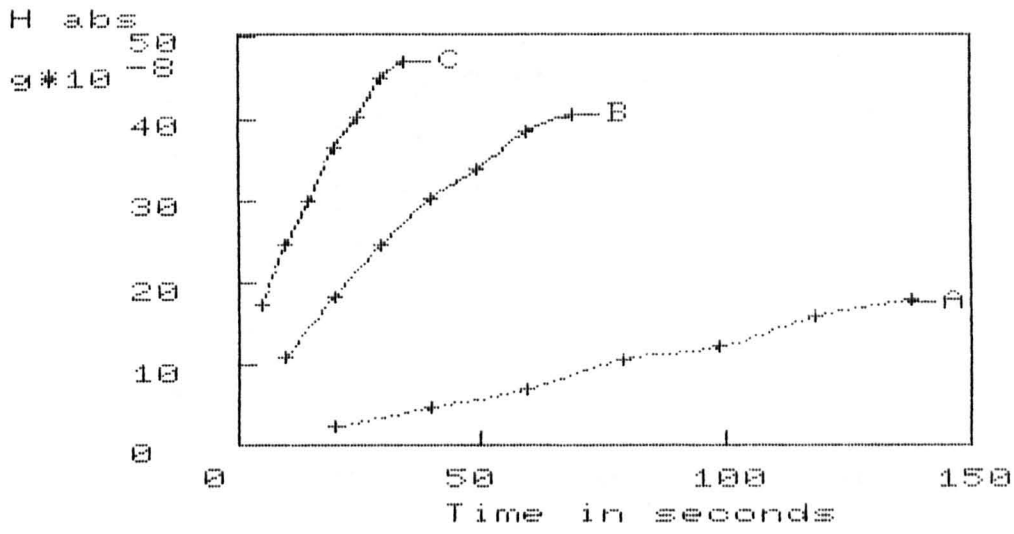


Fig. 26 Hydrogen absorption in Zr at various current densities

- A = 0.4 [mA/cm²]
- B = 0.8 [mA/cm²]
- C = 1.6 [mA/cm²]

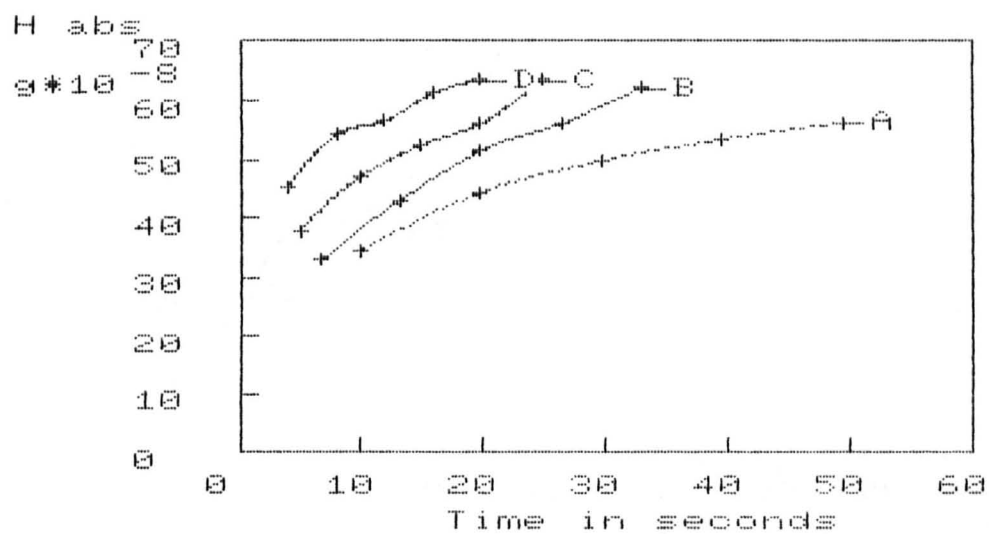


Fig. 27 Hydrogen absorption in Ni at various current densities

- A = 0.8 [mA/cm²]
- B = 1.2 [mA/cm²]
- C = 1.6 [mA/cm²]
- D = 2.0 [mA/cm²]

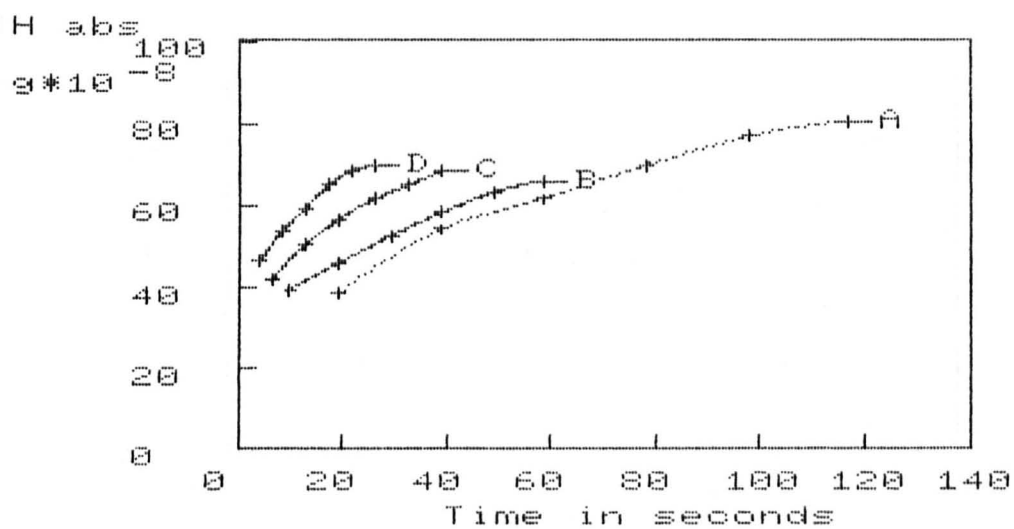


Fig. 28 Hydrogen absorption in Ag at various current densities

- A = 0.4 [mA/cm²]
- B = 0.8 [mA/cm²]
- C = 1.2 [mA/cm²]
- D = 1.8 [mA/cm²]

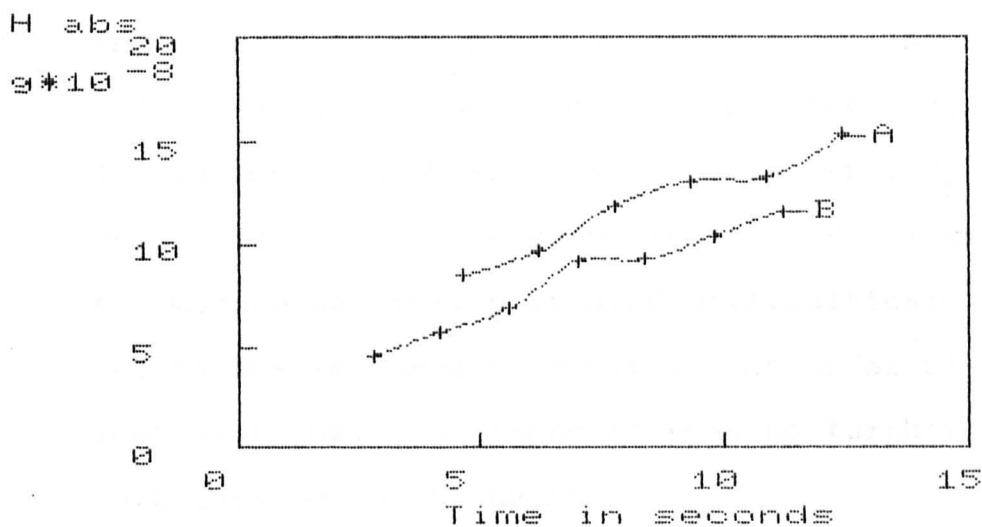


Fig. 29 Hydrogen absorption in Cd at the surface at various current densities

- A = 1.8 [mA/cm²]
- B = 2.0 [mA/cm²]

experiment results at 0.4 mA increments are shown in these graphs. In the case of Ga great difficulties were encountered in the preparation of a reliable electrode but preliminary experiments showed little sign of H absorption. Hg showed a very small tendency for hydrogen absorption but the introduction of a Hg electrode into the monitoring cell presented difficulties; furthermore, the values measured were within the order of the experimental error. For these reasons no further experiments were carried out using Hg.

The Hg/Cu amalgams which were prepared by dipping a Cu-wire for 24 h into Hg, showed no evidence of H absorption at any of the c.d.s studied, and only when the surface area was increased to 10 cm² could a very small H_{abs} trace be detected. No further studies were made of these extremely small absorption effects.

As can be seen from Figures 19-29 all metals studied show an increase in the rate of hydrogen absorption (h.a.r) with increase in applied c.d, and these results if plotted as rate of absorption (H_{abs}/t) vs $i^{1/2}$ give a straight line between 0.6 and 1.2 (mA/cm²). However, there are deviations from linearity above and below this range. Typical results are shown in Figures 31 and 32 for Cu and Ti, respectively.

Metals like Cd and Mo show very little (Mo) or no (Cd) increase in H_{abs} with increase in c.d.

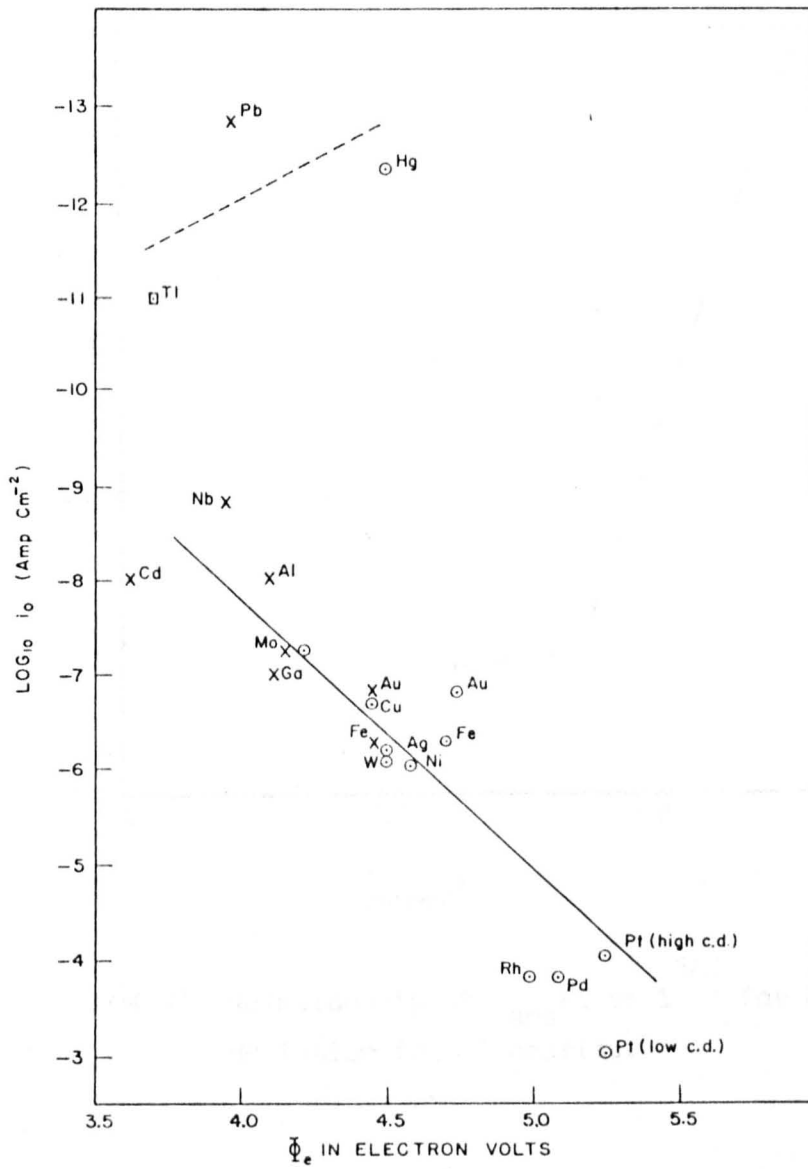


Fig. 30 Relation between workfunction and log exchange current after Conway and Bockris (152)

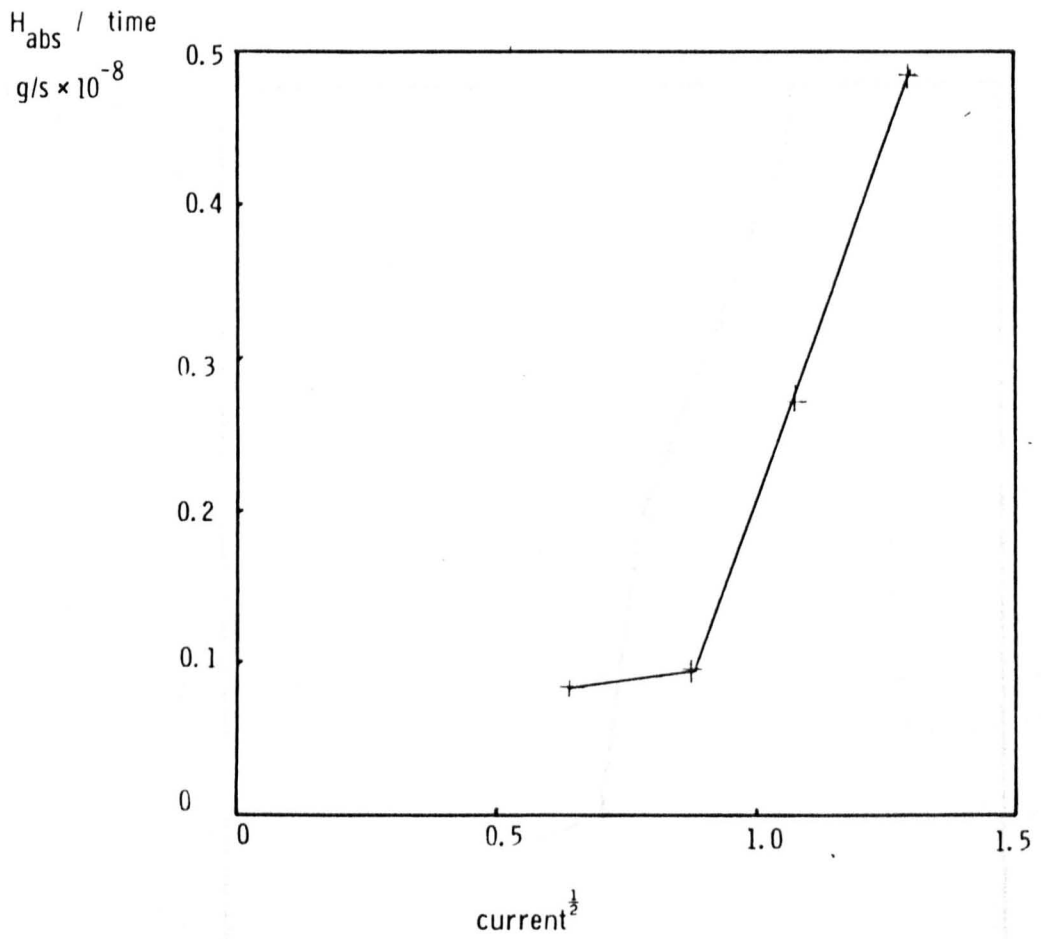


Fig. 31 Relationship of H_{abs}/t vs $i^{1/2}$ for Cu showing deviation from linearity.

$H_{abs}/time$
 $g/s \times 10^{-8}$

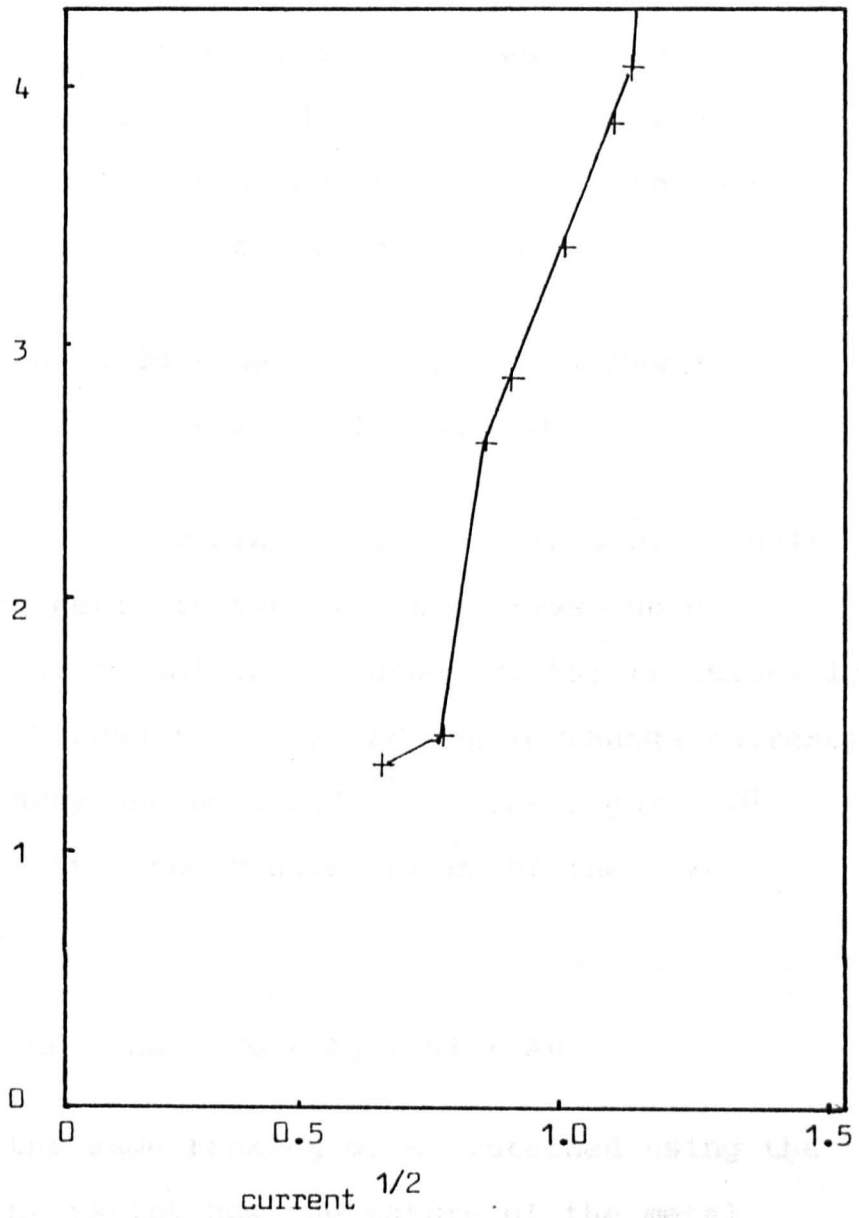


Fig. 32 Relationship of H_{abs}/t vs $i^{1/2}$ for Ti showing deviation from linearity.

6.1.2 Discussion

1. All metal-water investigations showed a tendency to absorb hydrogen at different rates.
2. Using the first it appears that the linear region

An attempt was made to rank the metals under study in order of their H_{abs} capabilities as assessed by the amount of H absorbed at a c.d of 1 mA/cm² applied for 40s. The results in ascending order of the rate of H_{abs} at constant c.d were found to be

Hg/Cu < Hg < Cd < Ga < In < W < Zr < Fe < Ti

Cu < Pb < Pt < Ag < Ni < Au < Mo

It was attempted to correlate these findings with their position in the periodic table, but no reasonable relation could be established. However, the relationship between the work function (ϕ_e) and log (exchange current), as shown by Conway and Bockris⁽¹⁵²⁾, see Figure 30 for the h.a.r, gives the ranking order of the work function to be

Cd < Ga < Cu < Ag < Ni < Au

which follows the same ranking order obtained using the P.E.T for demonstrating how the nature of the metal determines the rate of hydrogen absorption. Differences in the rate of H_{abs} were observed with Pt, Fe and Mo, which cannot be explained at the present time.

6.1.2 Conclusions

1. All metals under investigation showed a tendency to absorb hydrogen at different rates.
2. Using the P.E.T it appears that the linear region

of a H_{abs}/t vs $i^{1/2}$ plot is confined to 0.6 and 1.2 mA/cm² for Cu and Ti, which confirms work done by other investigators.

3. It is possible to rank metals in order of the rate of hydrogen absorption and to correlate this with the relationship between work function and log (exchange current),
4. All metals except Hg/Cu, Cd and Mo showed that the h.a.r was strongly dependant on applied c.d.

6.2 Hydrogen absorption by a gold electrode

6.2.1 Introduction

Gold is normally regarded as having no ability to dissolve hydrogen, and in 1959 Schuldinger and Hoare⁽⁷¹⁾ of the U.S Naval Research Laboratory, were unable to find any evidence that hydrogen could diffuse through gold. More recently, Chao and Costa⁽⁷²⁾ and Elkhaim⁽⁷³⁾ claim to have established experimentally that hydrogen dissolves in gold and can diffuse through it slowly at room temperature. They found that the reflective power of a polished unannealed gold electrode is reduced progressively when it is cathodically charged with hydrogen in sulphuric acid solution, and they attributed this change to dissolution of atomic hydrogen in the metal.

In a subsequent experiment Chao and Costa anodised the hydrogen - charged Au electrode at constant current density in H₂SO₄ and found that all potential - time curves exhibited two plateaux. One of these was attributed to the

oxidation of hydrogen adsorbed on the gold surface and the other to the oxidation of hydrogen which was diffusing from the bulk of the specimen. By performing a Devanathan experiment it was found that the time required to pass hydrogen through a 30 μm thick gold foil was 30 h, for a 50 μm gold foil 100 h, and 200 h was reported for a 75 μm gold foil. This very slow diffusion of H in Au has been used in the present work to study the sensitivity of the P.E.T method, and it has been found that H absorption can be evaluated in a very short time compared with the days or weeks required by other methods of studying diffusion.

6.2.2 Material and Experimental Procedure

The gold was supplied by Goodfellows Metals Ltd in the form foils with a thickness of 25 μm and had been pre-annealed by the supplier. Its nominal composition was

Element	Ag	Cu	Ni	K	Pb
ppm	300	500	100	15	15

The gold foil was cut to form electrodes of (0.5 x 1 cm) and these were then spot welded onto electrode holders as described in Chapter 4. They were then degreased using trichlorethylene (p.a grade) and the wire holding the electrode was laquered using 'Lacomite', leaving a total exposed surface area of 1 cm^2 .

The gold electrodes were placed in hydrogen-saturated 0.05M H_2SO_4 within the piezo-electric apparatus, and then cathodically polarised at 1 mA/cm^2 , the rate of absorption being evaluated by the method described in Chapter 5.

6.2.3 Results

As it can be seen from Figure 33 it is possible to monitor the rate of hydrogen absorption in gold using the P.E.T, and from the initial slope of the curve, which is quite constant, it would appear that the kinetics, which are diffusion controlled, provide no evidence of interference due to surface films. After charging the gold foil for 280s the curve becomes horizontal showing that saturation has been reached, and this corresponds with a value of 78 ppm for the *equilibrium* solubility of H in Au. The time required to reach saturation (280 s) is very small and is contrary to the results obtained by Chao and Costa who, using a Devanathan cell, obtained a breakthrough time of 6×10^3 min corresponding with arrival of H on the reverse of the foil.

This shows the limitations of the Devanathan method for studying H diffusion in metals such as Au, Nb, Cd, Pt and Al, in which the rate of diffusion is very small. This difference in results indicates a non-even distribution of gas throughout the foil, which has been demonstrated previously by Zabel and Peisl⁽⁷⁴⁾ and by Dörr, Bauer, Gruner and Rauch⁽⁷⁵⁾ who obtained a non-linear H distribution in niobium⁽⁷⁴⁾ and aluminium⁽⁷⁵⁾. It would appear that if such a non-linear distribution occurs, the diffusion values obtained by the Devanathan method are invalid, since no mathematical model is available to describe this phenomenon.

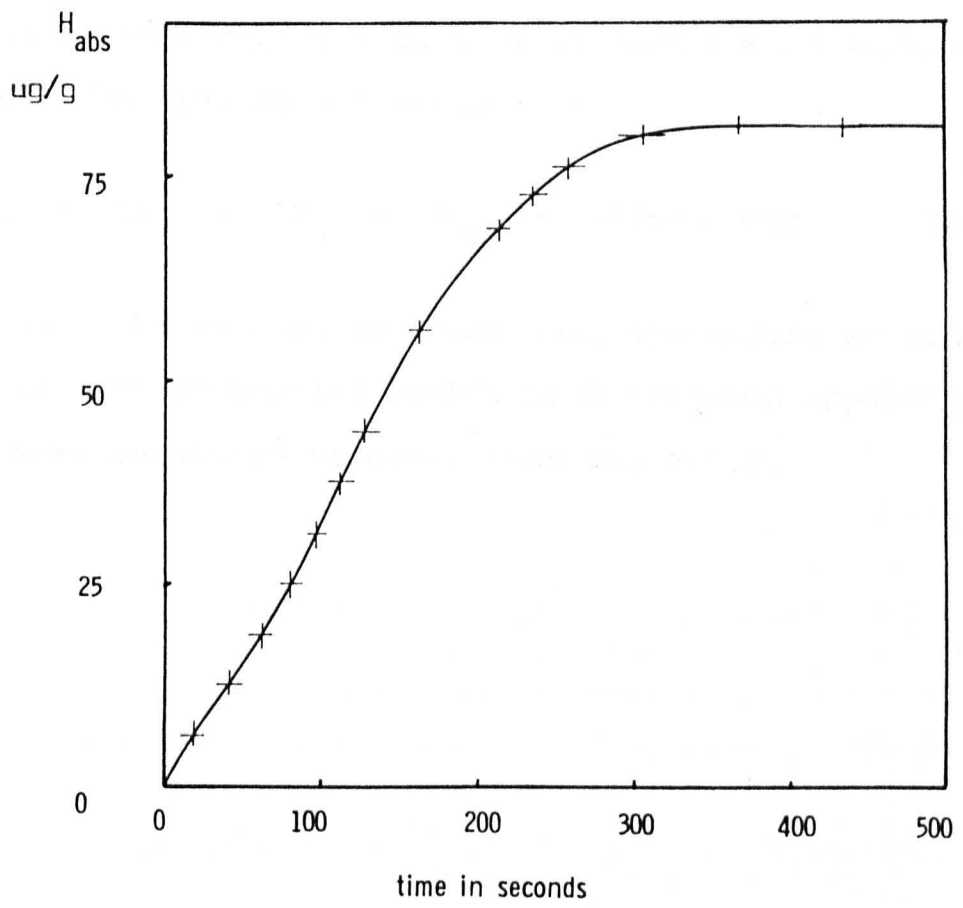


Fig. 33

Hydrogen absorption in gold

For these determinations Brauer et al have used a nuclear method based on the resonant reaction



whereas Zabel et al used an X-ray back scattering method. Both these methods require highly sophisticated apparatus, and are more sensitive to error than the P.E.T.

CHAPTER 7

7. HYDROGEN ABSORPTION IN TITANIUM

Titanium was discovered as early as 1791 but for 150 years there was hardly any practical use for it and it is only during the last 25 years that it has become more widely used and the subject of detailed studies in most countries of the world. This interest in titanium is explained by its technologically important properties, ie. a high strength at ambient and elevated temperatures, low density and a high resistance to corrosion. An effective method for the production of ductile titanium was proposed for the first time in 1940, but it was not produced in commercial quantities until 1948 when the annual production was about 2.5 ton. Since then the production of titanium has been increased steadily, and 30,000 tons were produced in the USA as early as 1957 and by 1976 world production amounted to 73,250 metric ton⁽⁷⁶⁾ .

The high rate of growth of production of Ti is due to the fact that at flight velocities in excess of 2000 km/h, the skin temperature becomes too high⁽⁷⁷⁾ for aluminium alloys to be used. Thus the demand is mainly for supersonic aircraft , although considerable amounts are used in the chemical industry for plants that have to resist corrosive acids.

The production of Ti and its alloys is complicated by problems arising from hydrogen embrittlement. It was found that hydrogen causes premature failure of components which in some cases was catastrophic. The situation became very serious in 1954 after the Pratt-Whitney company reported that aircraft parts made of Ti alloys suffered fracture resulting from the presence of hydrogen, and it was feared that this could limit the use of the metal in applications where high stresses were present. For this reason the cause of hydrogen embrittlement, and the means of preventing it, have been the subject of extensive research. Improved processes for the production of titanium sponge, the use of vacuum melting, and the occasional use of vacuum annealing to remove any hydrogen present, were in most cases effective in preventing hydrogen embrittlement. However, since modern industrial methods for the production of commercial titanium do not completely remove hydrogen, the problem arose of determining the maximum permissible content of hydrogen in titanium that could be tolerated without vacuum annealing, which is a laborious and time-consuming operation.

The object of the present work on Ti was to determine (a) the factors that influence the initial stages of hydrogen absorption and (b) the kinetics of formation of hydride layers on the surface of titanium.

7.1 Comparison between solid state vacuum extraction (VE) and P.E.T

7.1.1 Introduction

The solid-state vacuum extraction technique has been used in this work to establish the validity of the piezo-electric technique for determining the absorption of cathodic H into Ti. This technique was available in the laboratory since previous workers, Newman⁽⁵¹⁾, Phillips⁽⁷⁷⁾ and Phillips, Poole and Shreir^(79,80) have used it for studies of H absorption in iron, steel and in Ti. The technique adopted by these workers for Ti have been reproduced in the present using similar materials and conditions of H absorption.

7.1.2 Materials

The material used was commercially pure Ti (130 grade) supplied by IMI Ltd of nominal composition

Element	O	N	C	Fe	Si	H
wt %	0.125	0.01	0.03	0.05	0.04	0.002

It was supplied in form of cold-worked strip 8 cm wide and 0.01 cm thick. Titanium of higher purity (supplied by Goodfellow Metals Ltd) in the form of sheet of 25 cm x 25 cm with 0.025 mm or 0.001 mm thickness was also used. The nominal composition of this pure Ti is given below, and it should be noted that the values listed are the maximum possible.

Element	Al	Cr	Cu	Fe	Mn	Ni	Si
ppm	300	50	5	1500	100	50	300
Element	Sn	C	H	N	O		
ppm	200	300	60	150	2000		

This Ti had been given an anneal by the manufacturer, but it still showed a preferred grain orientation when analysed by x-ray diffraction. However, it was not given any further heat treatment, since this was found to cause distortion of the foil.

7.1.3 Specimen Preparation

Spade shaped specimens were cut with a charging surface $2 \times 1 \text{ cm}^2$. To prevent effects due to the rolling texture all specimens were cut so that their major axes were parallel to the rolling direction of the sheet. The specimens were then degreased by ultrasonic cleaning in acetone, and were then vacuum annealed at 900°C for 15 min to remove any traces of dissolved hydrogen.

The furnace consisted of a silica tube heated by a horizontally mounted Nichrome-wound furnace. Temperature control was achieved by using a Chromel-Alumel thermocouple and a 'Ether Transistrol' control in conjunction with a 'Variac' auto transformer. The silica tube was evacuated by a mercury-in-glass diffusion pump (Edwards E.M.G) backed by a two stage rotary pump (Metrovac D.R I-K.A.E.I Ltd) in conjunction with a liquid- N_2 cold trap, and by this means the pressure could be reduced to 10^{-5} torr. The vacuum

in the furnace tube was monitored by a Pirani-gauge head (Edwards A. 6B) and gauge (Edwards B5). After the annealing treatment the furnace was removed and the tube containing the specimens under vacuum was allowed to cool to ambient temperature. When the specimens were completely cold the vacuum was released and the specimens were removed from the tube. This treatment not only removed all the hydrogen but it also produced a clean surface, although it did result in an increase in grain size. The final step in specimen preparation was to spot weld a 10 cm length of nichrome wire to the shank of the specimen. This wire was led through two holes in a glass stopper (see section 4) and glued in place using 'Araldite'. The shank and wire were then coated with 'Lacomite' (Cannings Ltd) to insulate them.

7.1.4 Solutions

The solution used in the P.E.T cell, in which the specimens were charged with hydrogen was 0.05M H_2SO_4 , which was precharged with hydrogen; this acid was chosen since the corrosion rate of Ti at ambient temperatures is very small. At the same time, it had sufficient conductivity to allow c.ds of up to 3 mA/cm² to be passed without solution heating. All solutions were prepared from AnalaR grade reagents and distilled water. The technique differed from that used by Phillips⁽⁷⁷⁾ in that the electrolyte was de-oxygenated and saturated with hydrogen using a special charging vessel (see Chapter 4).

7.2 Estimation of absorbed hydrogen using P.E.T Cell

After surface preparations the electrode was introduced into the P.E.T cell. All bubbles adhering to the surface were removed and a zero reading was then taken which represented the e.m.f readout when the cell was free from gas bubbles. The electrode was then cathodically polarised at 1 mA/cm^2 . The periods of charging were normally 15 or 25 min, but when using the larger cell the times were increased to 55, 90, 120 and 900 min. The rate of hydrogen evolution was measured during the experiment and by comparing the values against those obtained using a Cu/Hg alloy electrode (in which H is insoluble), it was possible to calculate the rate of H - absorption during the charging process. After removing the specimen from the P.E.T cell it was washed in distilled water and its supporting wire was then cut off. The 'Lacomite' was then removed by acetone, the specimen was quickly dried in an air stream and small piece of pure Fe foil wrapped around it for magnetic manipulation in the tube furnace. It was at once introduced into the vacuum extraction apparatus (V.E.A) through a Hg trap by means of a magnet. The whole process, removing the specimen from the P.E.T cell and introducing the specimen into the VEA took only 30 - 40 s, which was necessary to avoid errors due to diffusion of hydrogen from the specimen.

7.3 The vacuum extraction apparatus (VEA)

The sample was heated in vacuum to remove all the hydrogen from the metal, and the hydrogen was simultaneously pumped

off and collected in an evacuated compartment of known volume. From the pressure and temperature of this volume of hydrogen it is possible to calculate the hydrogen content of the Ti. The apparatus used in this investigation, Figure 34, is basically the apparatus developed by Bearpack⁽⁸¹⁾ and modified by Phillips⁽⁷⁷⁾. The apparatus consists of three sections, which are described with reference to Figure 34.

7.3.1 Extraction Section

The specimens were introduced through a barometric Hg column (L) into a silica furnace tube (t), which was heated to the extraction temperature by the tube resistance furnace (K). The temperature was maintained at 700°C by means of a chromel-alumel thermocouple and 'Ether Transistrol' controller via a 'Variac' auto-transformer. The hydrogen evolved from the Ti was pumped off by a two-stage Hg-in-glass diffusion pump (Jencons Limited), (F) via the cold trap (E) which removed any water vapour present. After the completion of the analysis the specimen was transferred to the reservoir (B).

7.3.2 Analysis Section

The analysis section consisted of three volumes of known capacity V_1 , V_2 and V_3 linked in series by the cut-offs CO.2 and CO.3. All three volumes were connected to the evacuation section by the large Tap T_1 and cut off CO.1. The pressure in the analysis section could be measured either directly by means of the McLeod gauge (G) or

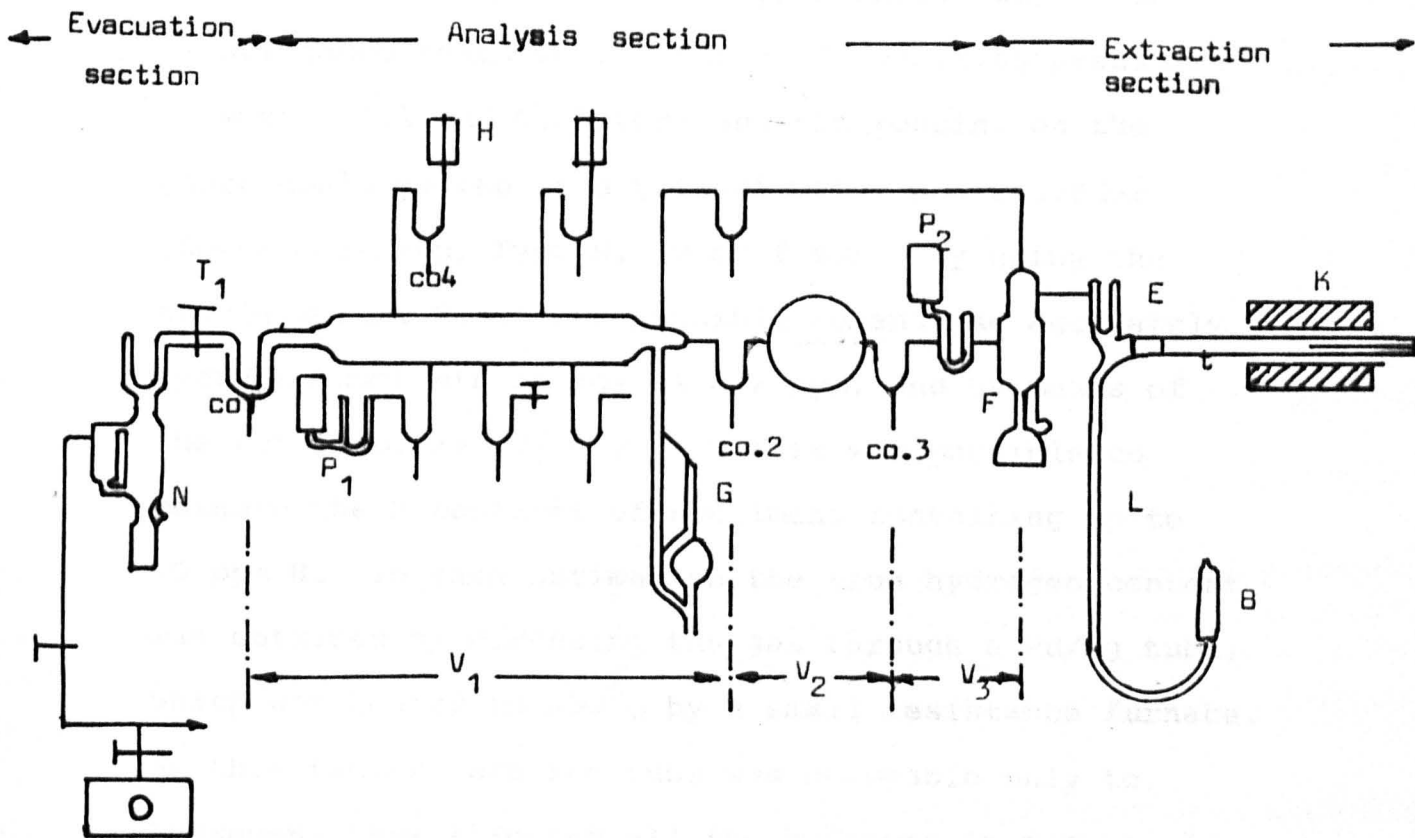


Fig. 34

Diagram of vacuum hot extraction gas analysis apparatus

by the Pirani gauges (P_1 and P_2) (Edwards Ltd). The Pirani gauge heads were capable of measuring pressures between 0.001 and 0.05 torr and the reading on the gauge could be fed to a potentiometer pen recorder (Leeds Northrup, Type S, 10 mV f.s.d). By using the single volume V_3 it was possible to analyse accurately hydrogen contents as low as 0.2 ppm, and by means of the total volume ($V_1 + V_2 + V_3$) it was possible to measure the H contents of specimens containing up to 10 ppm H. In each estimation the true hydrogen content was obtained by diffusing the gas through a Pd/Ag tube, which was heated to 450°C by a small resistance furnace. At this temperature the tube was permeable only to hydrogen, thus allowing all the hydrogen in the sample to diffuse into the atmosphere leaving the residual gases in the apparatus. From the difference between the initial and final pressure, an accurate estimation of the hydrogen content could be obtained.

7.3.3 Evacuation Section

A Hg-in-glass diffusion pump (M. Edwards B.5) guarded by a liquid N_2 cold trap (N) to prevent any Hg vapour entering the apparatus and backed by a two stage rotary pump (O), was used to evacuate the apparatus. The pressure which could be reached within the apparatus was 10^{-5} torr.

7.3.4 Calculation of results obtained by VEA

The volumes V_1 , V_2 and V_3 have been accurately measured by Bearpark 1966 who reported the following values

$$\text{Total volume } (V_1 + V_2 + V_3) = 2450 \text{ ml} \quad (67)$$

$$V_1 = 1140 \text{ ml}$$

$$V_2 = 1015 \text{ ml}$$

$$V_3 = 305 \text{ ml}$$

An extra volume V_4 was added to the apparatus by Phillips and was found to have a capacity of 145 ml, giving a total volume for the analysis section of the apparatus V_t of 2605 ml. If the pressure developed during analysis of a specimen at an ambient temperature of 25°C is P (torr) and the density of hydrogen is taken as $9 \times 10^{-6} \text{ g/cm}^3$ at N.T.P., then the mass of hydrogen w in the specimen is given by

$$w = \frac{P \times 2605 \times 273 \times 9 \times 10^{-5}}{760 \times 298} \quad (68)$$

$$w = 2.83 \times 10^{-4} P \text{ (g)} \quad (69)$$

Difficulties arose in cutting the specimens to the exact size of 2 cm^2 so a correction factor had to be employed, which consisted of multiplying the observed pressure by the ratio of the weight of 1 cm^2 of sheet/the weight of the actual specimen. The initial pressure of hydrogen was calculated by multiplying the reduced pressure by the ratio V/V_t , which had a value of 17.97, which was obtained by Phillips⁽⁷⁷⁾, and experimentally confirmed in the present work.

7.4 Results and Discussion

It can be seen from Figure 34A that a direct comparison of results obtained using the P.E.T and VEA methods was possible and highly reproducible.* At low hydrogen contents the VEA showed a high standard deviation ($> 13\%$) which became less ($> 5\%$) as the volume of H increased. The standard deviations of the results obtained by the P.E.T (see Figure 35) did not vary significantly during the duration of the experiment, although within a given period of time the deviation fluctuated. These results are discussed in detail in Section 7.6. It is evident that the VEA experiments gave a slightly lower hydrogen content than those obtained by the P.E.T. This can be explained by loss of H during the time interval between terminating the P.E.T experiment and inserting the specimen into the vacuum extraction apparatus.

These experiments show the advantage of the P.E.T method over the VEA, since it was possible with the former to follow the kinetics of absorption continuously from almost zero time. Very small changes in the rate of absorption can be monitored with high accuracy, and since these occur mainly in the initial stages of absorption, they are very difficult to monitor using the VEA. The VEA method gives values for the rates of absorption only with metals in which the ratio of surface area/mass is small (ie. not thin foils) so that the rate of desorption of hydrogen into the atmosphere is slow or where the metal forms a stable Me-H compound (eg. Ti). The number of points on the curve is limited also by the sensitivity

* 24 experiments

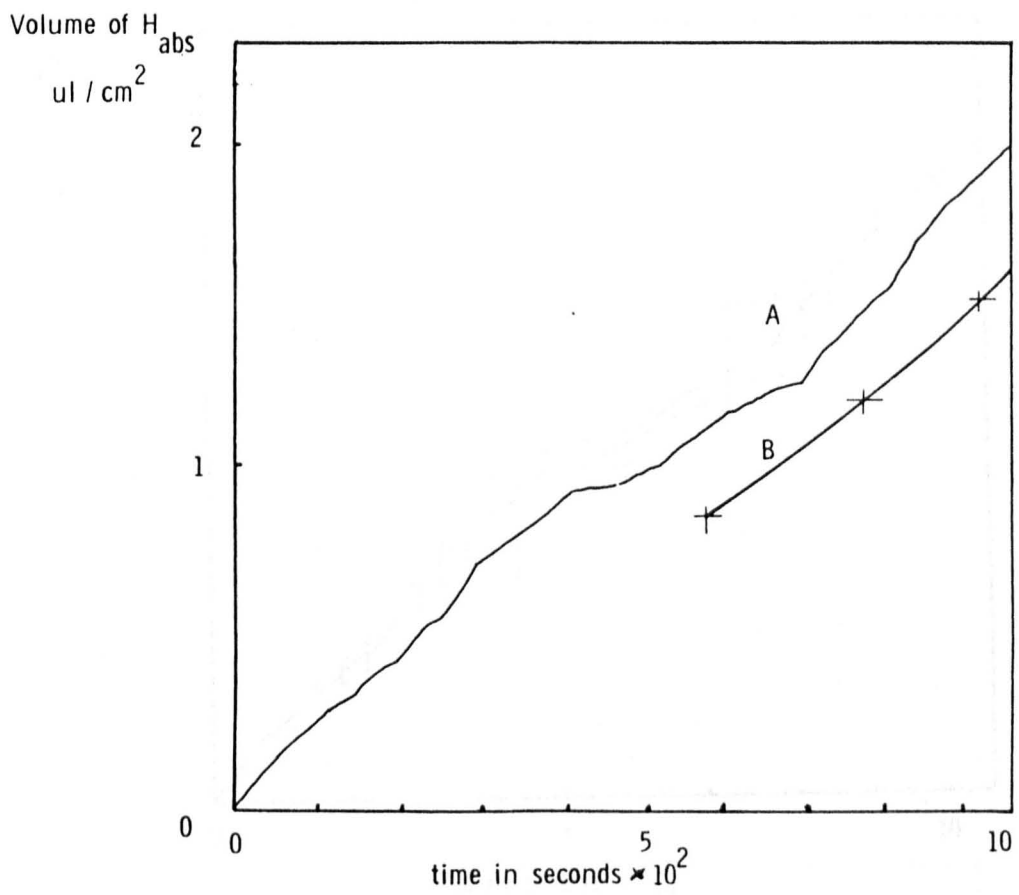


Fig. 34 A

Hydrogen absorption by Ti using two different methods

A - Piezo - electric technique (Goodfellow Ti)

B - Vacuum extraction method (Ti (130))

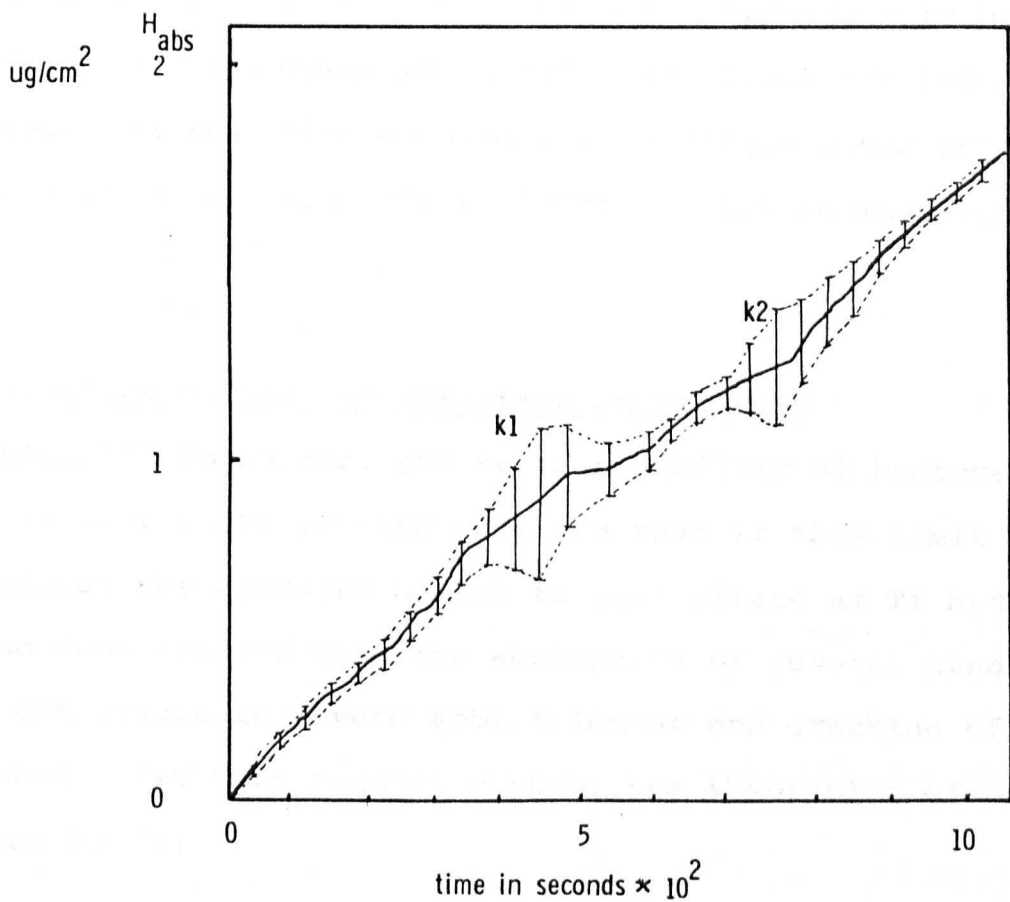


Fig. 35 Hydrogen absorption in Ti measured by P.E.T.

The rate of absorption is controlled, therefore, by both the nature of the surface and internal structure of the metal. The most important factor of importance is the nature of the oxide film and its degree of contamination. Other factors which are important are the composition, microstructure and temperature. Cowgill and his co-workers have shown that the oxide film acts as a barrier against the absorption of molecular hydrogen although it would not prevent absorption of H in the atomic form. Molecular hydrogen has to dissociate to atomic hydrogen before it is able to diffuse into the metal lattice.

of the apparatus. Thus, even though the results obtained by VEA and P.E.T correspond closely, the P.E.T has the advantage over VEA, that no losses of hydrogen occur into the atmosphere and that the H absorption can be measured from about 0 time.

7.5 Kinetics of hydride formation on titanium

Covington⁽⁸²⁾ found that the solid solubility of hydrogen in Ti is limited to 100-150 ppm, and that if this limit is exceeded the hydrogen begins to precipitate as Ti hydride. He also demonstrated that the absorption of several hundred ppm H can result in severe embrittlement and cracking of the metal. Two main factors control the absorption of hydrogen by Ti:

1. adsorption of H at the surface of the metal, and
2. diffusion of the adsorbed hydrogen into the bulk metal.

The rate of absorption can be controlled, therefore, by both the nature of the surface and internal structure of the metal. The surface properties that are of importance are the nature of the oxide film and its degree of contamination whilst the important internal properties are the composition, microstructure and temperature. Covington found that the air-formed oxide film acts as a barrier against absorption of molecular hydrogen although it would not prevent absorption of H in the atomic form, ie. molecular hydrogen has to dissociate to atomic hydrogen before it is able to diffuse into the metal lattice.

It appears, therefore, that surface films do not have a significant effect on hydrogen absorption, if the hydrogen is in the form of an atom.

The danger of Ti-hydrides is due to their very embrittling characteristics which can lead to catastrophic failures in metal parts, although the high capacity of Ti for H has important industrial applications for hydrogen storage. The problem which is dealt with in this Chapter, mainly concerns the initial stages of the hydrogen absorption and the formation of the lowest hydride. These investigations have been carried out on titanium with an air-formed oxide film on the surface.

7.6 Results

As can be seen from the H_{abs} vs time curves (see Figure 35) two kinks are clearly indicated on the graph, and by plotting the standard deviations for a large number of points it became apparent that these showed a periodic rise and fall of H_{abs} . The maximum st.d was found to be near to these two kinks, which indicates that at these points there is a change in the kinetics of the h.a.r (hydrogen absorption reaction). Ti is known to form three different types of hydride; a solid solution of H in Ti, (α - Ti), a Ti-hydrogen compound of the composition TiH, (β - hydride), and TiH₂ (γ - hydride), but at room temperature only α - and γ - hydrides are stable (see Figure 36). From Figure 35 it is possible that the first kink in the curve is caused

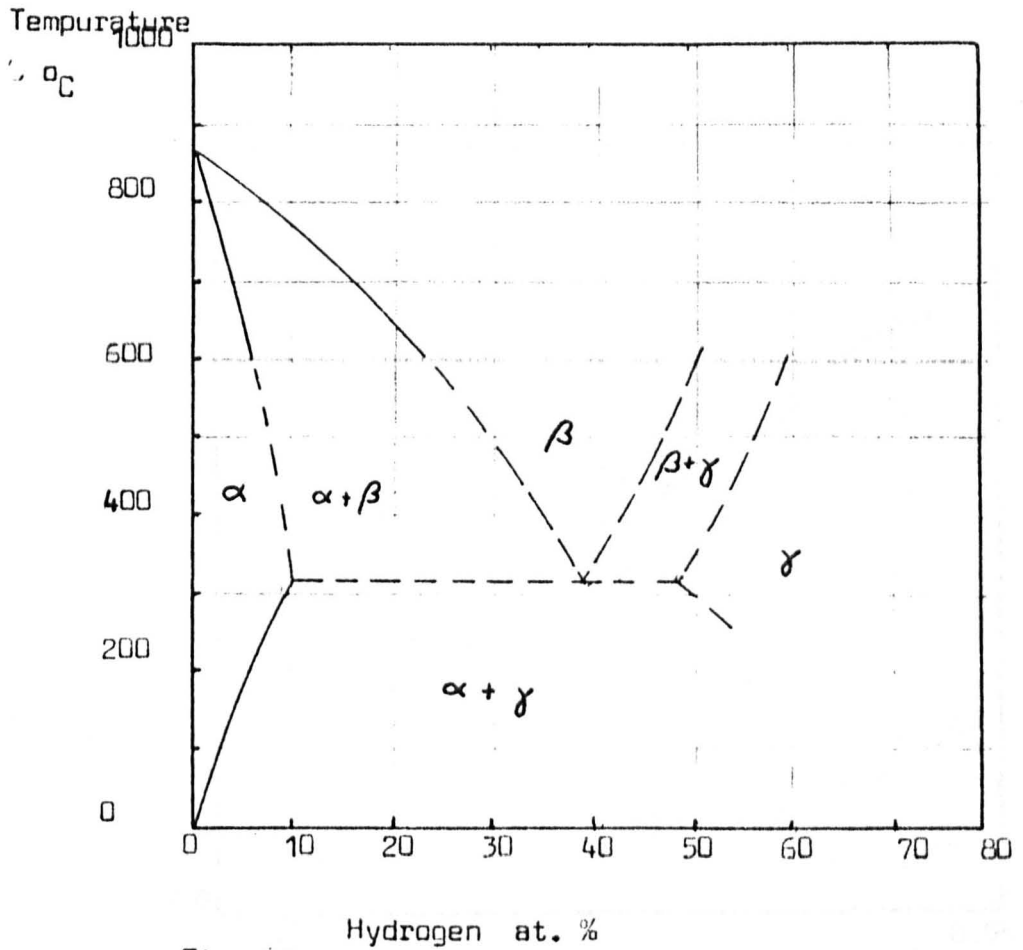


Fig. 36
 Phase diagram of the titanium - hydrogen system

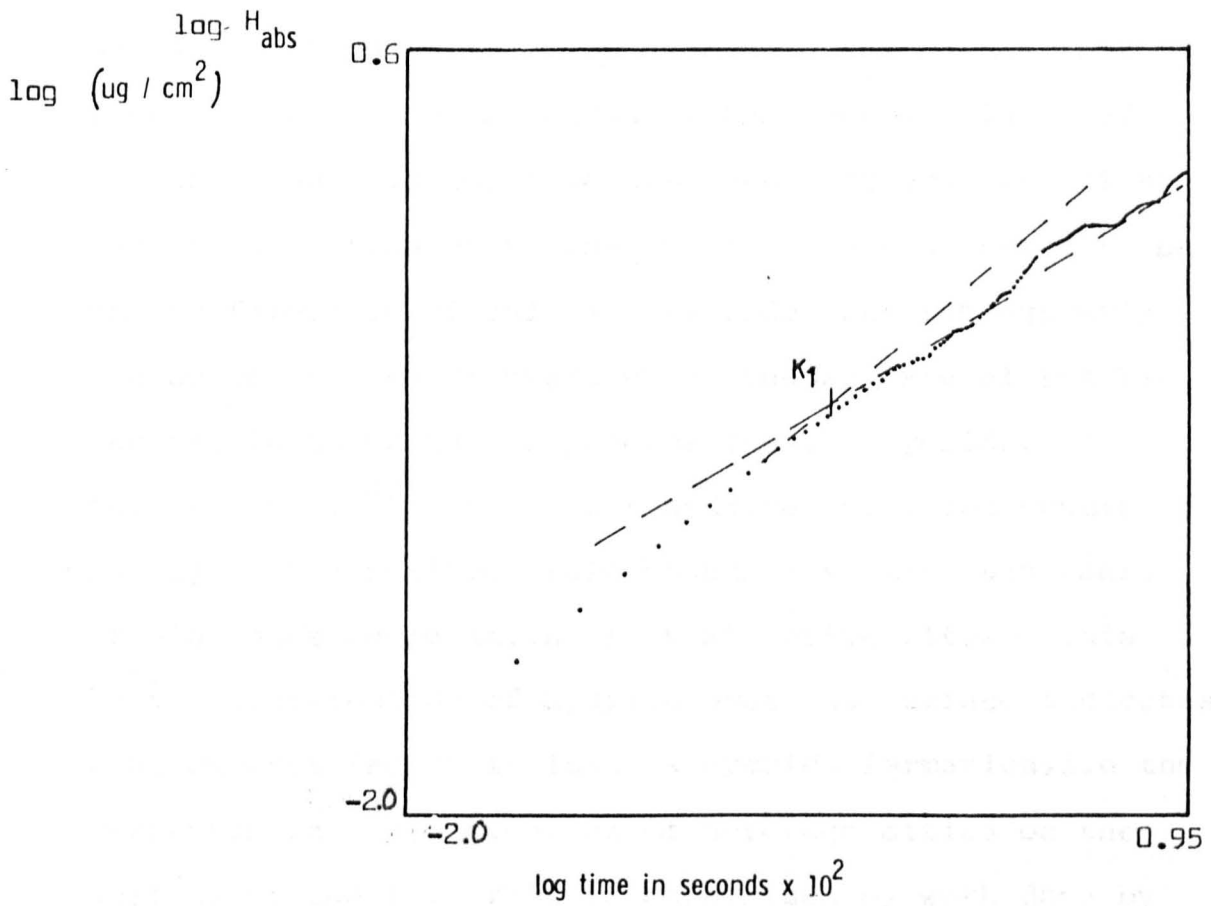
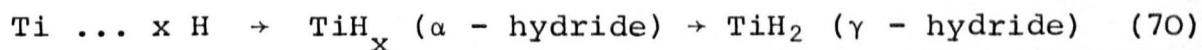


Fig. 37 H_{abs} in Ti plotted as $\log H_{\text{abs}}$ vs log time

by the formation of the γ - hydride. The change in the slope (kink K_1) in the curve is enhanced in Figure 37 in which $\log H$ vs \log time has been plotted. The first part of the graph up to the point K_1 is considered to be due to formation of only α - hydride, but subsequently the concentration of hydrogen at the surface of the Ti becomes large enough to produce the γ - hydride. Tsutsui et al⁽⁸³⁾ found that hydride formation occurs mainly at the surface grain boundaries, although there is also some segregation of it at active sites. This uneven distribution of hydride over the surface indicates that another factor influences hydride formation, i.e the variation in the energetics of heterogeneities on the surface of the Ti. This is emphasised by work done by Murai et al⁽⁸³⁾ who found a clear indication that in the earlier stages of H-absorption, hydride formation occurs at the grain boundaries. Murai also found that hydride formation occurs in three different stages which are accompanied by changes in the electrode potential, and these have been confirmed in the present work by galvanostatic measurements carried out simultaneously with the measurements of the h.a.r using the PET. These showed that changes in the potential occurred at the kinks K_1 and K_2 (see Figure 35). Even though these results are indirect evidence of γ - hydride formation at K_1 , it would appear that they give some evidence of changes in the kinetics of the h.a.r.

More prolonged experiments of > 16 h duration allowed a second effect to be observed. Figure 38, which manifested itself as sudden decreases in the rate of the h.e.r followed by slow increases until the initial rate of H evolution is reached again. These decreases occurred regularly after 2 hours of cathodic charging, but with further charging the length of the intervals increased. This phenomenon in conjunction with the rise and fall of the standard deviation may be explained by the following series of steps:

1. Discharges of the hydrogen at the surface of the electrode followed by diffusion of atomic H through the oxide film.
2. Continuous absorption of H at the metal/metal-oxide interface followed by transfer across the interface to form the α - hydride, which continues with consequent hydrogen saturation of the surface layers of the Ti.
3. Sudden formation of γ - hydride when the concentration of the hydrogen exceeds a limiting concentration



This limiting concentration for transition was established to be

$$\sim 1 \times 10^{-6} \text{ g cm}^{-2} \text{H}_{\text{abs}}$$

The formation (stage 3) of the stable compound TiH_2 consumes

H - evolution
 $g \times 10^{-6}/cm^2$

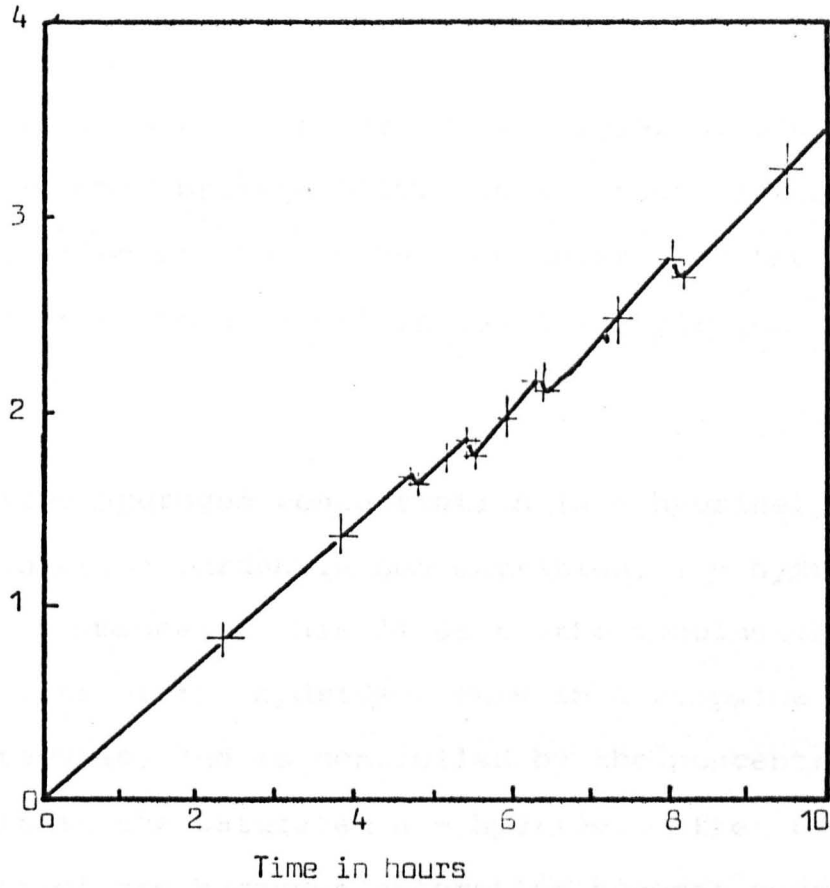


Fig. 38 Hydrogen evolution on pure Ti.

all the hydrogen stored in the surface layer of the metal, which is re-formed subsequently. This sudden decrease in the concentration of the α - hydride underneath the oxide layer leads to a slight increase in hydrogen absorption.

After the free hydrogen concentration (α - hydride) builds up to the reaction threshold concentration, γ - hydride formation recommences. This leads to the conclusion that the growth rate of the hydride occurs in a stepwise mode at regular intervals, and is controlled by the concentration of hydrogen within the saturated α - hydride. After 60 mins the kinetics of the hydrogen absorption becomes governed by cracks in the hydride. This can be seen in Figures 38A and 38B which shows the effect of formation of TiH_2 on the surface of the metal. Studies on Ti having oxide films of different thicknesses in 0.05M H_2SO_4 (section 7.8.1) show that under cathodic conditions ($E_H = - 0.8V$) the air-formed oxide film after periods of time greater than 1 h has no significant effect on the kinetics of the h.a.r. It is possible to show that after 1 h a continuous layer of hydride is formed on the surface of the metal, and that the subsequent absorption of hydrogen is controlled by the presence of cracks in this hydride.

7.7 Hydrogen absorption by Ti in solutions containing As

7.7.1 Introduction

As shown in the previous Chapter absorption of cathodic hydrogen is dependent on a variety of

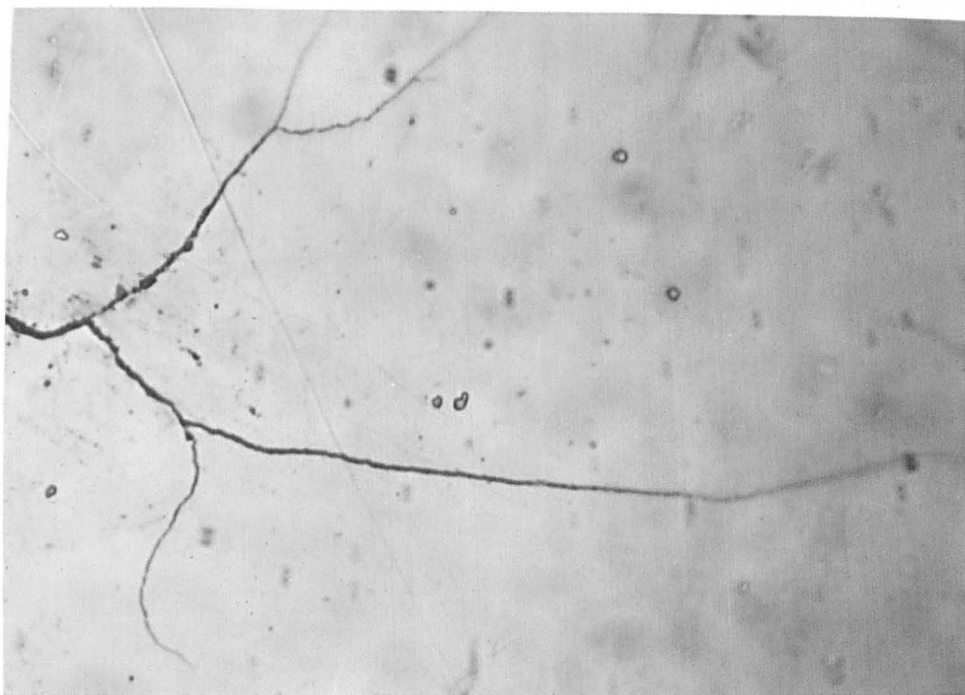


Fig. 38A Crack on surface of polished hydrided specimen (x 1000)

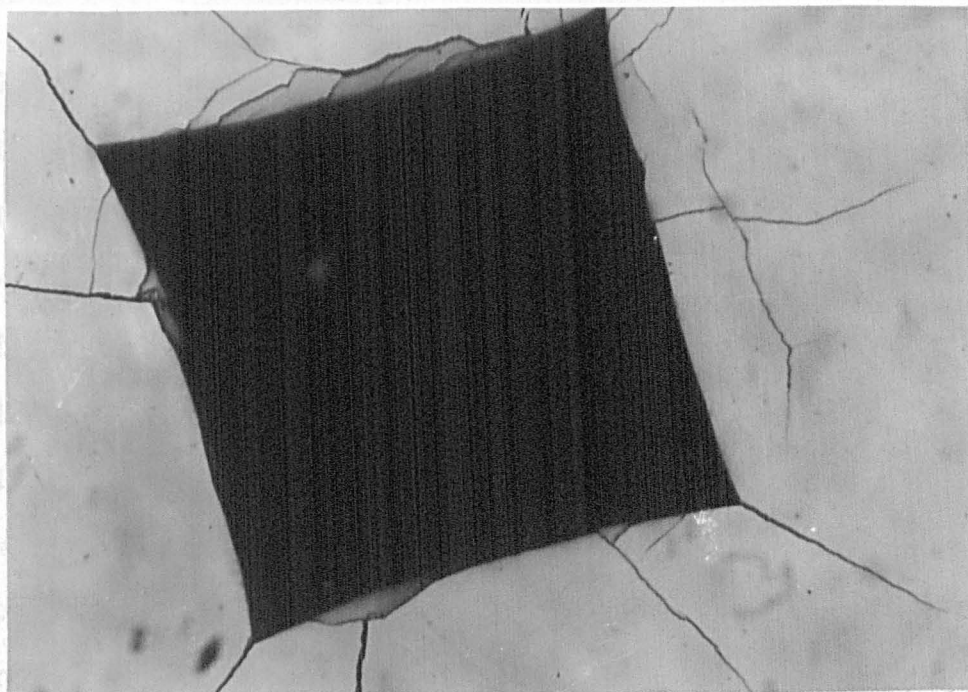


Fig. 38B Vickers diamond inprint on hydrided specimen showing crack propagation and indicating the brittle nature of TiH_2 (158)

different factors: ie. the nature of solution, material, temperature, microstructure, etc. It has also been shown that the nature of the surface in the later stages of hydrogen absorption, will be of significance owing to hydride formation and to its subsequent cracking.

It has been established that As increases the rate of H absorption in Fe and it was of interest to study whether this would apply for Ti cathodically polarised in acid solutions containing various concentrations of this promoter. This work has been supplemented by X-ray diffraction and X-ray microprobe analysis (JEOL).

7.7.2 Material and experimental procedure

The material used for metallographic study was pure Ti foil of 0.025 mm thickness supplied by Goodfellow Metals Ltd and 130 Ti sheet of 8 mm thickness. The foil and sheet were cut to form specimens of 10 x 10 x 0.025 mm and of 10 x 10 x 8 mm, respectively. Into the thick sheet a long brass nut of 1 mm diameter was introduced. This brass nut and all sides except one (10 x 10 mm) were laquered with 'Lacomite'. The remaining side was abraded on silicon carbide papers and then polished on 6, 1 and $\frac{1}{4}$ μ m diamond followed by a final polish using a slurry of γ - alumina suspended in 5% oxalic acid. Great care was taken to produce a completely flat surface. These thick specimens were

charged outside the cell, in a container in which the anode and cathode compartments were separated by a glass frit. The Ti was made the cathode and a Pt gauze the anode, and charging with hydrogen was carried out using 0.05M H_2SO_4 . The concentrations of As used were 2 ppm, 5 ppm and 10 ppm prepared from a stock solution of As_2O_3 dissolved in 0.05M H_2SO_4 . The same solutions were used for H_{abs} measurement using the PET. The specimens were the same as described in section 7.1.2.

In order to avoid changes in surface properties the specimens which were used for metallographic studies were used in the unetched condition. After cathodically charging the 8 mm thick specimen in the two compartment cell (charging time 9×10^3 s) they were rinsed in distilled water and then examined by a microprobe analyser.

The microprobe analyser uses a wave length dispersive system of analysis and the specimen is scanned with a narrow electron beam of approximately 1 μm dia, giving X-rays characteristic of the elements present, which are dependent on their atomic number. Light elements produce long wave length X-rays which are readily absorbed and hydrogen is therefore undetectable. The X-rays are resolved by a suitable diffracting crystal set at the appropriate Bragg angle and for this purpose either pentaerythritol set at $36^\circ 29'$

or quartz set at $48^{\circ} 32'$ was used, to detect the Ti K- α radiation.

The instrument was calibrated before use by recording the number of counts per second registered by a scintillation counter when a sample of pure Ti was scanned. The amount of Ti present in the specimen can then be estimated from the number of counts per second registered from the specimen, compared to that from the pure metal. To determine the distribution of As on the surface of the Ti a LiF crystal was used, the angle of incidence being $33^{\circ} 55'$. For determination of the state of the Ti-surface, electron back scattering experiments were performed and the influence of As on the formation of hydrides was studied by X-ray diffraction.

The apparatus used was a Philip's X-ray diffractometer using copper K- α radiation to determine the lattice spacings of pure Ti, titanium hydride and electro-deposited As. After examining the specimen they were rotated through 90° for a second examination to eliminate any effects attributed to preferred orientation in the specimen. The magnifications used in the microprobe analyses were x 300 and x 1000. The

experiments were only qualitative in nature, since it was only necessary to determine whether or not deposition of As occurred and the way in which As influenced hydride formation.

7.7.3 Results

The results obtained with the P.E.T are summarised in Figure 39, and as can be seen from curves 1 - 4 As in solution has a significant effect on the h.a.r on Ti. Curve 1 shows the hydrogen absorption rate in As-free acid the significant kinks K_1 and K_2 can be observed. However, additions of 2 ppm and 10 ppm As increase the rate of hydrogen absorption significantly, and it can be observed that no kinks can be seen in either, and that the curves are more linear than in the absence of As.

It can be seen that curves 1, 2 and 4 (Figure 40) have the same slopes in the initial stages of hydrogen absorption, but after 4×10^2 s there is a change in the slope of curve 1, indicating a

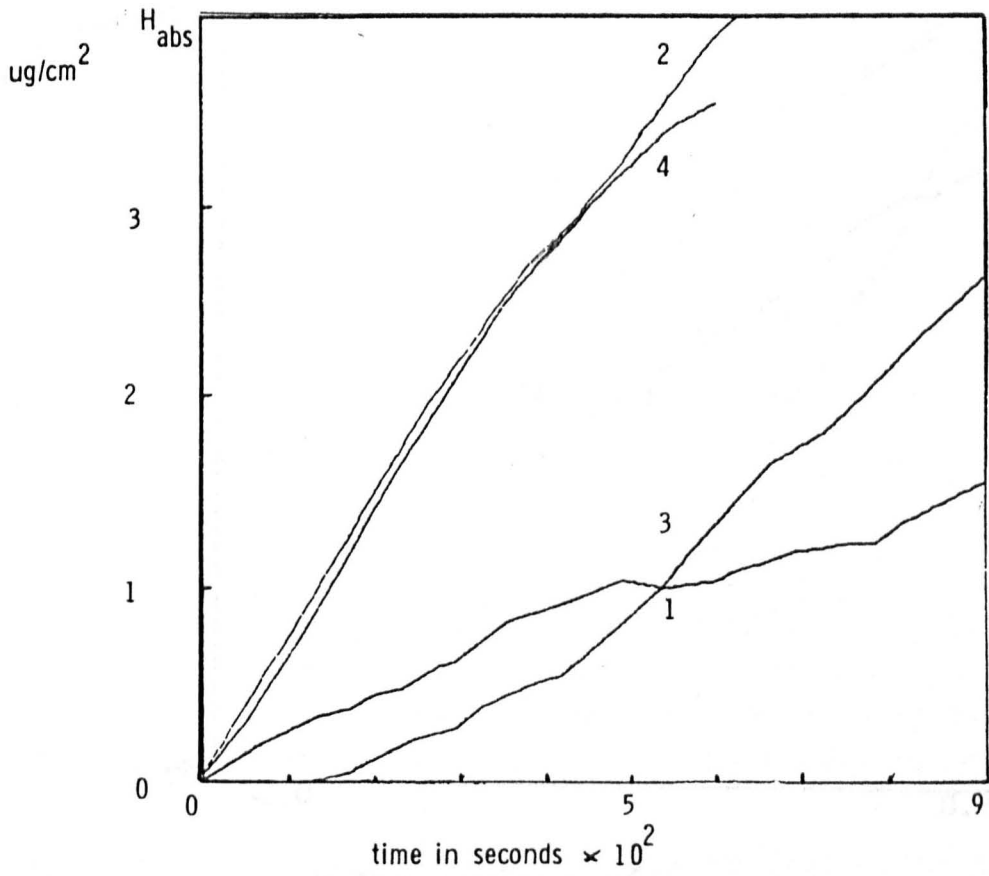


Fig. 39

Hydrogen absorption by Ti in 0.05 H_2SO_4 plus various concentrations of As in solution.

1. Ti - no As in solution
2. Ti - 2ppm As in solution
3. Ti - 5 ppm As in solution
4. Ti - 10 ppm As in solution

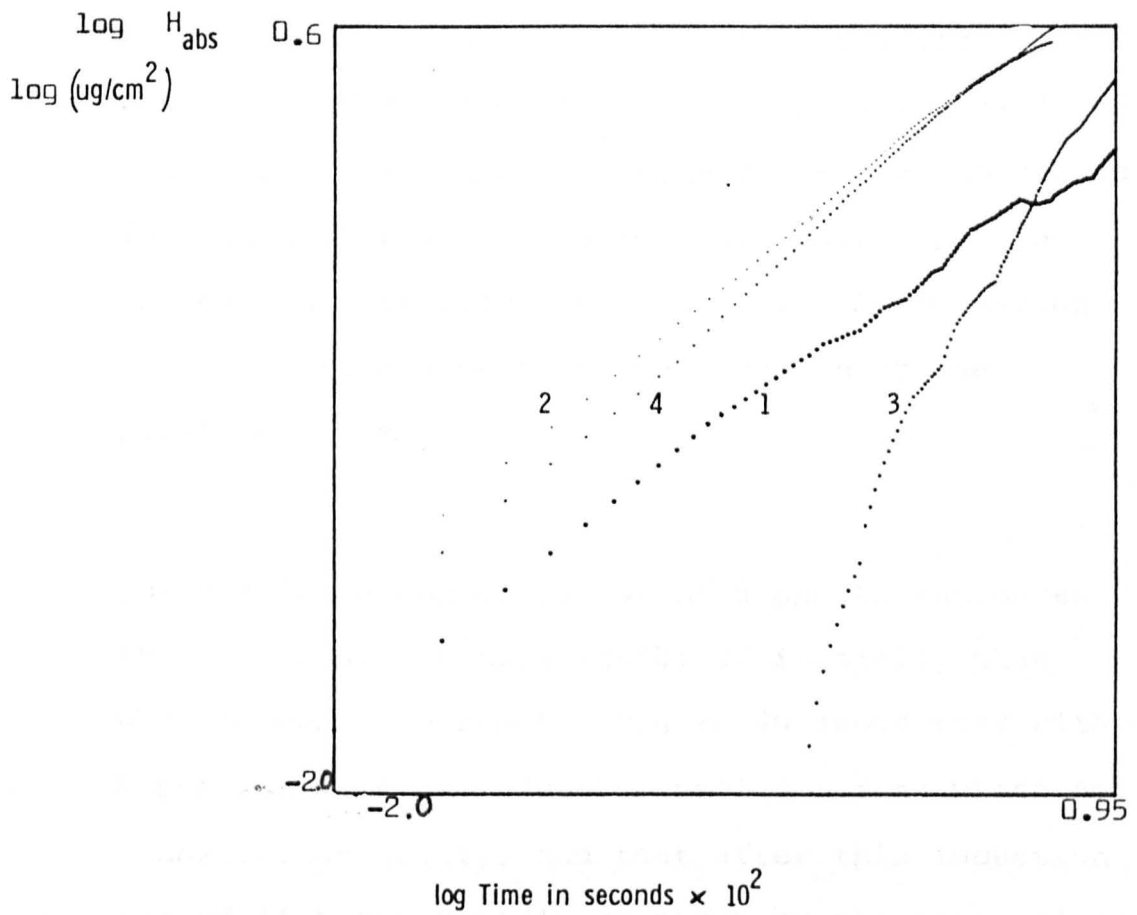


Fig. 40

Hydrogen absorption by Ti in 0.05 H_2SO_4 plus various concentrations of As in solution

1. Ti - no As in solution
2. Ti - 2 ppm As in solution
3. Ti - 5 ppm As in solution
4. Ti - 10 ppm As in solution

change in mechanism of the h.a.r. It would appear that the early stages of absorption follow different kinetics than the later stages in which it becomes controlled by the formation of the γ - hydride (see curve 1). In the case of the solutions containing As formation of γ - hydride appears to be hindered by the presence of As.

Curve 3 for a concentration of 5 ppm As indicates that the h.a.r is more inhibited initially than when 10 ppm is present. Figure 40 shows that with 5 ppm there is an induction period during which no H absorption occurs, and that after this induction period it rises rapidly as shown by the steep slope of curve 3. These results are not altogether surprising since Rhadhakrishnan and Shreir⁽¹⁰¹⁾ have shown that in the case of mild steel hydrogen absorption increases to a maximum and then decreases with increase in concentration of As. This has been established as due to deposition of elemental As at active sites.

These observations have been studied by examining the surface of the Ti by means of X-ray diffraction and microprobe analysis.

X-ray diffraction analysis of Ti specimens showed that after a period of cathodic charging with hydrogen of 180 mins duration γ - hydride could be detected at

the surface. But after introducing 2 ppm of As into the electrolyte, no hydride could be observed until after 720 mins of charging. Similar results were obtained with 5 and 10 ppm As in the electrolyte, showing that As has a pronounced effect in inhibiting the reaction of hydrogen with Ti to form γ - hydride.

The results of microprobe analysis are shown in Plates 41 - 44.

At 2 ppm As no deposited As was observed on the surface of the Ti nor was the diffraction pattern of Ti hydride detected when the surface was examined by X-rays. Thus As at this concentration appears to inhibit hydride formation. However, at 5 ppm it was evident that As had deposited at the grain boundaries. This can be seen by comparing Plate 45, an etched Ti specimen which clearly shows the grain structure of Ti, with Plate 41 which shows the surface of the Ti after charging in 0.5M H₂SO₄ + 5 ppm As.

The result of a microprobe analysis of the surface with respect to the concentration of As is shown in Plate 42, the separation of the two peaks corresponding to the average grain size. It should be noted that Plate 42 was taken at a higher magnification than Plate 41 and 45 to enhance the peaks due to As deposition.

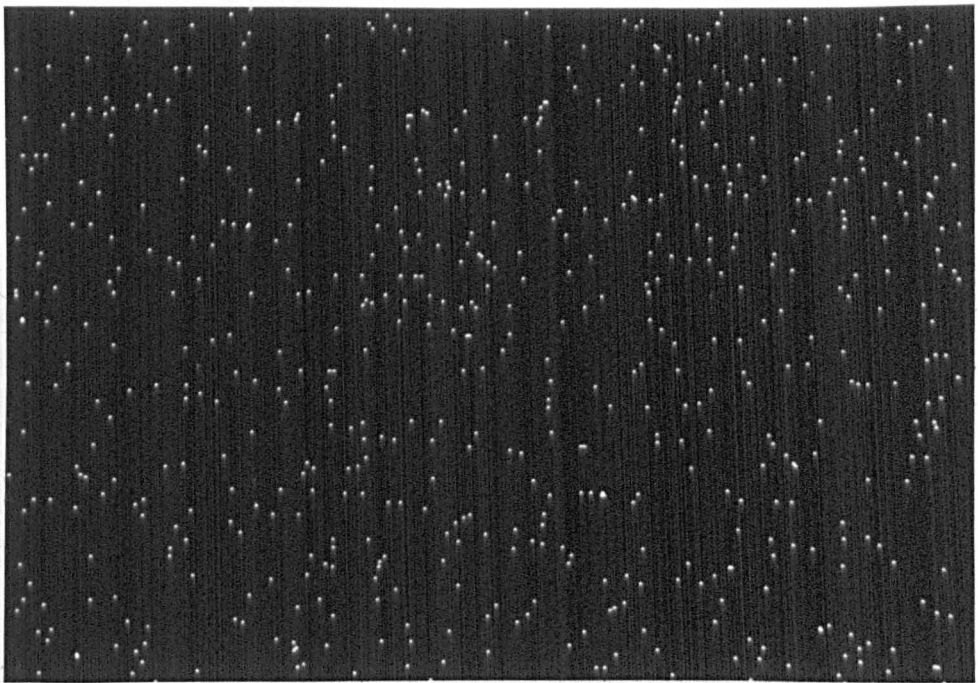


Fig. 41 Distribution of As over Ti surface after cathodically charging in 0.05 M H_2SO_4 + 5 ppm As ($\times 1000$)

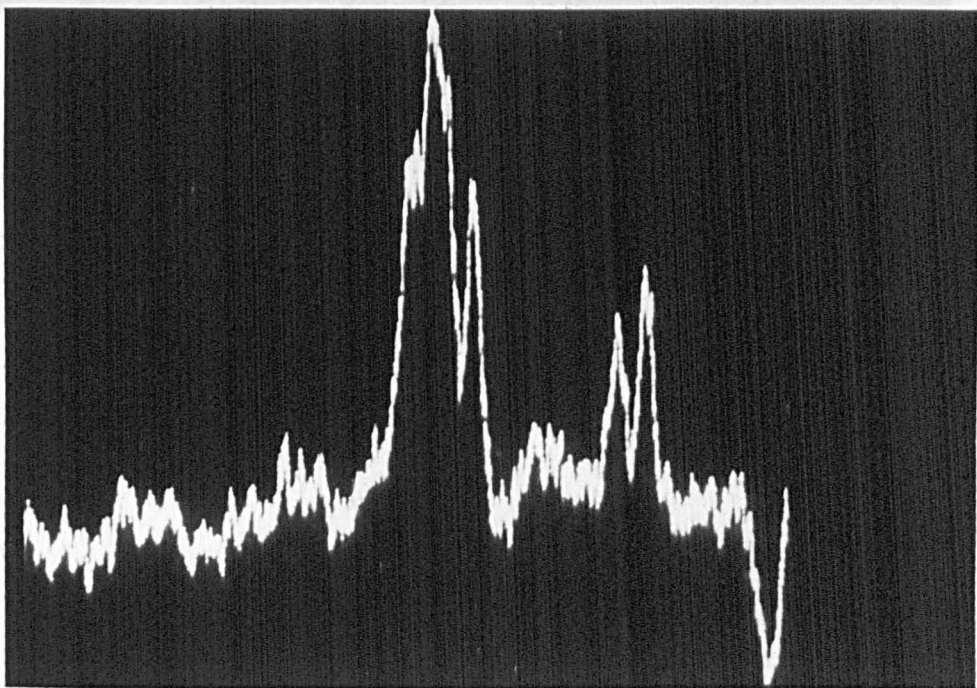


Fig. 42 Concentration profile of As. The distance of the two peaks corresponds with the average grain size. ($\times 2000$)

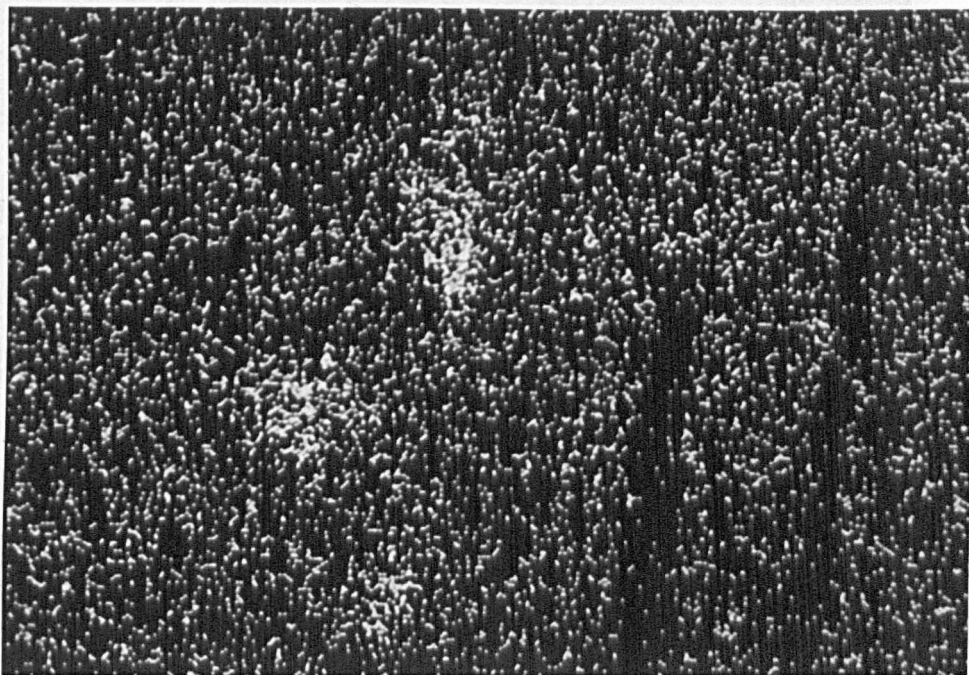


Fig. 43 Distribution of As after cathodically charging at
 1 mA/cm^2 in $0.05 \text{ M H}_2\text{SO}_4$ + 10 ppm As in solution
($\times 1000$)

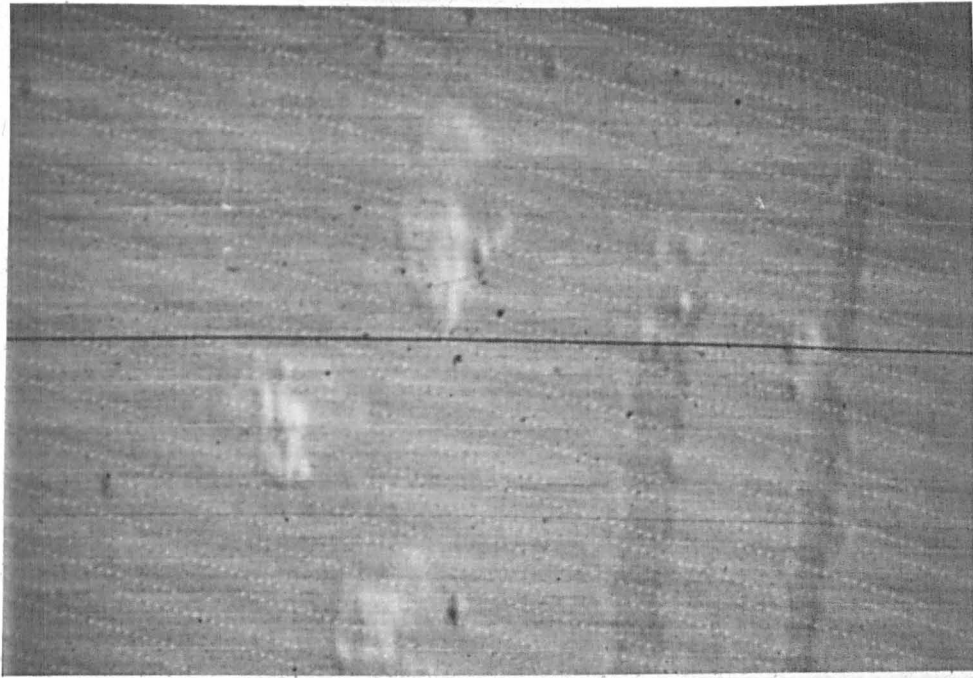


Fig. 45 Embryonation of pure titanium (× 1000)

Fig. 44 Structure of surface above Ti specimen (× 1000)

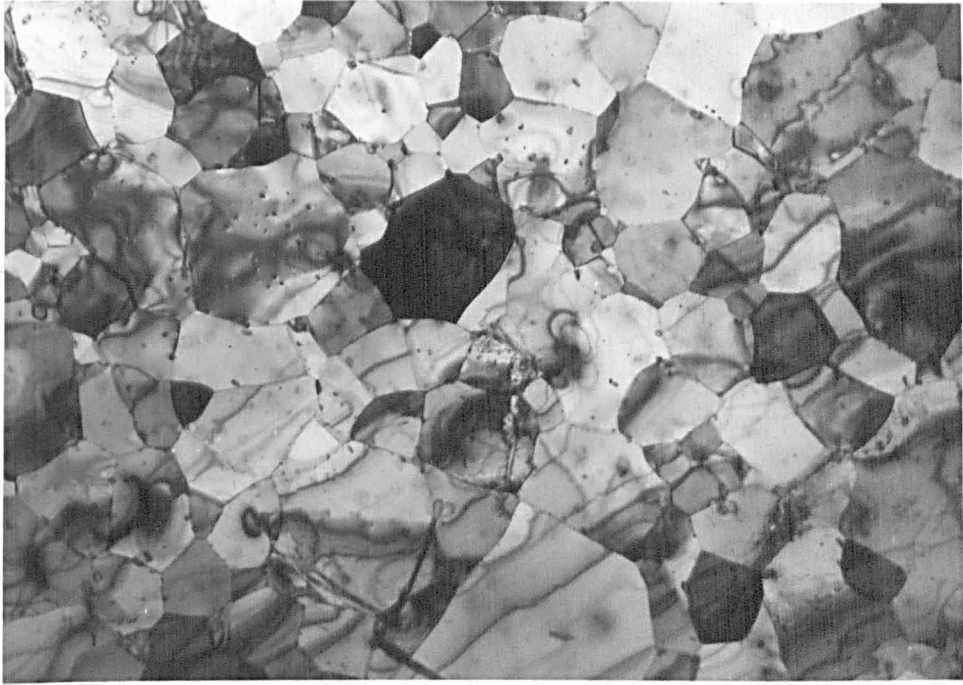


Fig. 45 Grainstructure of pure titanium (x 1000)

The average grain size was determined by counting the number of grains along one diagonal of Plate 45 and then dividing by the length of the diagonal. The grain size was also determined by X-ray diffraction and was established to be 4×10^{-3} cm.

Plates 43 and 44 show the microprobe analyses of Ti when 10 ppm of As was introduced into the electrolyte, and it can be seen from Plate 43 that As deposition occurs in a random manner, although three clusters indicating segregation of As appear in the l.h side of the picture, and there are two scratch-like areas at which As is absent on the r.h side. By looking at the surface using electron backscattering as in Plate 44, these clusters and the elongated areas can clearly be seen as strong disturbances of the surface geometry. Apart from these effects it would appear that deposition of As on the surface of Ti during cathodic polarisation in the acid containing 10 ppm As does not occur at preferred sites. The same results were obtained with solutions containing 15, 20 and 30 ppm As the only difference produced by these more concentrated solutions being the increase in the number of clusters on the surface.

7.7.4 Discussions and Conclusions

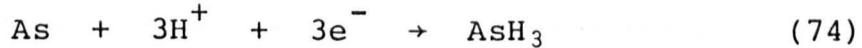
The values obtained by the P.E.T for hydrogen absorbed in Ti, when the electrolyte contains the H promoter As at different concentrations can be explained by considering the various steps involved.

1. If no As is present in the solution the h.a.r is controlled initially by the oxide film on the metal surface, but as cathodic charging continues the influence of the oxide film diminishes and absorption of H becomes controlled by hydride formation on the surface, which tends to block the active sites for H absorption, eg. grain boundaries. Thus after an initial period of charging the h.a.r becomes controlled by the growth of the Ti hydride. As the film of hydride thickens cracks are produced that allow access of H ions to the metal surface within these cracks, which thus determine the rate of the h.a.r.
2. If 2 ppm of As is present in the electrolyte the kinetics of the hydrogen absorption reaction change dramatically, and X-ray diffraction shows that hydride formation becomes inhibited.

Since no evidence of elemental As was found on the surface it is possible that the As ions are reduced to arsine. As in acid solutions is assumed to be present as AsO^+ , and the sequence of steps in which AsH_3 is produced may be represented as follows:



the electrodeposited As then being reduced cathodically to arsine.



This compound is thermodynamically unstable and tends to decompose into arsenic and hydrogen, and Moser and Bruhl⁽⁸⁵⁾ found that in aerated water brown precipitates were formed of either arsenic or a solid lower hydride. The E-pH diagram for As-H (Figure 46) shows that AsH₃ is unstable at E = -0.6 V vs SHE at pH 1-2, and will decompose following an equation proposed by Hicks⁽¹¹⁴⁾



However, in the present study using electron microprobe analysis no deposited As could be found when the concentration of As in the solution was only 2 ppm, suggesting that all the As was converted to arsine.

The As deposits on the surface in the elementary state. This cycle shown in equation 73 - 75 then repeats itself. This sequence of events occurs usually at the grain boundaries as was demonstrated by the detection of As at the grain boundaries in solutions of higher As concentration (5 ppm) by means of electron microprobe analysis and X-ray diffraction.

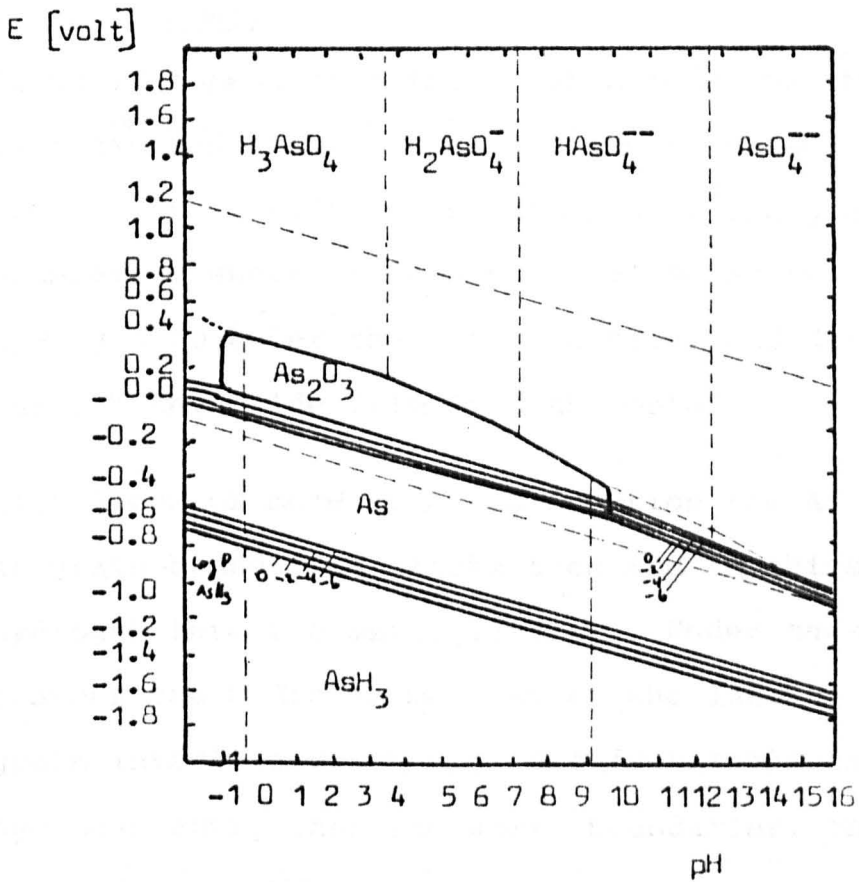


Fig. 46

Potential - pH equilibrium diagram for the arsenic - water system at 25°C

7.7.5 Summary

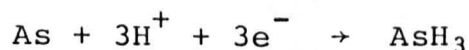
It would appear from the above discussion that cathodic reduction of the AsO^+ to form AsH_3 occurs and that this hydride is adsorbed at the grain boundaries where it decomposes allowing the hydrogen to enter the metal lattice, and diffuse through the oxide film into the metal.

With 5 ppm or more of As in solution the As deposited at grain boundaries blocks them and inhibits entry of hydrogen into the metal lattice. Under these circumstances the hydrogen must enter the lattice via the grain interiors which are less favourable sites for hydrogen entry than the grain boundaries, thus reducing hydrogen absorption.

At 10 ppm As in the electrolyte the Ti is fairly evenly coated with As which can then act as a collector for the hydrogen, and the kinetics of hydrogen absorption are controlled by the diffusion of hydrogen through this deposit. This explains the similar slopes of the curves 2 and 4 in Figure 40 for 2 and 10 ppm As, respectively. Curves 3 (5 ppm) and 4 (10 ppm) also shows the limitations of the P.E.T method if a secondary reaction takes up hydrogen or charge, since these losses will appear as absorbed hydrogen and thus give an erroneous high result.

Thus curves 3 and 4 in Figure 40 include charge consumed by hydrogen absorption plus the charge

consumed through cathodic deposition of As. By employing methods such as X-ray diffraction and electron-probe micro-analysis in conjunction with the P.E.T it was possible to establish the kinetics of H absorption even when elemental As is co-deposited with the hydrogen. In the case of curve 2, Figure 40, it would appear that no As deposition occurs although charge may be lost during the formation of AsH₃ by the reaction



7.8 Cathodic reduction of anodic oxide films on Ti

7.8.1 Introduction

From optical measurements⁽⁹⁴⁾ it appears that the oxide film formed on Ti in air at room temperature is about 1.7 nm thick after 2 h and 3.5 nm thick after 40-50 days. This growth follows either as logarithmic or inverse logarithmic law. All investigators^(88 - 92) agree that these air-formed films consist essentially of TiO₂ with a rutile structure, and that the lower oxides TiO₂ and Ti₂O₃ become detectable only at very high temperatures^(92, 93). A characteristic feature of titanium is its high solubility for oxygen, but below 500°C diffusion of oxygen into the metal lattice will be hindered by the oxide film on the surface⁽¹⁰¹⁾.

To produce different thicknesses of oxides on the surface of the Ti, heating Ti for extended periods over a range of temperatures is tedious, and an

Table 3. Thickness of oxide times on Ti
and related interference colours

Thickness of oxide (nm)	Wavelength (nm)	Colour
0	578	yellow
10	577	
20	579	
30	0	
40	466.8	blue
50	479	
60	483	
70	487	green
80	522	yellow
90	570	
100	573.6	
110	518.7	
120	605	red
130	00	
140	00	
150	469.6	blue
160	484.6	green
170	498.7	
180	547.6	yellow
190	560.5	
200	571.9	
210	594.2	Absorbing

easier way to achieve different thicknesses is to anodize it in a suitable electrolyte at various constant voltages. The thickness of the oxide film can be judged by the appearance of interference colours of the oxide film, and Table 3 shows the interference colours related to the thickness of the oxide film⁽⁹⁴⁾. For the measurement of the hydrogen absorption in Ti, if oxide films are present, three different thicknesses were produced 10-20 nm, 60 nm and 110 nm. All these films showed 1st and 2nd order colours. The anodizing of the pure Ti was performed in the cell shown in Figure 47. The electrodes were anodized at 60 V in 0.05M H₂SO₄ to give a given interference colour, which corresponded with a particular thickness and order. They were washed with distilled water and then introduced into the P.E.T cell. To obtain micrographs of the oxide film 130-Ti blocks were polished (see Chapter 4) and anodized as described above and then photographed at different magnifications (x 200, x 500, x 1200).

7.8.2 Results

As can be seen from Figure 48 the impression is created that there is an increase in hydrogen absorption with increase in the film thickness of the oxide, but this is misleading owing to errors introduced by electrochemical reduction of the anodic oxide film. Reference to the potential pH equilibrium diagram for the Ti-H₂O system indicates that titanium oxide

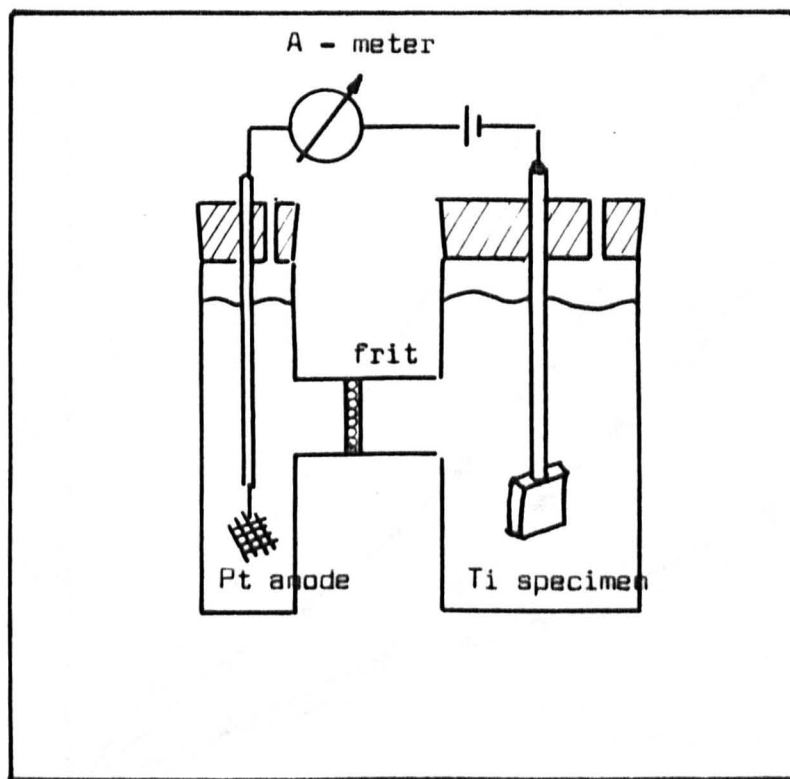


Fig. 47

Container for charging thick Ti - specimen

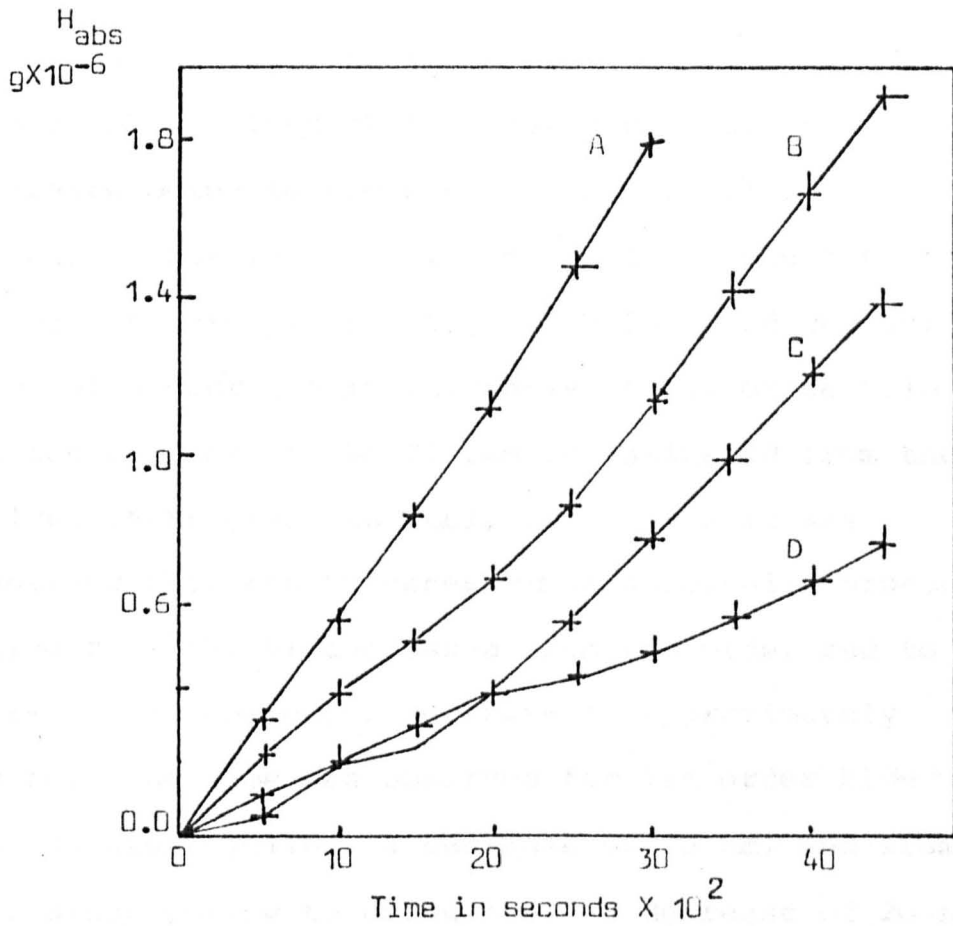


Fig. 48

Hydrogen absorption in anodized Ti

Curve	oxide film thickness, nm
A	110
B	60
C	10 - 20
D	air formed film

is not stable at potentials of - 0.6 to - 1.8 V and at pH 2, although this may not occur in practice owing to preferential H evolution however, observations of the colour of the specimen after cathodic polarization in H₂SO₄ produced evidence of a decrease in thickness of the oxide film on the surface of the Ti can be estimated from the colour chart given in Table 3⁽⁹⁴⁾ and it was observed that the thickness of an anodically produced oxide film (90 V) decreased from 2nd order red to first order yellow, a decrease of approximately 90 nm. The same was observed for 1st order blue to 1st order yellow, a decrease of 70 nm, and from 1st order yellow to colourless, a decrease of 20 nm. By assuming the reaction for the dissolution of rutile TiO₂ at potentials between - 0.6 and - 1.8 V at pH 2 to be:



It was possible to calculate the error introduced by the instability of the oxide film. Reaction ⁷⁵ was confirmed by adding H₂O₂ to the H₂SO₄, and the yellow colour produced showed that Ti²⁺ was present. (Ti³⁺ would give a violet colour.) At a cathodic c.d of mA/cm², at which the potential remains fairly stable at - 0.84 V (SHE) during the time of the experiment, it was possible to determine the charge consumed in electrochemically reducing a certain thickness of TiO₂ over a period of time of 5 x 10³(s): the thick-

ness was estimated from the change in colour.

The results obtained were for H_{abs} after 5×10^3 s.

Film thickness(nm)	20	60	110
Loss of charge(H in g)	4×10^{-6}	1.92×10^{-6}	2.81×10^{-6}

where the dissolution of TiO_2 calculated from the charge required to reduce TiO_2 to Ti^{2+} using equation 76

Film thickness(nm)	20	60	110
TiO_2 dissolved(H in g)	6.4×10^{-7}	1.9×10^{-6}	2.8×10^{-6}

Comparing both these results a great similarity can be observed which shows that in the case of 60 and 110 nm oxide film thickness all the charge is used to reduce the oxide film and no hydrogen absorption occurs.

It would appear that for hydrogen evolution and absorption, TiO_2 can be regarded as a cathodic depolariser. However, this effect only persists while the oxide film is greater than about 10 nm, and once the film decreases below this thickness it has no effect on hydrogen absorption. In the present work it was shown that if the cathodic current was switched off no further dissolution of the oxide film occurred even over a period of several days.

This could explain observations by Phillips and Shreir⁽⁷⁹⁾ that the anodic oxide film did not affect the kinetics of the h.a.r as evaluated by determining the H by solid state vacuum extraction.

Similar experiments were performed in the present work using Ti on which the 1st order blue oxide film was formed by high temperature oxidation at 800°C.

In the present study the Ti specimens were polarized at a high cathodic current for a time and under these conditions the anodic oxide film is removed according to equation 76. However, in the presence of a thermal oxide film the P.E.T gave no indication of hydrogen absorption into the metal, and no dissolution of the oxide film could be observed after 1 day, but after 4 or 5 days under cathodic polarization a partial flaking of the oxide was observed. It would appear that the thermal oxide film gives far greater protection against hydrogen absorption in 0.05M H₂SO₄ under cathodic polarization, than that given by anodic oxide films. This could be explained by the porous nature of the anodic oxide films as compared to the non-porous nature of the thermal oxide scale.

CHAPTER 8

8. HYDROGEN ABSORPTION IN Al

8.1 Introduction

Aluminium and the aluminium alloys lend themselves to many engineering applications because of their combination of lightness with strength, their high corrosion resistance, their thermal and electrical conductivity, their heat and light reflectivity, and their hygienic and non-toxic qualities. The variety of fabricated forms in which they are available also enhances their utility⁽⁹⁵⁾ .

Aluminium is a very reactive metal with a high affinity for oxygen, Shreir⁽⁹⁵⁾ . The metal is nevertheless highly resistant to most natural atmospheres and to a great variety of chemicals. Its resistance is due to the inert and protective character of the aluminium oxide film which forms on the metal's surface. In most environments, therefore, the rate of corrosion of Al decreases rapidly with time and in only a few cases, eg. in caustic soda, does the corrosion rate approximate to linear. A corrosion rate increasing with time is rarely encountered with Al, except in aqueous solutions at high temperatures and pressures.

The main interest in studying hydrogen absorption in Al is in relation to the possibility that this can give rise to hydrogen stress cracking at high strength Al alloys. This will be considered subsequently.

As far as the hydrogen evolution reaction is concerned, ample polarization data exist mainly for pure aluminium (99.9%) (96 - 104). However, it is well known that the polarization vs c.d relationship in aqueous media depends strongly on the impurities in the metal (96,100,101). Many workers have (103 - 105) stated that at neutral pH, hydrogen discharge occurs predominantly at precipitated impurities which are more electropositive than Al, resulting in local alkalisation and leading to the formation of pits. Conflicting accounts have been presented concerning the nature of attack in slightly acid solutions (101, 104, 107). Most of the work done on aluminium is concerned with cathodic polarization studies in different environments and very little work has been published on the rates of hydrogen absorption and the determination of the diffusion coefficient of hydrogen (D_H). The values available (summarised in Table 4) (108 - 112) give diffusion coefficients for Al that are valid only at very high temperatures. These have been determined mainly by Sievert's method, in which the metal is molten and the volume of the gas system above the molten metal is determined at a given temperature and pressure. This volume is referred to as the 'hot volume'. The system is then evacuated and a known quantity of H gas is introduced into the system at the same temperature. After certain intervals of time the decrease in the pressure of H gas is measured by a pressure gauge, and from the difference between the two volumes it is possible to calculate the amount of gas absorbed into the molten metal.

Table 4. Diffusion coefficients for aluminium at high temperatures obtained by various workers

$D(\text{cm}^2/\text{s})$	$T(^{\circ}\text{C})$	$D_0(\text{cm}^2/\text{s})$	Method	Ref.
	400-630	3.8×10^{-2}	Vacc.Extr.	108
	450-600	1.2×10^5	"	108
	450-600	1.2×10^{-9}	"	109
	450-600	0.12	"	109
	450-600	1.1×10^{-5}	"	109
1.13×10^5	570		"	110
1.26×10^5	585		"	110
1.47×10^5	600		"	110
1.62×10^5	615		"	110
1.86×10^5	630		"	110
	570-630		Capillary	113
0.7586×10^3	943		"	112
0.8670×10^3	960		"	112
1.365×10^3	1018		"	112
2.438×10^3	1103		"	112
3.631×10^3	1173		"	112
4.786×10^3	1228		"	112
5.623×10^3	1258		"	112

The data obtained in this work for determining hydrogen solubility and diffusivity in the hot solid state using extracting method, in which D_0 is determined by charging a specimen with H in a Sieverts' type apparatus, and then vacuum extracting the hydrogen from the metal.

The problems encountered using vacuum extraction have been discussed in the literature, and for example Brandt (5) reported that one of the most difficult problems in determining the true hydrogen content of aluminium is control of the surface gas, i.e. hydrogen gas adsorbed by the oxide film. He prepared specimens by charging the Al cathodically with hydrogen gas, and prior to vacuum extract-

Several variations of this method are still used to measure H - absorption rates in Al. The advantage of using a molten metal under vacuum is that the kinetics of absorption are not affected by continuous protective films of oxide. This removal of the oxide film on aluminium is important for desorption and absorption studies which are both affected by the oxide film.

Hydrogen effusion from the metal is affected by the oxide film, and this in turn affects the rate of H - diffusion within the bulk material. This combined with the low solubility of H in Al, makes it very difficult if not impossible to employ a desorption method such as the Devanathan cell method for determining diffusion coefficients. One other obstacle is the danger of pitting of the very thin Al foils that must be used in the Devanathan cell. These effects are described by several authors^(113 - 115). The third established method for determining hydrogen solubility and diffusivity is the hot solid state vacuum extraction method, in which D_H is determined by charging a specimen with H in a Sieverts type apparatus, and then vacuum extracting the hydrogen from the metal.

The problems encountered using vacuum extraction have been discussed in the literature, and for example Brandt⁽⁵⁾ reported that one of the most difficult problems in determining the true hydrogen content of aluminium in control of the 'surface gas', ie. hydrogen gas absorbed by the oxide film. He prepared specimens by charging the Al cathodically with hydrogen gas, and prior to vacuum extract-

ion the oxide film was removed by dry machining in C.P benzene. The disadvantage of this technique is the impossibility of obtaining any exact details of the kinetics of the hydrogen absorption and the rate controlling factors, since removal of the oxide film must also have removed the surface layers of Al in which there would be the high concentration of H. The second obstacle in determining the true H content within Al using the hot vacuum extraction method will be the temperature of 550° - 650°C used in this method. Magnesium which is present even in high-purity Al at very low concentrations (100 ppm) will evaporate rapidly under these conditions and will then be deposited on the cooler parts of the apparatus where it will act as a getter for hydrogen gas by reacting to form MgH_2 . This effect will diminish the quantity of H gas measured quite significantly and to an extent that is dependant on the quantity of Mg present in the Al rather than on the actual amount of H present, thus the presence of an oxide film on the surface and the presence of Mg in the Al make the use of solid-state hot-vacuum extraction very unreliable.

Because the piezo-electric technique is based on absorption of hydrogen and not on desorption it is possible to monitor the absorption of hydrogen continuously, and the limitations inherent in the vacuum - extraction method and the Devanathan cell method do not apply. It is evident, therefore, that the P.E.T is particularly suitable for measuring hydrogen absorption by metals that have stable oxide films on the surface.

8.2 Material and Experimental

The material used was pure Al (supplied by Goodfellow Metals Ltd), which had been pre-annealed by the supplier. Its nominal composition and the thicknesses of the foils are given in Table 5.

Table 5. Maximum impurities and thicknesses of Al specimens

Material	Purity(%) [*]	Thickness(mm)	Cu	Fe	Mn	Si	Zn(ppm)
Al	99.6	0.0015)				
Al	99.6	0.003)				
Al	99.6	0.006)				
Al	99.6	0.008)	1000	7000	1000	500 1000
Al	99.99	0.010)				
Al	99.99	0.015)				
Al	99.5	0.025	(household foil)				

*The purity of Al given is the minimum figure.

The electrodes were cut to 0.5 x 1 cm, a copper lead attached by spot-welding and the specimens were then ultrasonically cleaned in benzene. Determination of hydrogen absorption was carried out in the piezo-electric cell in which the specimens were cathodically polarized at 1mA/cm² in 0.05M H₂SO₄.

8.3 Effect of thickness of foil on D_H in Al and Fe

Aluminium foils of different thicknesses were polarized at a constant c.d of 1mA/cm², and it can be seen from Figure 50 that the rate of H absorption (slope of H_{abs} vs t curve) increases with foil thickness. These unusual results confirm the work of Frank et al⁽¹¹⁵⁾ who found using iron foil membranes that when the membranes had thicknesses less than

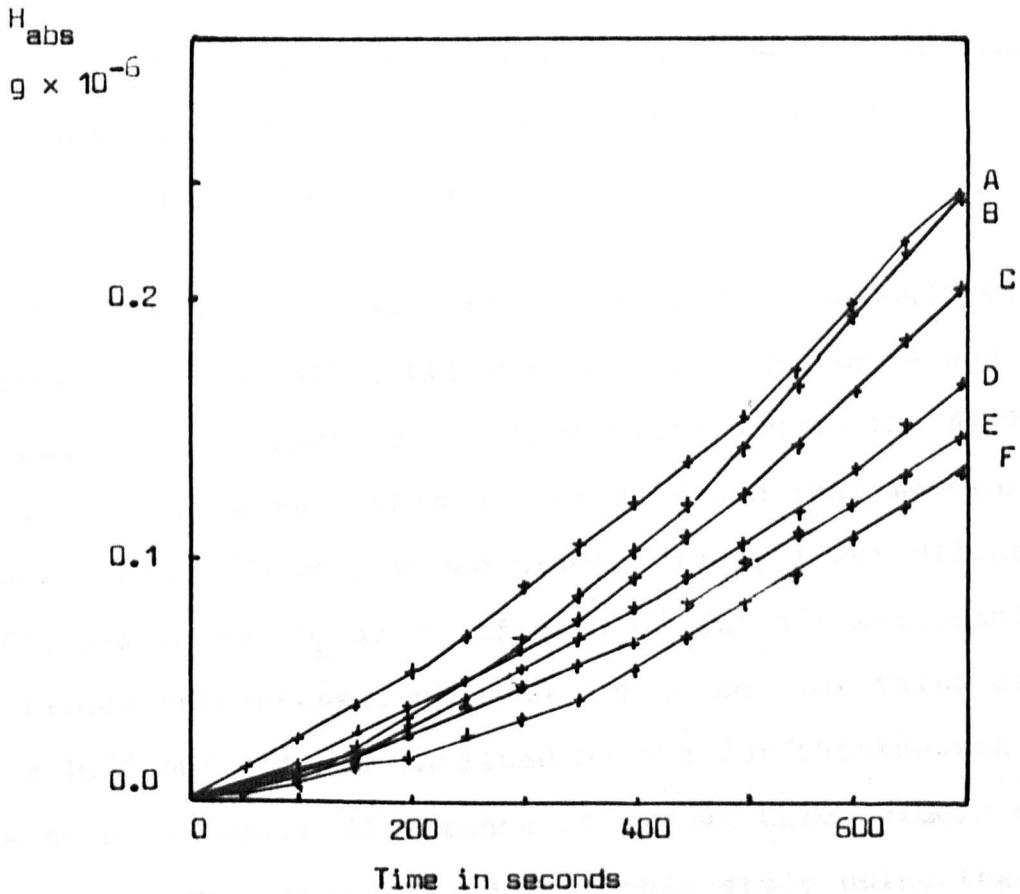


Fig. 50

Hydrogen absorption in aluminium foils of different thicknesses

A = 0.015 mm

B = Al - 3Mg = 0.0025 mm

C = 0.0125 mm

D = 0.008 mm

E = 0.006 mm

F = 0.0015 mm

0.8 mm the diffusion coefficients were much smaller than those obtained with thicker specimens (all other conditions being identical).

This thickness effect was investigated independently by Raczynski⁽¹¹⁶⁾ at 90°C, who used cathodic hydrogen and the time - lag method in his investigations on the diffusion of H in pure Fe. This author reported that membranes thinner than 0.77 mm yielded progressively lower diffusion coefficients, eg. D_H in Fe of $2 \times 10^{-5} \text{ cm}^2 \text{ s}^{-1}$ was obtained for larger thicknesses, whereas a much smaller value of $7.0 \times 10^{-8} \text{ cm}^2 \text{ s}^{-1}$ was obtained by him for thicknesses less than 0.1 mm, a difference of almost three orders of magnitude. Work performed during this study using the Devanathan method for pure Fe foils of a thickness of 0.5 mm gave a $D_H = 6 \times 10^{-5} \text{ cm}^2 \text{ s}^{-1}$, whereas for foils of 0.08 mm $D_H = 2 \times 10^{-7} \text{ cm}^2 \text{ s}^{-1}$ was obtained. No results can be given for thinner foils because of the danger of pinholes within the foil which makes the technique used very unreliable. Using the P.E.T the value obtained for pure Fe (Figure 51) for thicknesses > 0.1 mm was established to be $2 \times 10^{-6} \text{ cm}^2 \text{ s}^{-1}$, which is in very good agreement with values given in the literature. The equilibrium solubility in Fe was determined as $S_H = 1 \times 10^{-2} \text{ g H}_{\text{abs}}/\text{g Fe}$. The anomalous thickness effect has also been reported for iron by Palczewska and Ratajczk⁽¹¹⁷⁾ who observed the passage of hydrogen produced from the gas phase by a high voltage discharge.

IMAGING SERVICES NORTH

Boston Spa, Wetherby

West Yorkshire, LS23 7BQ

www.bl.uk

**PAGE MISSING IN
ORIGINAL**

H_{abs}
 $g \times 10^{-6}$

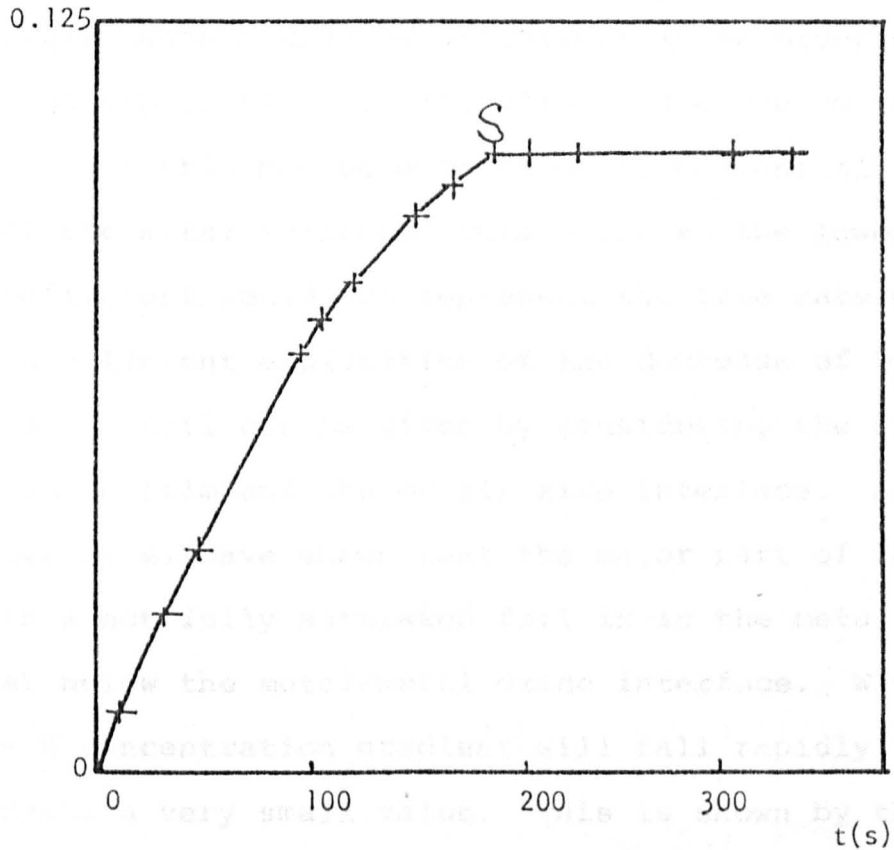


Fig. 51

Hydrogen absorption in Fe-foil
of 0.005 cm at 1 mA/cm².

An important phenomenon observed in their work was the low D_H obtained on fully out-gassed membranes; D_H values obtained after precharging were higher by approximately an order of magnitude. One explanation of this effect is given by Wach⁽⁶²⁾, who considers that this may be attributed to mechanical distortion of the metal surface. This being so the lower diffusion coefficient would not represent the true rate of diffusion. A different explanation of the decrease of D_H with thickness of foil can be given by considering the effect of both the oxide film and the metal/oxide interface. Studies of Al by Bauer et al have shown that the major part of the absorbed H in a not fully saturated foil is in the metal situated just below the metal/metal oxide interface. Within the foil the H concentration gradient will fall rapidly until it attains a very small value. This is shown by the schematic diagram Figure 52A, in which the initial positive slope of the C_H vs thickness curve is due to rapid loss of H by effusion from the metal's surface. This surface effect can be neglected if the surface area/volume ratio of the metal is small (ideally a sphere), but will become of increasing significance as the ratio increases, tending to a maximum in an extremely thin foil. The effect will be enhanced if charging and H absorption take place on both sides of the foil; similar effects occur in heat transfer from one side to the other of a metal plate, and in the capacitance of a foil which has a dielectric film on both sides of a foil of a 'valve' metal.

In the case of Al this anomalous thickness effect was observed only when the foil was $> 20 \mu\text{m}$.

Table 6. Diffusion coefficients obtained using different methods with membranes of various thicknesses

Membrane thickness d cm	Apparent D cm ² sec ⁻¹	Material	Source	Ref.
0.076	5.0 x 10 ⁻⁶	mild steel	Frank, Swets & Fry	115
0.012	1.4 x 10 ⁻⁸	mild steel	Alikin	118
0.02	3.8 x 10 ⁻⁷			
0.042	2.0 x 10 ⁻⁶			
0.078	3.4 x 10 ⁻⁶	mild steel	Palczewska & Ratajczyk	117
0.12	3.1 x 10 ⁻⁶			
0.16	2 x 10 ⁻⁶	mild steel	Schuetz & Robertson	119
0.1	2.8 x 10 ⁻⁶	mild steel	Veysseyre, Azou & Bastien	67
0.0254	2.3 x 10 ⁻⁷	mild steel	Davis	120
0.077	-	iron	Devanathan & Stachurski	102
0.017	2 x 10 ⁻⁷	iron	Kuznietsov & Subbotina	121

Table 6A Diffusion coefficients for hydrogen in
 α -iron and mild steel

D ($\text{cm}^2\text{sec}^{-1}$)	Material	Authors	Ref.
4.28×10^{-8}	iron	Barrer	122
1.5×10^{-5}	iron	Sykes, Burton and Gegg	123
1.64×10^{-5}	iron	Geller and Sun	124
4.2×10^{-6}	iron	Stross and Tompkins	125
8.6×10^{-6}	iron	Stross and Tompkins	12
8.2×10^{-6}	iron	Eichenauer et al	126
6.4×10^{-6}	mild steel	Smialowski	127
5.0×10^{-6}	mild steel	Frank, Swets and Fry	115
4.4×10^{-7}	mild steel	Frank, Swets and Fry	115
1.0×10^{-5}	iron	Raczynski	116
4.4×10^{-6}	iron	Johnson and Hill	118
2.2×10^{-7}	iron	Johnson and Hill	128
1.6×10^{-5}	iron	Raczynski and Stelmach	129
4.6×10^{-6}	iron	Wagner and Sizmann	130
5.0×10^{-7}	mild steel	Eschbach et al	131
6.26×10^{-5}	iron	Bryan and Dodge	132
3.4×10^{-7}	mild steel	Plusquellec et al	133
4.0×10^{-7}	iron	Schwarz and Zitter	134
6.25×10^{-5}	iron	Beck et al	135
2.7×10^{-5}	iron	Heumann and Primas	136
5.5×10^{-5}	iron	Guntherschulze et al	137
8×10^{-6}	iron	Guntherschulze et al	137
2×10^{-6}	mild steel	Schuetz and Robertson	138
5×10^{-7}	iron	Baranowski et al	139
3×10^{-7}	mild steel	Palczewska and Ratajczyk	117
2×10^{-6}	mild steel	Palczewska and Ratajczyk	117
1.4×10^{-8}	iron	Alikin	140
2.9×10^{-6}	iron	Veysseyre, Azou and Bastian	67
8.3×10^{-5}	iron	Devanathan and Stachur- ski	102

H concentration

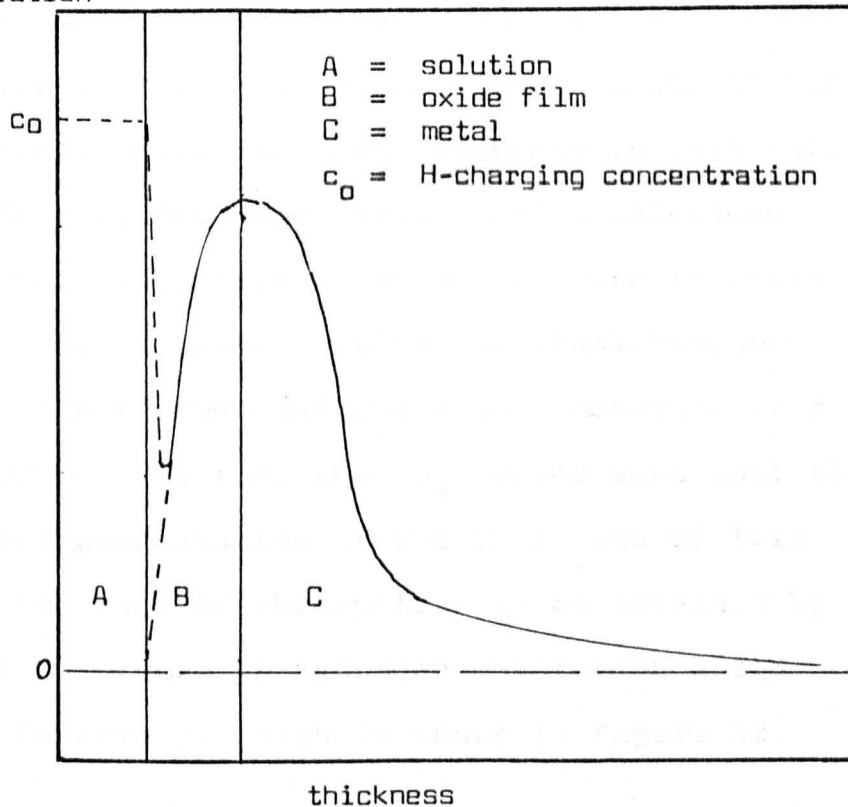


Fig. 52A Schematic diagram of H concentration :
within Al foil.

diffusion coefficient is not sufficient to explain the fact that the rate of H absorption in Al foil is independent of foil thickness. It is suggested that the rate of H absorption in Al foil is controlled by the rate of H diffusion in the oxide film. The rate of H diffusion in the oxide film is independent of foil thickness because the diffusion coefficient of H in the oxide film is very small. The rate of H diffusion in the metal is independent of foil thickness because the diffusion coefficient of H in the metal is very large. The rate of H absorption in Al foil is independent of foil thickness because the rate of H diffusion in the oxide film is independent of foil thickness.

6.3 Hydrogen Absorption in Aluminum Foil

Commercial Al foil is of relatively high purity, but it is probable that in comparison with pure foil the rolling texture and the thicker oxide film on the surface will have some effect on the rate of H absorption. Experiments

8.4 Aluminium Foils

To prove the validity of this theory, experiments were carried out on Al foils of various thicknesses as described in the last section. As can be seen from Figure 50 the rate of absorption decreases with decrease in foil thickness, which follows from the theoretical predictions discussed above. Extensive experimental work is still required to quantify these results for aluminium, but the experiments performed and the values obtained from the literature support the fact that D_H varies with foil thickness. A better presentation of the influence of foil thickness on the rate of absorption can be obtained by plotting foil thickness vs hydrogen absorption after various time intervals, which is shown in Figure 52.

It can be seen that with Al the region of a low diffusion coefficient is reached when the foil thickness is less than 0.0015 cm and to stabilise this diffusion coefficient a rapid drop in the rate of absorption at the surface of the metal has to occur. Thicker foil of thicknesses > 0.0015 cm have very little or no influence on the diffusion of hydrogen atoms, and a constant diffusion coefficient at constant temperature and current density will be obtained, irrespective of thickness.

8.5 Hydrogen absorption in domestic Al foil

Domestic Al - foil is of relatively high purity, but it is probable that in comparison with pure foil the rolling texture and the thicker oxide film on the surface will have some effect on the rate of H absorption. Experiments

Foil thickness

(mm)

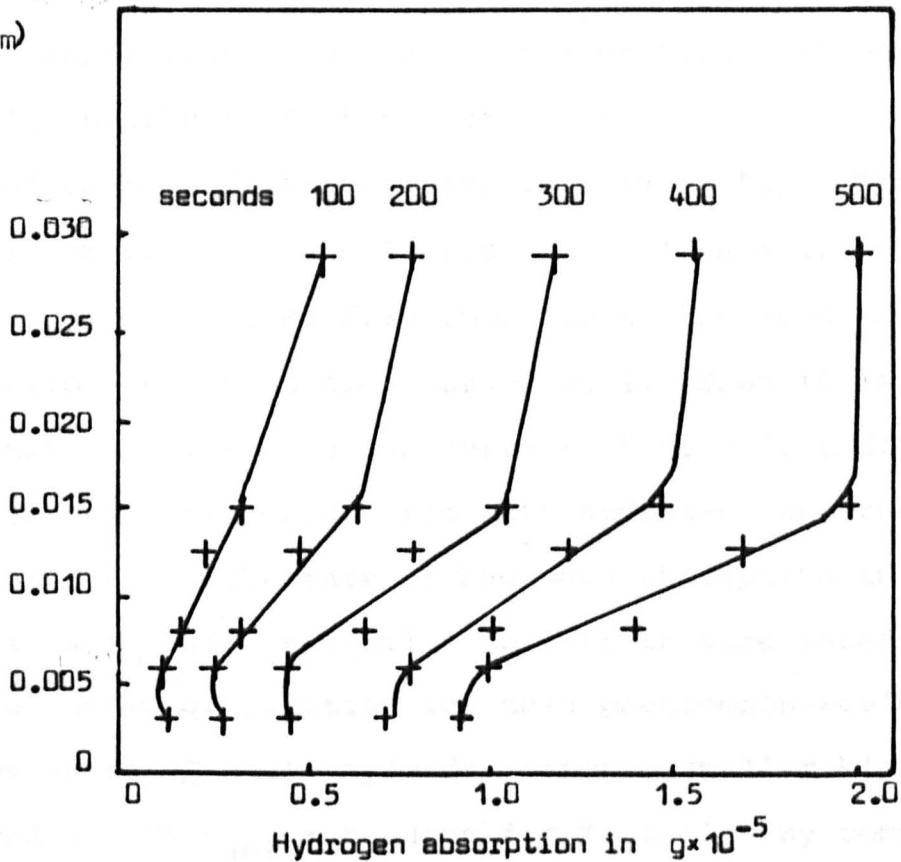


Fig. 52

Influence of foil thickness on hydrogen absorption after a given time

... pure aluminum with that in beryllium
 Figure 52 showing that after 100 seconds it can be shown
 that over a foil thickness of 0.015 mm the hydrogen absorption
 increases sharply. This is due to the fact that aluminum hydroxide
 stands in the way of hydrogen, therefore, to explain this
 difference in the absorption of an unstable Al-hydride (AlH₃)
 at the oxide-metal interface as an intermediate step. This
 hydride will decompose rapidly and will give up hydrogen
 into the metal lattice. Following this theory, the rate
 of H absorption into aluminum should be controlled by the
 formation and the decomposition of AlH₃ at the metal/oxide
 interface



with this foil showed that the time taken for a steady rate of absorption to occur is greater than that obtained with high purity foil of the same thickness, although the rates of absorption are comparable (Figure 53). This initial non-linearity indicates the influence of the relatively thick oxide film compared to the much thinner oxide film present on high purity foil. Thus it is possible that the kink K₁ on the curve in Figure 53 indicates saturation of this oxide film with hydrogen, and that once this occurs the rate of hydrogen absorption in a domestic foil will be similar to that in pure annealed foil. An alternative explanation for this phenomenon would be the formation of an Al hydride, since a smaller kink was observed on the H_{abs} - t curve for Ti foil. By comparing hydrogen absorption in pure aluminium with that in Duralumin (Figure 54), and taking short time intervals it can be shown that even for pure Al the rate of diffusion does show irregularities, whereas the H_{abs} rate for Duralumin increases steadily. It is possible, therefore, to explain this difference by the formation of an unstable Al-hydride (AlH₃) at the oxide-metal interface as an intermediate step. This hydride will decompose rapidly and will give up hydrogen into the metal lattice. Following this theory, the rate of H absorption into aluminium should be controlled by the formation and the decomposition of AlH₃ at the metal/oxide interface



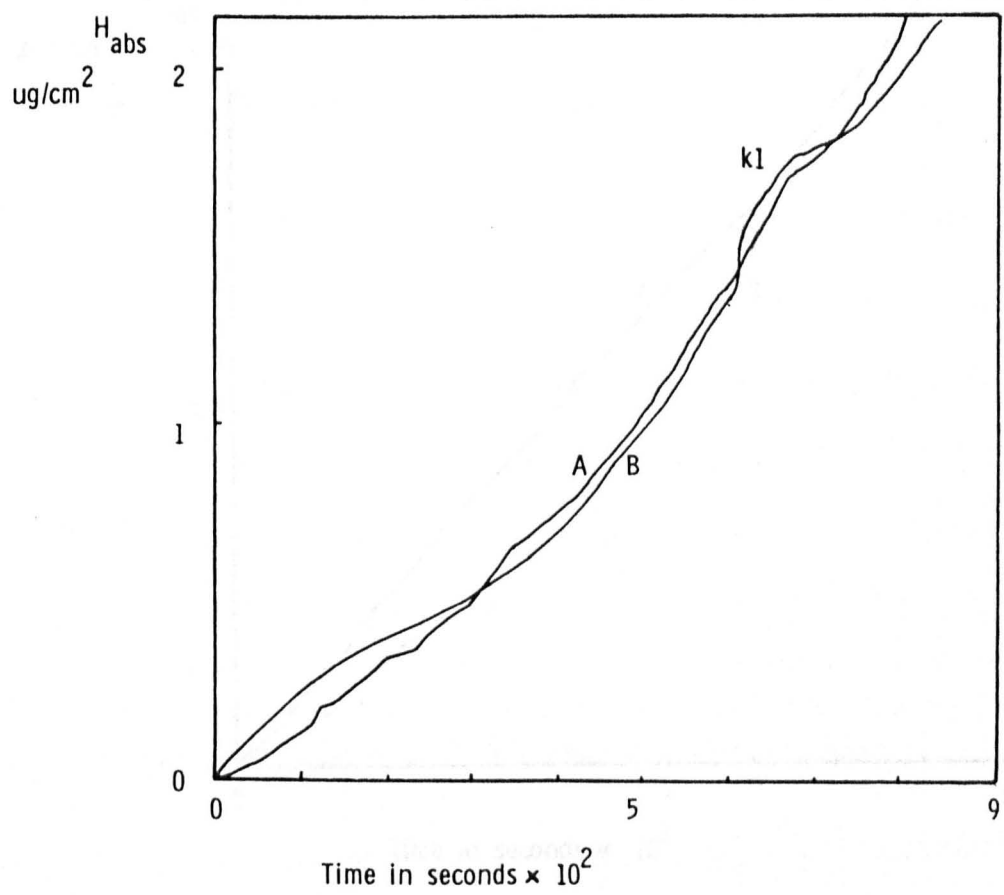


Fig. 53

Hydrogen absorption in Al (A) and household foil (B)

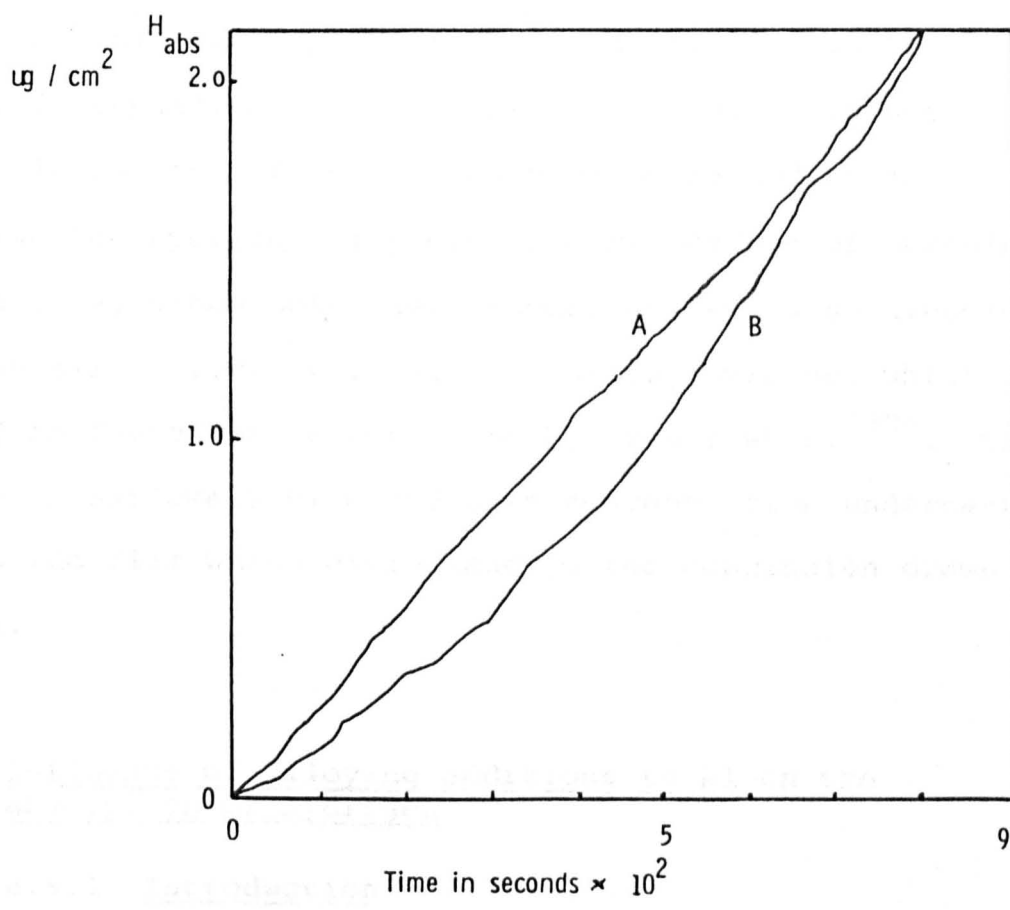


Fig. 54

Hydrogen absorption in Al (B) and Duralumin (A)

In the first part of the report it is proposed that crack propagation is caused by the preferential distribution of the metal atoms at a grain boundary (141) attributed cracking to preferential dissolution of the grain boundary precipitates. This was recently confirmed by Sedriks et al (142) who suggested that preferential adsorption of hydrogen at grain boundaries leads to rupture of the passive film and subsequent local dissolution of the PPF.



IMAGING SERVICES NORTH

Boston Spa, Wetherby
West Yorkshire, LS23 7BQ
www.bl.uk

**PAGE MISSING IN
ORIGINAL**

The difficulty in supporting this theory lies in the rapid decomposition of the hydride so that it is not possible to study this by a desorption method or to observe the hydride using electron microscopy or scanning microscopy, since both these techniques would be hindered by the oxide film. The only supporting evidence which could be found was in work done by Brauer et al⁽³⁰⁾. They found an extremely high hydrogen concentration underneath the oxide film which could lead to the conclusion drawn above.

8.6 Influence of alloying additions to Al on the absorption of hydrogen

8.6.1 Introduction

It is well known that high-strength precipitation-hardened aluminium alloys are susceptible to intergranular stress corrosion cracking (SSC) in environments ranging from moist air to various aqueous solutions, and mechanisms which have been proposed fall into three classes.

In the first category it is proposed that crack propagation occurs by preferential dissolution of the metal at the crack tip. Dix⁽¹⁴¹⁾ attributed cracking to preferential dissolution of the grain boundary precipitates, while more recently Sedriks et al⁽¹⁴²⁾ suggested that preferential slip in the precipitate-free zone (PFZ) would cause rupture of the passive layer and subsequent local dissolution of the PFZ.

The second group of theories consider that the crack propagates by mechanical fracture. The most recent mechanical model for SCC is based on hydrogen embrittlement of the lattice. Speidel⁽¹⁴³⁾ has shown that cracking of high strength aluminium alloys takes place in gases containing water vapour and has this attributed to hydrogen entry into the matrix^(144 - 151). Koch⁽⁷⁸⁾ proved that high-strength Al alloys are susceptible to hydrogen embrittlement by ionizing molecular H between a tungsten electrode and an aluminium specimen. The positively charged ions moved towards the specimen's surface and penetrated the oxide film.

Aluminium hydride has been reported to be unstable in environments containing moisture⁽¹⁴⁸⁾. Therefore, it is difficult, if not impossible to detect hydrides after the specimen has been exposed to laboratory air. It appeared from Koch's work that the porous layer which resulted from the sputtering inhibits hydrogen entry into the lattice.

In the present work the effects of alloying additions to Al have been studied to determine how they affect the rate of H absorption.

8.6.2 Material and Experimental

The aluminium alloys were supplied by Goodfellow Metals Ltd in the pre-annealed form. The electrodes were cut into shape, and cleaned as described in Chapter 5.

Their nominal compositions were:

Electrode	Cu	Cr	Fe	Mg	Sn	Zn	Ti (ppm)
Al-3Mg	1000	5000	500	2.5-3.5%	500	2000	1000
Al-5Mg	1000	4000	300	4.5-5.5%		1000	
Al-4Cu-1Mg	3.8-4.4%		100	0.8-1.3%			

The thickness of the foils was 0.025 mm.

Duraluminium ^{was} workhardened, no heat treatment was applied, no further information was obtainable from Goodfellow metals.

8.6.3 Results and Discussions

As can be seen from Figure 55, curve C for Al, which has been discussed in Section 8.4 has the lowest rate of hydrogen-absorption in comparison with Al-3Mg and Al-5Mg. The appearance of curve C has been discussed in detail in the previous Chapter. Alloying additions of Mg increase the rate of H absorption significantly, as can be seen from curves 1 and 2, and this can be explained by the possible formation of the compound MgH_2 at the grain boundaries and/or by solubility of H in the Mg. It can be seen from the kinks K1 and K2 in curves 1 and 2 that hydride formation is possible. This was established by Tuck⁽¹⁴⁹⁾ who found a layer of corrosion product along internal grain boundaries in Al/Mg alloys. This product which surrounded each grain consisted of a complex mixture of AlH_3 , $Al(OH)_3$, MgH_2 and diaspore $Al_2O_3 \cdot H_2O$.

This hydride formation and the fact that it proceeds along grain boundaries gives an indication that addition of Mg influences the lattice to an extent that enables the hydrogen to penetrate into the alloy along the grain boundaries. The formation of a second hydride MgH_2 in Al-Mg alloys would indicate a much higher hydrogen saturation point than that in pure aluminium. By adding Cu to the Alloy, as in

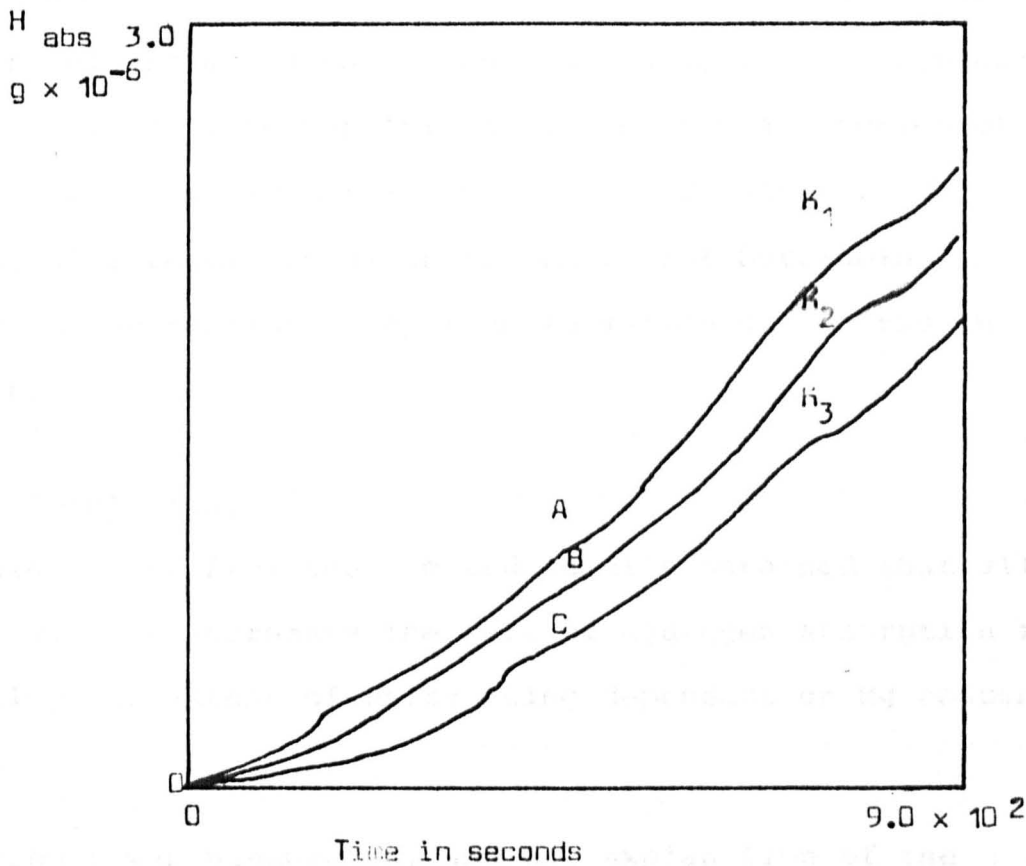


Fig. 55

Hydrogen absorption in :

A = Al - 5 Mg

B = Al - 3 Mg

C = Al

Duralumin, the formation of hydrides can be suppressed (see Figure 54, curve A). Little indication is given of any irregularities in the graph and its appearance approximates to linear; in the initial stages the absorption of hydrogen observed is larger than that for pure Al. The absence of irregularities in the curve for Duralumin indicates suppression of hydride formation due to the Cu content.

8.6.4 Conclusions

It would appear from the limited results obtained that alloying Al with Mg increases the rate of hydrogen absorption into the alloy the extent of which being dependant on Mg concentration.

This result was unexpected, and one explanation of the phenomenon could be that Mg in solid solution in Al might cause a lowering of the Fermi level of the alloy, and facilitate the transformation of atomic H to the H⁻ ion and consequently the entry of the latter into the alloy.

There is evidence in the literature that entry of H into Al/Mg alloys occurs preferentially at grain boundaries, since Tuck⁽¹⁴⁹⁾ identified Mg at these sites. This may indicate that hydrogen embrittlement may be responsible for the failure of Al/Mg alloys under certain environmental conditions.

Addition of Cu to the alloy, as in Duralumin, results in a linear curve, indicating that hydride formation is diminished if not completely suppressed. In the case of Duralumin the slight increase in the rate of H absorption

in the initial period may be due to the presence of Mg (1%) in the alloy.

One further consideration, not quantified in these experiments, is the possible role of Cu and Mg oxide impurities within the Al oxide surface layer, which may have a promoting effect on the H uptake in the initial stages. This would explain the more rapid initial increase of hydrogen absorption in Al-Mg and Duralumin compared with pure Al.

8.6.5 Determination of hydrogen equilibrium solubilities and diffusion coefficient in pure Al

Very little information can be found in the literature on hydrogen diffusion coefficients in pure aluminium at low temperatures for the reasons described in Chapter 7. The values available are limited to very high temperatures as shown in Table 4 and no values could be found for the equilibrium solubilities of hydrogen in Al. In the present work a major objective was to establish these values by means of the piezo-electric technique, which has proved to be one of the most suitable tools for this kind of measurement. The material used for this work was pure Al of various thicknesses, (supplied by Goodfellow Metals Ltd) of nominal composition given in Section 7.1.2. The thicknesses used were 0.0015 mm, 0.003 mm, 0.006 mm, 0.008 mm, 0.0125 mm, 0.015 mm and 0.025 mm. They were cut into spatular - shaped electrodes of dimensions of 10 x 5 mm, which were spot welded to the electrode holder as described in Chapter 4. They were then ultrasonically

degreased in benzene and introduced into the P.E.T cell. The experimental procedure has been described in Chapter 4.

8.6.6 Results

The diffusion coefficient of cathodic hydrogen in Al was obtained by determining the time at which pure Al of various thicknesses becomes saturated with hydrogen. From this it is possible to determine the diffusion coefficient using the Einstein-Smoluchowsky equation as described in Chapter 2.

Figure 56 shows the trace of the rate of hydrogen absorption up to the point of saturation, which was taken as point S where the extent of hydrogen absorption suddenly decreases to almost zero. This as shown in Figure 56, was determined for several thicknesses of Al. The times for saturation for some thickness of foil and the parameters used to calculate D_H are given in Table 8.

Table 8
Parameter used to calculate D_H

<u>Foil thickness</u>					
<u>x(cm)</u>	<u>t(s)</u>		<u>Δt(s)</u>	<u>Δx(cm)</u>	<u>$D(\text{cm}^2 \text{ s}^{-1})$</u>
0.0003	80.7)	64.3	0.0005	1.9×10^{-9}
0.0008	145)			
0.0008	145)	133	0.0007	1.8×10^{-9}
0.0015	278)			

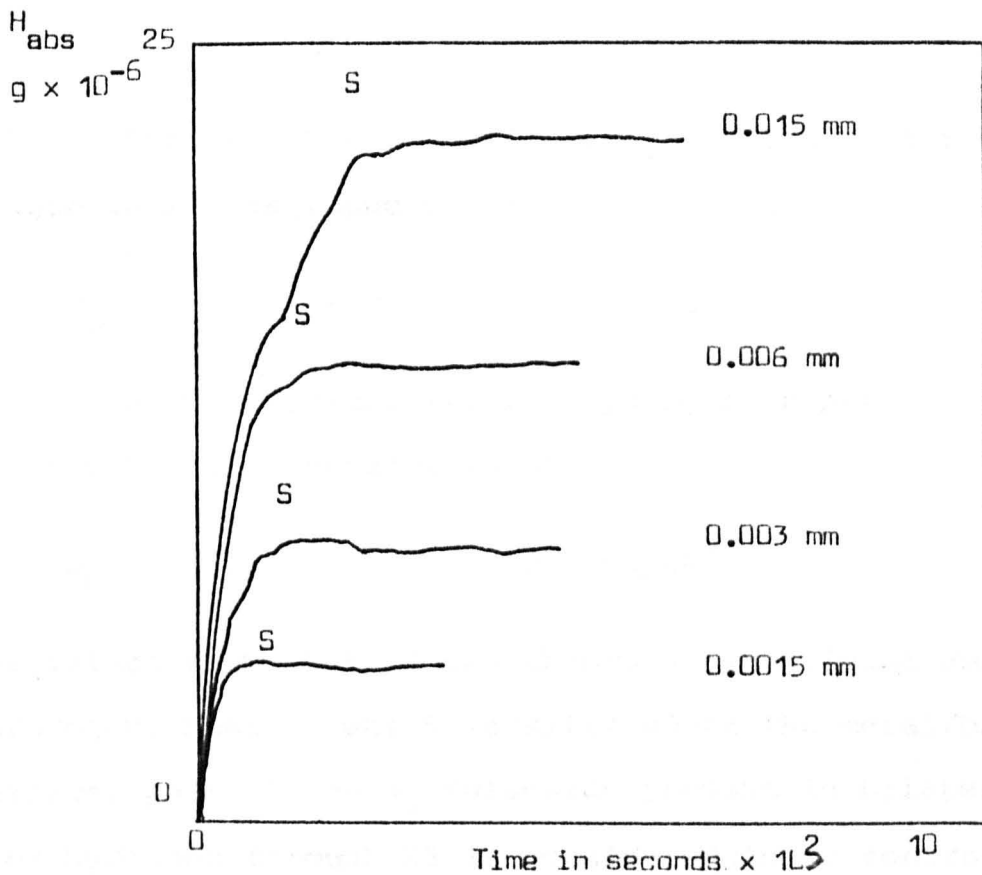


Fig. 56

Hydrogen absorption in Aluminium foils of different thicknesses charged at 1 mA/cm^2 in $0.05 \text{ M H}_2\text{SO}_4$

By this method the average diffusion coefficient for hydrogen in Al was found to be

$$D_H = (1.87 \pm 0.04) \cdot 10^{-9} \text{ cm}^2\text{s}^{-1}$$

and the equilibrium solubility for hydrogen in pure aluminium has been determined as

$$S_H = (1.0 \pm 0.14) \cdot 10^{-4} \text{ gH/gAl}$$

These values show that Al can absorb a significant amount of hydrogen, most of which is situated at the metal/oxide interface, possibly as H_2 molecules present in blisters. The diffusion of hydrogen through Al is considered to be controlled by this interface and it has been found that hydrogen is able to penetrate air formed oxide films of thickness between 10-20 Å. According to the literature the species that enters the oxide is the H^+ ion, which then reacts with the surface of the Al to form an intermediate hydride which rapidly decomposes; the hydrogen then enters the metal lattice as described in equations 79 and 80. The hydrogen in the bulk material will be mainly situated at the grain boundaries, and the quantity of hydrogen absorbed will depend on the content of Mg, as shown by Brauer et al⁽⁸⁵⁾ and Tuck⁽¹⁴⁹⁾.

8.6.7 Cathodic absorption of H in Al using As-containing charging solutions

Previous studies of hydrogen absorption in the presence of an inhibitor or promoter of the hydrogen absorption reaction has been confined largely to pure iron and to steels of

different compositions. Very little work has been carried out on the promoting action of As on hydrogen absorption by Ti and there appears to be no published work on its effect on hydrogen absorption by Al in its alloys. This is due to the insensitivity of previous experimental techniques. However, the P.E.T has shown that it can be used to study the promoting action of As on the absorption of H by Al, Al alloys and Ti. The alloys used were pure Al, Al-5Mg and Al-4Cu-1Mg, in the form of foils which were 0.02 mm thick. The composition of these foils has been given in the previous Chapter, and the preparation of specimens has been described in Chapter 4. The solution in which the experiments were carried out was 0.05M H₂SO₄ and the arsenic concentrations in the acid were 2 ppm, 5 ppm and 10 ppm. The foils were cut into electrodes of 1 cm² surface area and charged at a current density of 1 mA/cm² at room temperature. The time of each experiment was 150 min.

8.7 Results

Fig 57 shows the effect of As on the absorption of hydrogen by Al, and it can be seen that low concentrations of As (2 ppm) have the greatest promoting effect on the hydrogen absorption reaction, (h.a.r), whereas at 5 ppm As and above the effect is reversed and As acts as an inhibitor. The explanation for this effect follows closely that outlined in the previous Chapter for Ti, which divided the reaction taking place into three different stages.

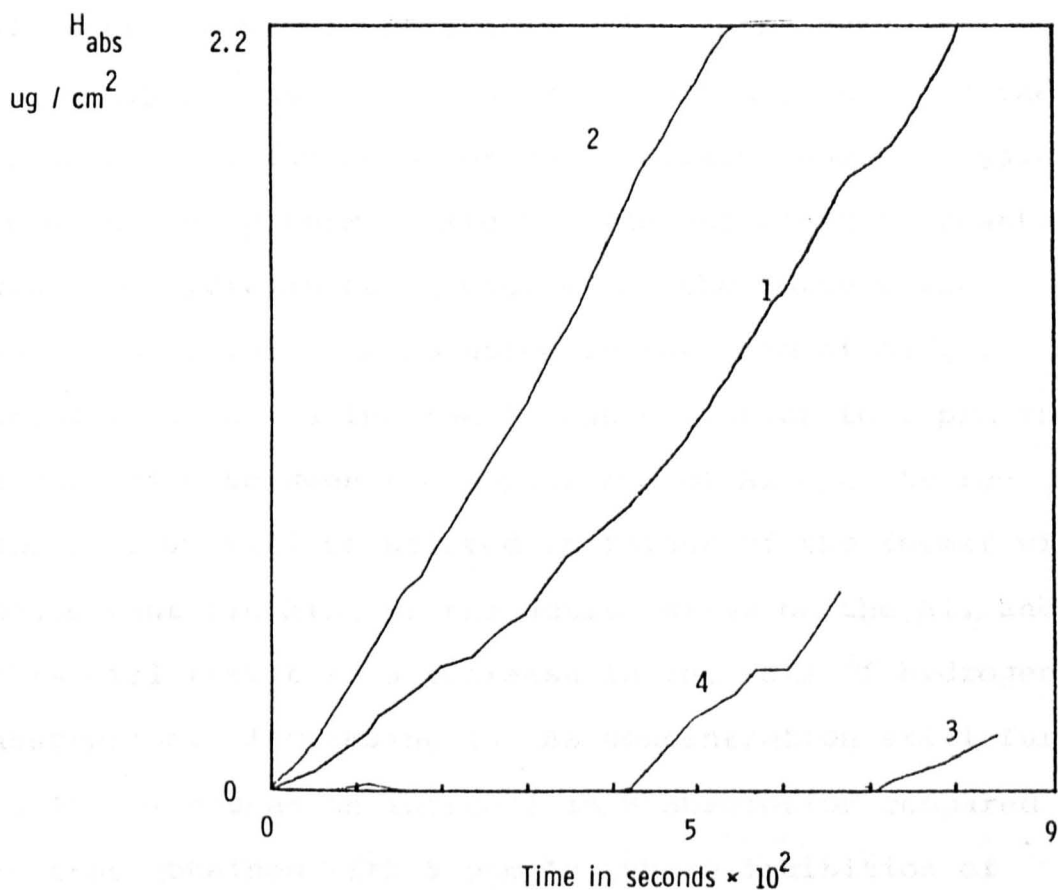


Fig. 57

Hydrogen absorption by Al in 0.05 M H_2SO_4 plus various concentrations of As in solution

1. Al - no As in solution
2. Al - 2 ppm As in solution
3. Al - 5 ppm As in solution
4. Al - 10 ppm As in solution

First the formation of AsH_3 which decomposes at active sites on the metal surface, and liberates hydrogen (possibly H^+) and As. The H^+ then diffuses through the oxide film to the metal oxide interface, where it gains an electron to form atomic H. The deposited As reacts with the hydrogen being evolved at the surface and passes back into the solution in the form of AsH_3 . Second, by increasing the As concentration to 5 ppm the equilibrium between the deposition of As and its re-dissolution will be shifted in favour of the former with consequent blocking of the active sites on the Al, and this will result in a decrease in the rate of hydrogen absorption. Increasing the As concentration still further to 10 ppm causes an increase in H absorption compared to that obtained with 5 ppm As, where inhibition of absorption occurs, and As was shown to have deposited evenly over the surface of the Al.

Consultation of Figure 57 shows (a) curve 2 is more linear than curve 1 although both depart from linearity and (b) the incubation time for curve 3 is more prolonged than that for curve 4. The reason for the promoting action of 2 ppm As cannot be explained satisfactorily at present.

By increasing the As concentration to 5 and 10 ppm a larger incubation time is observed as shown in curves 3 and 4. This is due to the deposition of the As on the surface and a decrease in the absorption of hydrogen.

The different times required for the commencement of absorption indicates that different periods of time are required to attain an equilibrium between As and AsH_3 (see Chapter 7).

Figure 58 shows the effect that the same concentrations of As have on hydrogen absorption into Al - 5 Mg, and it can be seen from curves 2 and 3 that the region of significant promoting action now commences at 5 ppm rather than 2 ppm as in the case of pure Al. This can be explained by an increase in the active sites resulting from the presence of Mg as an alloying addition.

By increasing the concentration of As to 10 ppm (curve 4) an inhibiting effect is observed similar to that for pure Al, and it is apparent that even when more active sites are present, increasing the concentration of As results in a blocking of these sites and a decrease in hydrogen absorption. This may explain why the absorption of hydrogen takes place at less active sites at which absorption is much slower than at active sites, such as grain boundaries, slip lines, or precipitates of the alloying addition.

By adding copper to the aluminium as in Duralumin a completely different pattern of results is obtained. This is shown in Figure 59 where all concentrations of As

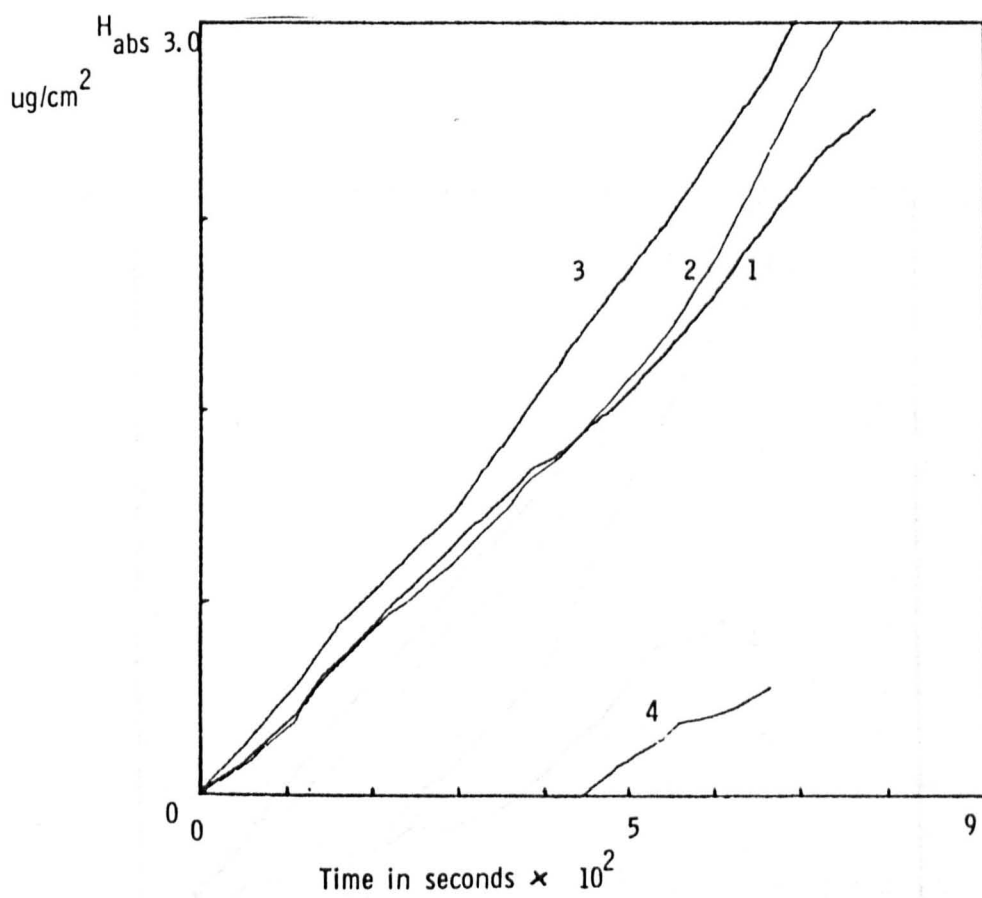


Fig. 58

Hydrogen absorption by Al - 5 Mg in 0.05 M H_2SO_4 plus various concentrations of As in solution

1. Al - 5 Mg - no As in solution
2. Al - 5 Mg - 2 ppm As in solution
3. Al - 5 Mg - 5 ppm As in solution
4. Al - 5 Mg - 10 ppm As in solution

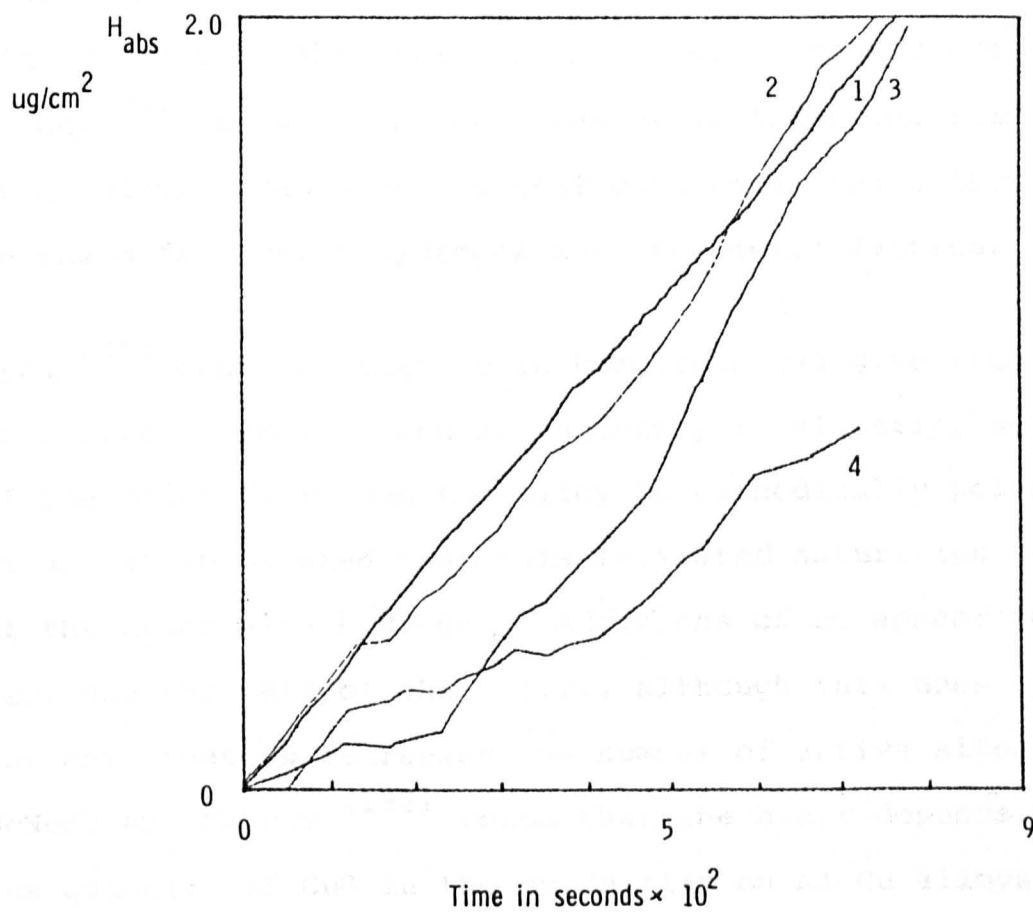


Fig. 59

Hydrogen absorption by Duralumin in 0.05 M H₂SO₄

plus various concentrations of As in solution

1. Duralumin - no As in solution
2. Duralumin - 2 ppm As in solution
3. Duralumin - 5 ppm As in solution
4. Duralumin - 10 ppm As in solution

producing an inhibiting effect. It appears that in the case of Duralumin, arsenic is acting purely as an inhibitor for the h.a.r., and comparison with Figure 42 shows that Duralumin and pure Al are similar with respect to absorption of hydrogen. Furthermore, Goshey⁽¹⁶¹⁾ showed that CuO present in the oxide film on Duralumin does have a significant retarding effect on the diffusion of hydrogen into the metal lattice.

Tuck⁽¹⁴⁹⁾ observed that Cu in Duralumin can give rise to blister formation and subsequent partial stripping of the oxide film when the alloy is cathodically polarized, and considered that this indicated saturation of the alloy with hydrogen. Additions of Cu appear to decrease the rate of the h.a.r., although this does not mean that Cu decreases the number of active sites. McNeab and Forster⁽¹⁵³⁾ found that the h.a.r depends on the quantity of CuO in the oxide film on Al-Cu alloys and that the simple diffusion model is not applicable if Cu is present. Figure 59 shows that curves 2 to 4 are non-linear in comparison with curve 1, which represents hydrogen absorption in the absence of As, and this is a clear indication of the change in the hydrogen entry kinetics. More careful metallographic work is required to determine the influence of Cu in the alloy, As in the solution and of Cu ions within the aluminium oxide lattice on the kinetics of the h.a.r.

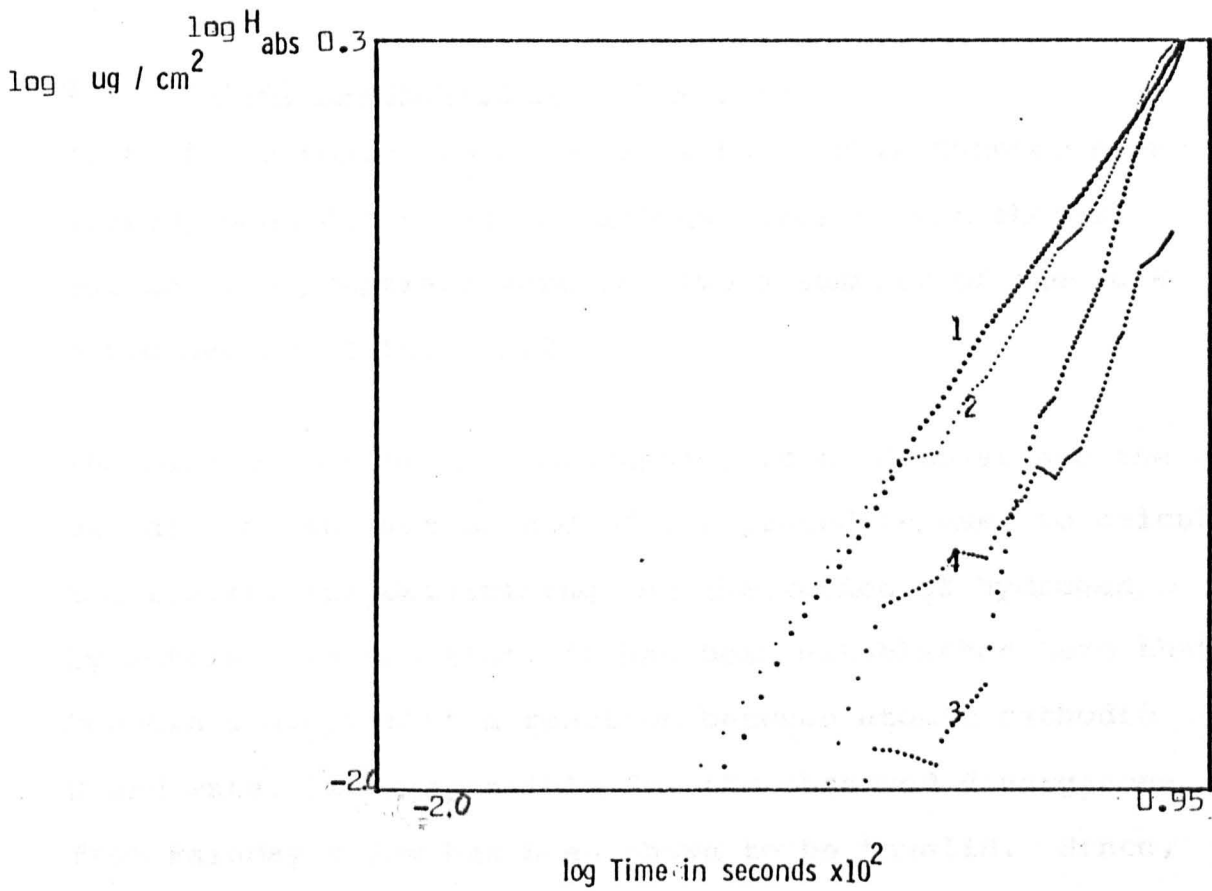


Fig. 60 Hydrogen absorption in Duralumin (Al - 4Cu - 1Mg) plus various concentration of As in solution

1. Duralumin - no As in solution
2. Duralumin - 2 ppm As in solution
3. Duralumin - 5 ppm As in solution
4. Duralumin - 10 ppm As in solution

CHAPTER 9

9.1 General Discussion and Conclusions

Most of the topics to be dealt with in this Chapter have already been discussed in various parts of the thesis, but it is appropriate here to give a summary of the work performed using the P.E.T.

The main object of this discussion is to demonstrate the validity of the method and of the procedure used to calculate the results for determining the absorption of hydrogen by metals. In addition, it has been established here that Meadows concept that a reaction between atomic cathodic H and water was responsible for the observed divergences from Faraday's law has been shown to be invalid. Since, it was not possible for him to reproduce his results, he questioned the validity of the method to give quantitative determinations of hydrogen absorption. Although he assumed that the solutions used for his work had been pre-saturated with hydrogen, this has been shown in the present work not to be the case. It has also been shown that if the solution is fully saturated with hydrogen gas by sparging for long periods with gaseous H, it is possible to obtain reproducible H-absorption results.

Furthermore Meadows quantum-mechanical approach in which he postulated electron clusters of multiples of $1/6$ leading to discrepancies from Faraday's law cannot be reproduced if the solution is fully saturated with hydrogen gas.

By using point electrodes of very small surface area it was possible for him to obtain the theoretical volume of cathodic hydrogen as calculated from Faraday's law. However, the reaction between water molecules and the hydrogen ions that was postulated by Meadows should not be dependent on the shape or area of surface of the electrode.

The main finding by Meadows was the limited validity of Faraday's law, which appears to be supported by work done by Palit^(154,155) whose experiments showed that electrolysis of dilute aqueous electrolyte solutions at low current densities gave H_2 and O_2 volumes that were less than those predicted by Faraday's law. Palit stated that as the ion population decreased the greater the departure from Faraday's law. These findings are strongly opposed by Konya⁽¹⁵⁶⁾ who considers that Palit's results do not invalidate Faraday's law and that the anomalies observed were probably due to contamination of the solution, and the failure by Palit to take into account all of the electrode processes which take place. In the case of O_2 evolution at a Pt anode impurities adsorbed on the surface during electrolysis may inhibit certain steps in the anode process so that a large amount of H_2O_2 accumulates in the anode compartment, part of which diffuses into the cathode compartment where it decomposes or is cathodically reduced. Although an intensive literature survey has been carried out to find work supporting the hydrogen cluster theory advanced by Meadows, no evidence could be found in the literature which supports the

formation of H_4 , H_5 , even H_6 molecules. It is possible that metastable atomic hydrogen can persist for a short time in solution during cathodic H_2 evolution at a Pt-electrode, but this possibility is overcome by saturating the solution with both gaseous H and cathodic hydrogen.

It was possible using this procedure not only to get excellent reproducibility (st. $D \pm 0.01 \times 10^{-6}$ g H for 1×10^{-6} g $H = 1\%$) and to establish experimentally the theoretical hydrogen evolution rate as calculated by means of Faraday's law. This was achieved by using a Cu/Hg electrode in which hydrogen is practically insoluble and this provided a means of producing a calibration curve for determining the solubility of hydrogen in electrodes of other metals.

The calculation was done using a mathematical model based on proportionalities, which gave a quantitative estimate of the hydrogen gas absorbed into a metal electrode during a given period of time. An extensive computer programme was used to provide a means of calculating as many points as possible.

The apparatus developed by Meadows was limited to the exact measurement of only 10 - 50 μ l of evolved hydrogen gas. By designing a P.E.T cell with larger piezo-electric crystals it was possible to collect 1000 μ l of hydrogen gas, and to thereby extend the time of the experiment to up to 15h. Comparison of the results obtained with the

P.E.T with other methods, such as solid-state vacuum extraction and the hydrogen permeation method showed good agreement. These comparisons were performed using metals such as Fe and Ti for which values of diffusion coefficients and equilibrium solubilities are well established. The good agreement confirms the validity of the P.E.T technique and the mathematical approach adopted.

A question that has to be answered is the advantage of the P.E.T if other well established methods are capable of yielding accurate results. The main value of the P.E.T method lies in its high sensitivity and the fact that the results are obtained in the form of an e.m.f that can be recorded on a chart recorder. It is sufficiently sensitive to determine H - absorption in metals such as Al, Au, Pt, Cd and Al - xMg, all of which have very low hydrogen solubilities.

Other experiments not reported in the thesis have shown that the P.E.T method can also distinguish between different surface treatments of the same metal, which is not possible with the other two methods mentioned above.

The determination of equilibrium solubilities using the permeation method is based on a questionable mathematical approach, ie. that the concentration gradient within the metal is linear. The P.E.T can also detect the influence of the oxide film on hydrogen absorption, since it is capable of measuring hydrogen absorption in very thin foils where the surface film has a significant effect in comparison with the bulk metal; this does not apply to the

permeation method.

Its advantages over the solid-state vacuum extraction method are its much higher sensitivity and the facility it affords for measurements to be recorded from the beginning and throughout the experimental period. The accuracy attained is comparable with the ion beam method but the nuclear method is very slow, cannot be used in situ, and requires a great deal of expensive equipment.

A limitation of the P.E.T was demonstrated by measuring the h.a.r on Ti when an oxide film of < 20 nm was present at the surface of the metal. If this oxide film is anodically formed it is unstable when cathodically polarized to a potential of $- 0.8V$ in a solution of pH of 1 - 2 at room temperature. This introduces a second reaction in addition to the h.a.r., ie. the slow dissolution of the oxide film. This dissolution of the oxide film takes up charge which introduces an error due to the charge consumed in reducing the oxide. In the case of Ti oxides, this error can be allowed for, by observing the change in interference colours which accompany the change in oxide film thickness, thus enabling an accurate calculation of the true quantity of hydrogen absorbed.

In the case of Ti oxide it has also been shown that this produces a barrier against hydrogen absorption but only if the oxide film is thicker than 20 nm. This is in conflict

with the work done by Phillips et al⁽⁷⁹⁾ who found that when an oxide film was present the results were not reproducible. Haynes⁽¹⁵⁷⁾ confirms that oxide films on Ti act as a barrier to hydrogen absorption, and that this is largely due to the layer enriched in oxygen at the metal oxide interface.

As has been shown, it is possible using the P.E.T to calculate the true absorption of H into Ti even if the anodic oxide film is slowly dissolving during the charging process. Much greater difficulties are encountered if promoter metals such as As are deposited on the surface during the H - charging process.

In the case of the h.a.r on Al and its alloys using an electrolyte containing As it has been established using microprobe analysis that deposition of As on the surface of the Ti occurs if the concentration of As in the solution exceeds 5 ppm. This reduction to elemental As will consume charge which although it cannot be estimated must be very small in comparison with the ability that As has of increasing the amount of hydrogen absorbed by the Al. The shape of the E - t curves, particularly the departures from linearity, any kinks can give an indication of the kinetics of the system.

In the study of hydrogen absorption by Al-Mg alloys it was shown that H absorption increased with increase in the concentration of Mg.

Furthermore, from the departure of the H_{abs} -t curves for the Al - 3Mg and Al - 5Mg alloys from linearity it would appear that this corresponds with hydride formation. This not only confirms the work of several other authors but also yields absolute values from which it is possible to determine the period of charging required for hydride formation.

9.2 Conclusions

1. It has been shown that the P.E.T provides a means of obtaining accurate data on the solubility of hydrogen in a range of metals such as Fe (high interstitial solubility), Ti (high absorption due to hydride formation) and Pt, Au, Cu, Al alloys (very low solubility). Calibration of the method is achieved using a Hg-Cu electrode in which H is practically insoluble, and at which hydrogen evolution conforms with Faraday's law. Thus the difference in the rate of H evolution at the surface of the metal under study and that evolved at a Hg-Cu electrode represent solubility of hydrogen in the former.

2. The solid vacuum-extraction method was used to repeat the work done by Phillips, Poole and Shreir on Ti, and their results have been confirmed by measuring also hydrogen absorption using the P.E.T. These experiments established that the P.E.T was of a comparable sensitivity to the solid-state vacuum-extraction method for studying the dissolution of hydrogen in a metal such as Ti in which

hydrogen is highly soluble. An advantage of the P.E.T is that results can be obtained rapidly and that the kinetics of dissolution can be determined continuously.

3. By comparing the P.E.T with the permeation method as developed by Devanathan, it was shown that it was possible to obtain accurate diffusion coefficients and equilibrium solubilities for metals such as Fe and Al by means of the P.E.T.

In the case of Fe the results obtained agreed very closely with those obtained using the permeation method.

The solubility of H in Al is so low that it is difficult to study using the permeation method, but by using the P.E.T it was not only possible to determine the equilibrium solubility but also the diffusion coefficient for Al. This demonstrates that the P.E.T is a more powerful tool than the permeation method for studying H absorption by metals which have a very low solubility of hydrogen, eg. Au, Pt, Al, Cd and Al alloys.

4. It was possible by means of the P.E.T in conjunction with X-ray diffraction to propose a theory to explain the stepwise kinetics of H absorption by Ti during cathodic charging in 0.05M H₂SO₄. These steps appear to be as follows:

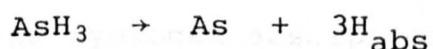
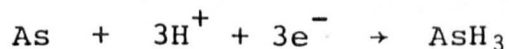
- i) Diffusion of the hydrogen ion through the oxide film and discharge at the metal oxide interface, followed by diffusion of hydrogen atoms into the metal lattice and the formation of a saturated solid solution of H and Ti.
- ii) After reaching a certain threshold concentration the hydrogen in the Ti-lattice reacts suddenly with the Ti to form a stable γ -hydride (TiH_2). During the formation of the α -hydride* the concentration of free hydrogen atoms again builds up until the threshold value is reached and a second layer of γ -hydride is formed.
- iii) When the titanium surface is evenly coated with γ -hydride the h.a.r becomes controlled by cracks that have formed in the hydride.
- iv) Oxide films on Ti (anodic or thermal) have a significant inhibiting effect on the rate of hydrogen absorption which contradicts the results obtained by Phillips et al on the behaviour of anodic films which these workers found had little effect in preventing hydrogen absorption. To inhibit H absorption the anodic film on Ti must be thicker than 10 nm.

* A solid solution of hydrogen in Ti.

- v) Anodic oxide films on Ti dissolve when the metal is cathodically polarized in 0.05M H₂SO₄.
- vi) If the oxide film is produced by heating it to 800°C the structure is predominantly rutile, and the oxide is in a lower energetic state than the low temperature anodic oxide film so that it is not possible to reduce this film cathodically.

5. By adding concentrations of 2,5 and 10 ppm As and studying hydrogen absorption using the P.E.T and the deposition of As on the surface by electron microprobe it was possible to propose a model to account for the promotion action of this metalloid. The main results may be summarised as follows:

- (a) When the concentration of As in the H₂SO₄ solution is 2 ppm it is assumed that it is present as AsO⁺. This cation is completely reduced to As at the grain boundaries, and this in turn is reduced completely to AsH₃, which is thermodynamically unstable and decomposes according to the reaction



and the hydrogen liberated entering the lattice at the grain boundaries.

However, if the concentration of As in the solution

is 5 ppm not all of the deposited As is reduced to AsH_3 and the unreduced As blocks the active sites of the metal and thus inhibits the h.a.r.

(b) At 10 ppm As in solution the metalloid was found to be evenly deposited over the whole surface of the metal, and the hydrogen was practically the same as for 5 ppm As in the solution.

6. By using the P.E.T it was possible to determine the diffusion coefficient of hydrogen in Al as

$$D_H = (1.87 \pm 0.04) 10^{-9} \text{ cm}^2 \text{ s}^{-1}$$

and the equilibrium solubility as

$$S_H = (1.0 \pm 0.14) 10^{-4} \text{ gH/g Al}$$

Alloying Al with 3 and 5% Mg resulted in a significant increase in the rate of hydrogen absorption, which has been explained by the formation of Mg H_2 in the alloy. However, Mg hydride was not detected in Duralumin suggesting that Cu (4%) inhibits hydride formation in this alloy. Unfortunately, this could not be confirmed by studying a 1% Mg-Al alloy, which was not available in the form of thin sheet.

By measuring the hydrogen absorption rates in Al and its alloys in the presence of 2, 5 and 10 ppm of As in the solution was promoted in both Al and Al-Mg whereas this concentration was inhibiting for Duralumin. At 5 and 10 ppm of As in the solution the h.a.r was inhibited for all alloys

of Al studied. These results show the value of the P.E.T for studying various phenomena associated with hydrogen absorption where other methods are ineffective, eg. the absorption of hydrogen by Al.

9.3 Future Work

Future work using the P.E.T could be pursued in the following fields.

1. Further studies on the absorption of hydrogen in metals with particular reference to the effect of stress.
2. Work on the effect of oxygen and other gases in metals.
3. Industrial applications.

9.4 Further Work on H Absorption

- (a) It would be of great interest to study the influence of stress on the hydrogen absorption of metals such as Al and its alloys and Ti, which could be done in situ. A cell for applying a stress during charging the metal with H has been designed as shown in Figures 61, 62.
- (b) To use a rotating disk electrode of the metal under study that could be introduced into the measuring compartment of the P.E.T cell and the evaluation of the quantities of H absorbed and the changes in potential.

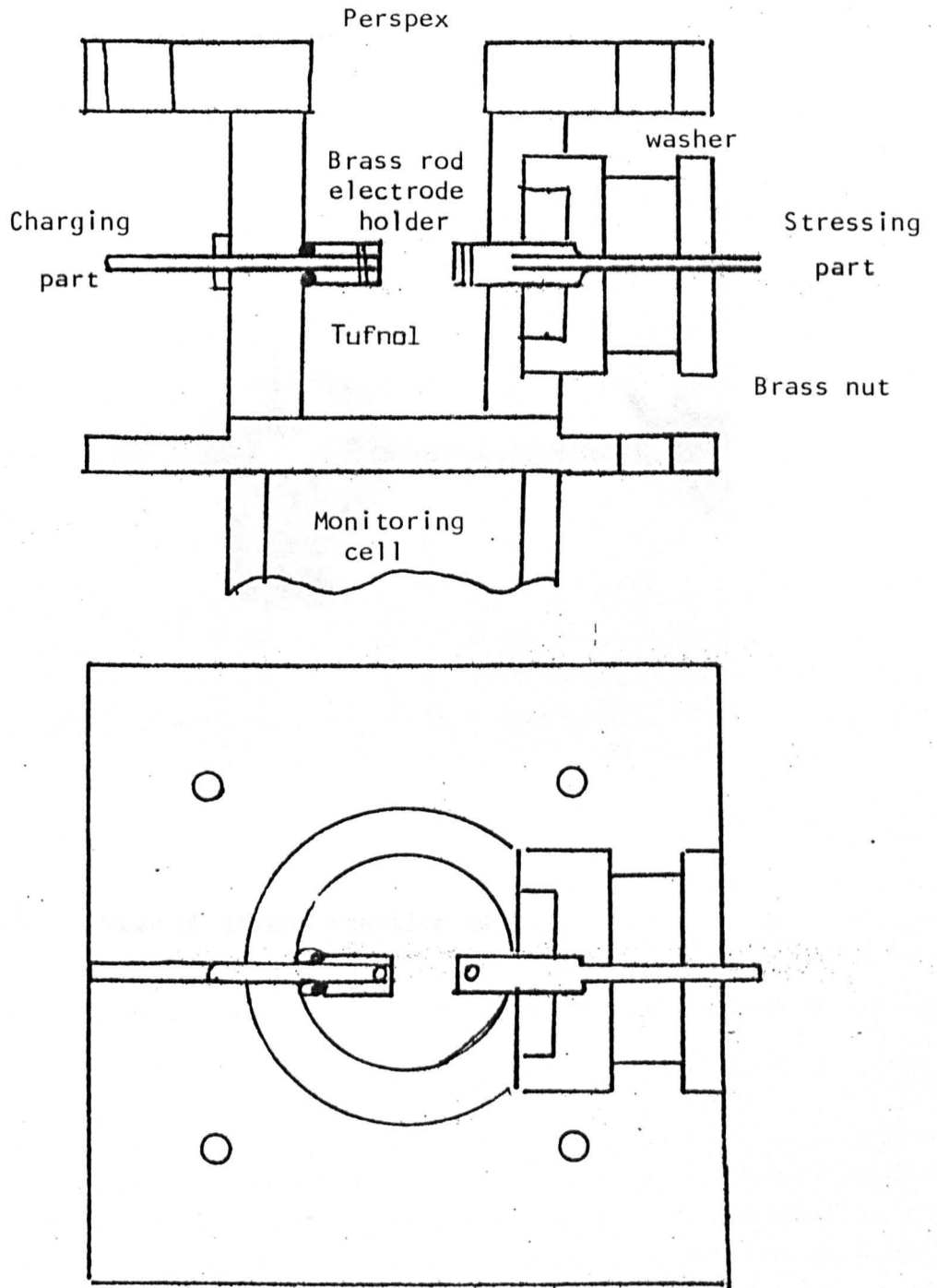


Figure 61 Stress reaction cell
(Scale 1:1)

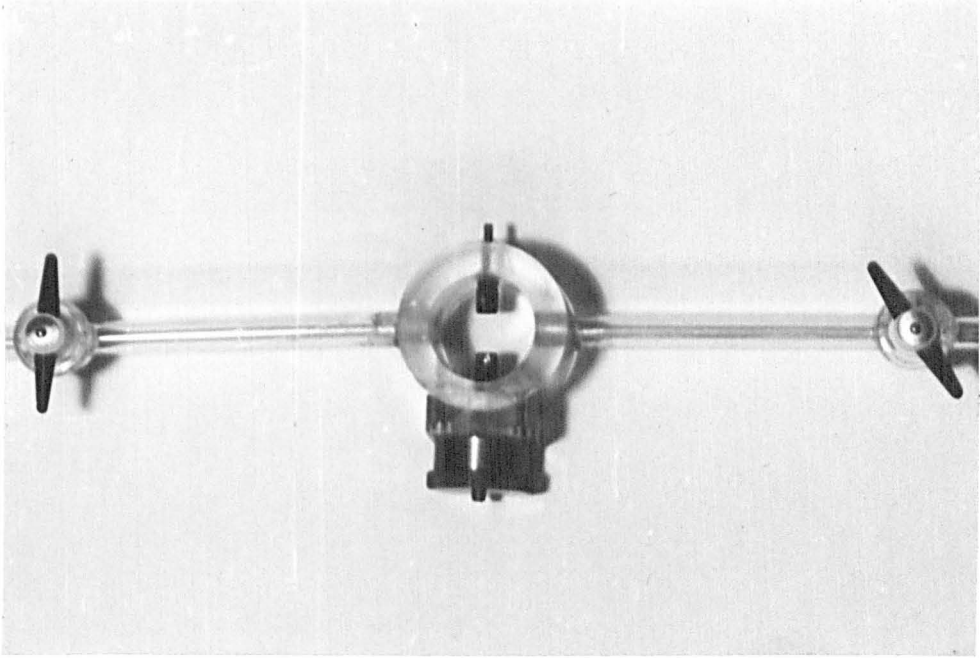


Fig. 62 View of stress reaction cell

IMAGING SERVICES NORTH

Boston Spa, Wetherby

West Yorkshire, LS23 7BQ

www.bl.uk

**PAGE MISSING IN
ORIGINAL**

- (c) To combine micro ellipsometric measurement with the P.E.T cell to quantify the growth of hydride films on the surface of a metal.

The second proposal is mainly concerned with work done at the anode of the cell to analyse oxygen absorption and oxide film formation on a variety of metals. The third field of work is to explore the potential of this method in industrial applications such as

1. A gas detector for measuring leakages in pipeline joints.
2. Measurement of overprotection of cathodic protection systems on ships hulls and oil rigs by estimating H evolved.
3. Applications in laboratories for measuring initial gas evolution produced by heating organic substances.

All these proposals show the great variety of subjects in which the P.E.T may be of great value.

REFERENCES

1. W.R. Opie and N.J. Grant: Foundary, 1950, 78 (10), 104-9, 209-10.
2. W.R. Opie and N.J. Grant: Trans.AIME, 1950, 188, 1237-47.
3. H.C. Vacher and L. Jordan: J.Res.Nat.Bur.Stan., 1931, 7, 375-40.
4. D.J Carney, J.Chipman, and N.J. Grant: J.Met., 1950, 397 (Trans AIME, 188).
5. J.L. Brandt and C.N. Cochran: J.Met., 1956, 8, 1672-4.
6. R. Parry: J.I.S.I., 1872, VII,238
7. R. Eborall and C.E. Ransley: J.Inst.Metals, 1945, 71, 525-52.
8. C.E. Ransley and D.E.J Talbott: J.Inst.Metals, 1955-G, 84,445-52.
9. Imperial Chemical Industries Ltd: Analysis of Titanium and its Alloys, 3rd Ed., 1959, pp 41, 71.
10. V.I. Lakonsky: Automat. Svarka, 1958, (2), 81-91.
11. R.K. McGeary: 'Zirconium and Zirconium Alloys', 168-75: 1953, Cleveland, ASM.
12. T.D. McKinley: Trans.Met.Soc. AIME, 1958, 212, 563-71.
13. C.E.A.S Hanakan: ISI, Special Rept., No 68, 1960.
14. L. Moreau, G. Chauchdron and A. Portevan: CR Acad.Sci., Paris, 1935, 201, 221-14.
15. E. Schmid and H.D Graf v. Schweinitz: Aluminium, 1939, 21, 772-8.
16. E.G. Bobalek and S.A. Shrader: Ind.Ens.Chem. (Anal.Ed), 1945, 17, 544-53.
17. M. Codell and G. Norwitz: Anal.Chem. 1956, 28, 106-10.
18. R.B Nunemaker and S.A Shrader: Anal.Chem, 1956, 28, 1040-2.
19. F. Sauerwald: z.anors.chem., 1948, 256, 217-225 (Met. Abst., 1951-2, 19, 856).
20. G.A. Moore: Trans. AIME, 1945, 162, 404-11.

21. P.F Chretien, H.A Nipper and E. Piwowarsky: Aluminium Archiv, 1939, (23), 29 pp.
22. W. Mannchen and W. Fischer: Metall, 1957, 10 (516), 191-5.
23. A.N. Zaidel, and A.A. Petrov: Zhur.Tekhn.Fiz, 1955, 25, 2571-3.
24. C.E. Ransley, D.E.J. Talbot and H.C. Barlow: J.Inst. Metals, 1958, 86, 212-19.
25. M. Codell and G. Norwitz: Anal.Chim.Acta, 1958, 18, 265-9.
26. R.M. Cook and J.D. Hobson: JISI, 1951, 169, 24-5.
27. Y. Dardel: Trans. AIME, 1949, 180, 273-86.
28. Y. Dardel: *ibid.*, 1948, 175, 497-515.
29. R. Eboral: Determination of Gases in Metals. ISI Special Report No.68, 1960, p 195ff.
30. R. Doerr, E. Brauer, R. Gruner, F. Rauch: Hydrogen detection in Metals by means of a new nuclear physical method. Hydrogen in Metals International Meeting, March 1979, pp 409.
31. W.A.Lanford, and H.P. Trautvetter, Appl.Phys.Letters 28, 566 (1976).
32. L.C. Northcliffe and R.F. Schilling. Nucl.Data Tables A7, 233 (1970).
33. C. Rolfs and W.S. Rodney. Nucl.Phys., A 235, 453 (1974).
34. E. Ligeon and A. Guirarch, Radiation Effects, Vol 22, pp 101-105, 1974.
35. D.A. Leich and T.A. Tombrello, Nucl.Instr. Methods 108, 67 (1973).
36. B. Pedersen (1965) Tidsskr.Kjemi.Bersv.Met., 25, 63.
37. R.M. Cotts, Ber.Brunsenes. Phys.Chem., 76, 760 (1972).
38. T. Springer (1972). "Springer Tracts in Modern Physics", Vol 64. Springer Verlag Berlin, N.Y.
39. W. Gissler (1972). Ber.Bunsenges.Phys.Chem. 76, 770.
40. K. Skold and G. Nelim (1967). J.Phys.Chem. Solids 28, 2369.

41. B. Alefeld (1972). Kerntechnik, 14, 15.
42. M.A.V. Devanathan and Z. Stachurski, J. Electrochem. Soc., Vol III, No 5, 619ff (1962).
43. Y.U.H Fukai and Shigeo Kazama. Acta.Met. Vol 25, pp 59-70, 1977.
44. T.P. Radhakrishnan. PhD University of London, 1966.
45. M.A.V. Devanathan and Z. Stachurski. Proc.Roy.Soc., 270 A (1962), 90.
46. M.A.V. Devanathan. O.N.R Technical Report No 4, 25-8, (1961).
47. W. Baukloh and A. Zimmermann. Eisenhüttenwesen 9, 459, (1935).
48. M. Smialowski and Z. Szklarska. Bull.Acad.Polerrcl.III, 2, 73, (1954).
49. L.D. McGraw, W.E. Ditmars, C.A. Snarely and C.L. Faust. N.A.C.A., T.N. 3164., 243ff, (1967)
50. H.Z. Siebert. Anorg.Allgem.Z.Chem., 274, 24, (1953).
51. J.F. Newman, thesis, University of London, (1968)
52. Angerstein - Kozłowska. H.Bull.Pol.Anod.Sci.Ser.Sc.Chim, 7, 881, (1959).
53. M. Ailes and L.L. Shreir. Electrochem.Acta II, 193 (1966).
54. R. K. Pöpperling, thesis, Technische Hochschule Aachen, (1976)
55. B.E. Conway. Theory and principles of electrode processes. Ronald Press, New York, 1965.
56. M.I. Tempkin, zh. Fiz. Khim. 15 (1941) p 296.
57. J.O.M. Bockris, J. McBreen, L.Nanis. J.Electrochem.Soc., 112 (1965) p 1025.
58. A.K.M. Shamsul Huq and A.J. Rosenberg. J.Electrochem.Soc., 111, 270 (1964).
59. E.J. Kelly. J. Electrochem.Soc., 112, 124, (1965).
60. R.Dretwell. MSc thesis. Sir John Cass College (1968).
61. A.Fick. Pogg. Ann. 94, 59 (1855).
62. S.P.Wach, thesis, University of Surrey (1966).
63. C. Wert and C. Zener. Phys.Rev., 76, 1169 (1949).

64. A. Ferro. Appl.Phys., 28, 895 (1957).
65. W.A. Rogers, R.S. Buritz and D. Alpert. J.Applied Phys., 25, 868(1954).
66. H.L. Eschbach, F. Gross and S. Schulien. Vacuum, 13, 543(1963).
67. H. Veysseyre, P. Azou and P. Bastian. Rev.Met.Mem.Sci., 61, 203 (1964).
68. L. Nanis and J. McBreen. NASA Accession No N64-22051 Report No AD 43914, avail. OTS, 17pp. (1964)
69. J. O.M. Bockris and A.J.N. Reddy. Modern Electrochemistry, Vol 1, 305 f (1970).
70. A. Meadows and L.L. Shreir. Corr.Sc. 17, 1015ff (1977).
71. S. Schuldinger and J. P. Hoare, Can.J.Chem., 37, 228 (1959).
72. F.Chao and M. Costa. Compt.Rend., Sev.C, (1977).
73. F.Chao, M. Costa and P. Elkhaim. *ibid.*, 28, (17), 639ff(1977).
74. K. Zabel and J. Peisl. Hydrogen in Metals, Int.Conf., March(1979), Munster, W Germany.
75. R. Doerr, E. Brauer, R. Gruner and F. Rauch, Hydrogen in Metals, Int.Conf., March (1979) Munster, W Germany.
76. J.D.Edwards and P. Robbins. , Guide to non-ferrous metals and their markets (Kogan Press, 1979) p 146.
77. I.I. Phillips., thesis, University of London (1972).
78. G. H. Koch, NACE, Vol. 35, No. 2, February, (1979)
79. I.I. Phillips, P. Poole and L.L. Shreir. Corrosion (1972), 12, 855-866.
80. I.I. Phillips, P. Poole and L.L. Shreir. Corrosion (1974), 14, 533-542.
81. J. P. Bearpark, thesis, University of London, (1966)
82. L.L. Covington. Int.Corr.Forum, April 1975, Toronto, Canada.
83. Tosuke Murai, Mitsuo Ishikawa and Chihatoski Miura. Corrosion, 26, 177-183 (1977).
84. M. Tsutsui, N. Fujise. Nippon Kinzoka Gakkaishi, (1975), 39 (5), 460-6).

85. E. Brauer, R. Doerr, H. Zuchner. Z.Phys.Chem.,26,435, (Frankfurt am Main) (1976).
86. R.J. Wasilewski and G.L. Kehl. Metallurgica, Vol 50 (1954), p 225.
87. T.P. Papzoglou and M.T. Hepworth. Diffusion of hydrogen in titanium. Trans.AIME, Vol 242, No.4 (1968) pp 682-5.
88. G. Hass. J.Americ.Ceram.Soc., 33 (1950) 353.
89. W. Kinna and W. Knorr. Z.Metallk. 47 (1956) 594.
90. T. Hurlen. J.Inst.Met. 89 (1960) 128.
91. A.E.Jenkins. J.Inst.Met., 82 (1953) 213.
92. J.W. Hickmann and E.A. Gulbrandsen. Analyt.Chem., 20 (1948) 158.
93. T. Hurlen, H. Kjollesdal, J.Markali and N. Norman. Central Inst.Ind.Res. Oslo-Blindem, Apr. 1958.
94. E. Roberts. Unpublished results, City of London Polytechnic,1981.
95. L.L. Shreir. Corrosion, Newnes-Butterworths, London-Boston 7:21, 87, 93.
96. C.L.M. Cottrell. Nature, 170, 1079 (1952).
97. W.J. Barnett and A.R. Trojano. J.Metals, 9, 486,(1957).
98. R.W.Buzzard and H.E. Cleaves. Nat.Bur.Standards, Circular No 511, (1951).
99. P. Cotterill. Progress in Materials Science, d, 201, (1961).
100. M. Smialowski, 'Hydrogen in steel'. Pergamon Press, London (1962).
101. H.W. Neville and E.K. Rideal. Proc.Roy.Soc.,A153, 89 (1936).
102. M.A.V Devanathan and Z. Stachurski. J. Electrochem. Soc., 111, 619 (1964).
103. T.C. Franklin and P.E. Hudson. Electrochem.Soc., 114, 568, (1967).
104. I. Langmuir. Am.Chem.Soc., 40, 1361 (1918).
105. J.O.M. Bockris and D.F.A Koch. J.Phys.Chem.,65, 1941 (1961).

106. A. Sieverts. Z.Physk.Chem., 60, 169 (1907).
107. M.H. Armbruster. J.Amer.Chem.Soc., 65, 1043 (1943).
108. W. Eichenhauer and A. Pebler. Z.Metallk, Vol 46 (1955) pp 373-8.
109. W. Eichenhauer. Z.Metallk, 69 (1961) pp 105-112.
110. I. Andreev, A.F. Vyatin, B.V. Leuchuk, V.I. Telkov and A.L. Rabinovich. Izv.Vyssh.Uchebn.Zaved, Tsvetn.Metall., 1975 (5), 123-8.
111. S. Matsuo and T. Hirata. Diffusion of hydrogen in Al. J.Japan, Inst.Met. Vol 31, No.4 (1967) pp 590-3 (Japanese).
112. L.E. Ronsley and D.E.J. Talbot. Z.Metallk.,Vol 46 (1955) p 328-37.
113. K. Papp, E. Kovacs-Csetenyi. Sr.Met.,(1977), 11(11), 921-923.
114. J. Hicks, Comprehensive Chemistry, Cleaver-Hume Press, London p.431,(1963).
115. R.C. Frank, P.C. Swets and L. Fry. J.Appl.Phys.,29, 892 (1958).
116. W. Raczynski. Archiwum Hutn., 3, 49 (1958).
117. W. Palczewska and I. Ratajczyk. Bull.Acad.Polon.Sci., Ser.Sci.Chim., 9, 267 (1961).
118. V.P. Alikin. Izv.Estestvennonauch.Inst.Pri.Permsk. Univ., 14, 19 (1960).
119. A.E. Schuetz and W.D. Robertson. Corrosion, 13, 437 (1957).
120. H.C. Davis. A.R.E. (Farnborough). Private Communication.
121. V.V. Kuznietsov and N.I. Subbotina. Elektrokhimiya 1, 1096 (1965).
122. R.M. Barrer. Trans.Farad.Soc., 36, 1235 (1940).
123. C. Sykes, H.H. Burton and C.C. Gegg. J.I., 156, 155 (1947).
124. W. Geller and T.H. Sun. Arch.Eisenhuttenw.,21, 423 (1950).
125. T.M. Stross and F.C. Tompkins. J.Chem.Soc., 155, 230 (1956).
126. W.H. Eichenhauer, Kunzig and A. Pebler. Z.Metallk., 49, 220 (1958).

127. M. Smialowski. *Neue Hütte*, 2, 621 (1957).
128. E.W. Johnson and M.L. Hill. *Trans.Met.Soc., AIME*, 218, 1104 (1960).
129. W. Raczynski and S. Stelmach. *Bull.Acad.Polon. Sci.Ser.Sci.Chim.*, 9, 633 (1961).
130. R. Wagner and R. Sizmann. *Arch. Eisenhüttenw.* 18, 193 (1964)
131. H.L. Eschbach, F. Gross and S. Schuhen. *Vacuum*, 13, 543 (1963)
132. W.L. Bryan and B.F. Dodge. *A.I.Ch.E.J.*, 9, 223 (1963).
133. J. Plusquellec, P. Azou and P. Bastien. *Mem.Sci., Rev.Met.*, 60, 111 (1963).
134. W. Schwarz and Zitter. *Arch.Eisenhuttenw.* 36, 343 (1965).
135. W. Beck, J.O.M. Bockris, J. McBreen and L. Norris. *Proc.Roy.Soc.*, A.290, 220 (1966).
136. T. Heumann and D. Primas. *Z.Naturforsch.* 21a, 260 (1966).
137. A. Guenterschulze, H. Betz and H. Kleinwaechter. *Z.Physik* 111, 657 (1938/9).
138. A.E. Schuetz and W.D. Robertson. *Corrosion*, 13, 437 (1957).
139. B. Baranowski, Z. Szklarska-Smialowska and M. Smialowski. *Bull.Akad.Poln.Soc. (Cl.111)*, 5, 191 (1957).
140. V.P. Alikin. *Izv.Estestvennonauch. Inst.Pri.Perm'sk. Univ.*, 14, 19 (1960).
141. E.H. Dix. *J.Trans.ASM*, Vol.42, p.1057 (1950).
142. A.J. Sedriks, P.W. Slattery and E.N. Pugh. *Trans.AMS*, Vol.62, 238 (1969).
143. M.O. Speidel. *Hydrogen in Metals*. Ed. I.M. Bernstein and A.W. Thorrupen ASM, p 249 (1974).
144. P.J. Gest and A.R. Troiano. *Corrosion*, Vol.30, P 274 (1974).
145. A.W. Thompon and I.M. Bernstein. *Reviews on Coatings and Corrosion*, Vol.2, p 3 (1976).
146. G.M. Scamans, R. Alani and P.R. Swan. *Corrosion Sc.*, Vol.16, p 443 (1976).

147. J.L. Nelson. PhD thesis, University of Illinois at Urbana Champaign (1976).
148. M. Appel and J.P. Frankel. J.Chem.Phys., Vol.42, p 3984 (1965).
149. C.D.S. Tuck and G.M. Scamans. Engineering Materials, Chicago (1977).
150. E.N. Pugh. The Metals Soc., London, p 493 (1977).
151. J. Albrecht, B.J. McTiernan, I.M. Bernstein and A.W. Scripta Met., Vol.11, p 893 (1977).
152. B. E. Conway and J. O'M. Bockris, J. Chem.Phys.,26, 532, (1957)
153. A. McNeab and Foster. AIME, p 1022, Vol.233 (1965).
154. S.R. Palit. Ind.J. Physics, p 79, Vol.45 (1971).
155. S.R. Palit. J.Sci.Ind.Res., p 435, Vol.31 (1972).
156. J. Konya. J.Electrochem.Soc., Vol.126, No 1, p 54 (1979).
157. R. Haynes. J.Inst.Metals, 8(7), 249-252 (1961).
158. R. F. K. Herzog. Trace analysis by mass spectrometry, Academic Press, New York, pp.57, 1972
159. M. Bodenstein., Z. Elektro. Chem.,23, 517, (1922)
160. G. Borelius and J. Lindblom, J. Am. Physik., 82, 201, (1927)
161. S. Goshey, Werkstoffe und Korrosion 25,p 565, (1974)